Phenomenological Aspects of Neutrino Oscillations

A thesis submitted for the award of the degree of
Doctor of Philosophy in Physics

by

Soumya C
(12PHPH09)

Under the guidance of
Prof. Rukmani Mohanta

School of Physics
University of Hyderabad
Hyderabad-500 046, India

April 2017

Declaration

I hereby declare that, this thesis entitled **Phenomenological Aspects of Neutrino Oscillations** submitted by me under the guidance and supervision of Prof. Rukmani Mohanta is a bonafide research work which is also free from plagiarism. I also declare that it has not been submitted previously in part or in full to this University or any other University or Institution for the award of any degree or diploma. I hereby agree that my thesis can be deposited in Shodhganga/INFLIBNET.

A report on plagiarism statistics from the University Librarian is enclosed.

Place: Hyderabad
Date:

Soumya C
Reg. No. 12PHPH09

Certificate

This is to certify that the thesis entitled **Phenomenological Aspects of Neutrino Oscillations** submitted by Soumya C bearing registration number 12PHPH09 in partial fulfilment of the requirements for award of Doctor of Philosophy in the School of Physics is a bonafide work carried out by her under my supervision and guidance.

This thesis is free from plagiarism and has not been submitted previously in part or in full to this or any other University or Institution for award of any degree or diploma. Further, the student has the following publications before the submission of the thesis for adjudication.

1) C. Soumya and R. Mohanta, European Physical Journal C **76**, 302 (2016), (ISSN No: 1434-6052 (online)), Chapter 3.

2) C. Soumya, K. N. Deepthi, and R. Mohanta, Advances in High Energy Physics **2016**, 9139402 (2016), (ISSN No: 1687-7365 (online)), Chapter 4.

3) C. Soumya and R. Mohanta, Physical Review D **94**, 053008 (2016), (ISSN No: 2470-0029 (online)), Chapter 5.

4) Soumya C. and R. Mohanta, European Physical Journal C **77**, 32 (2017), (ISSN No: 1434-6052 (online)), Chapter 5.

Further, the student has passed the following courses towards fulfilment of coursework requirement for Ph.D:

Course Code	Name	Credits	Pass/Fail
PY801	Advanced Quantum Mechanics	4	Pass
PY803	Advanced Statistical Mechanics	4	Pass
PY804	Advanced Electromagnetic Theory	4	Pass
PY821	Research Methodology	4	Pass

Prof. Rukmani Mohanta
Thesis Supervisor
School of Physics
University of Hyderabad

Prof. Bindu A. Bambah
Dean
School of Physics
University of Hyderabad

Date:

Acknowledgements

As my thesis work has reached its culmination, I would like to acknowledge the unconditional support offered by all in the years of my university education. There are numerous people without whom this work would not have been possible.

First of all, I would like to thank my supervisor Prof. Rukmani Mohanta, who was kind enough to take me under her guidance and had the patience to teach me. Her intellectual guidance and inspiring suggestions have droved me into the exciting field of Neutrino Phenomenology. Further, her constant support and encouragement in both academics and non-academics have shaped this thesis work. For me, she is an icon of patience, dedication and hard work. She has inspired and motivated me during the difficult times when I needed words of encouragement.

I would like to express my gratitude to the present Dean Prof. Bindu A. Bambah, who is always an inspiration. My heartfelt thanks to former Deans: Prof. S. P. Tiwari, Prof. S. Chaturvedi, and Prof. R. Singh for providing all the academic facilities.

I would like to thank Prof. P. K. Suresh, who was my M.Sc. project supervisor. My sincere thanks to doctoral committee members Prof. E. Harikumar and Dr. Soma Sanyal for their valuable suggestions to improve the quality of my work. I would like to thank all my M.Sc. teachers, especially Prof. A. K. Kapoor, Prof. V. S. S. Sastry, Prof. Ashok Chatterjee, Prof. M. Sivakumar, Prof. S. Dutta Gupta, and Prof. V. Seshubai for my understanding of other areas of physics. I am thankful to Dr. Ashok Vudayagiri for helping me at various stages. I also thank Dr. Barilang Mawlong for being so friendly and giving the suggestions.

My thanks to Prof. Anjan K. Giri for his motivational suggestions. I would like to thank Prof. Srubabati Goswami for helping me during my stay at Physical Research Laboratory. I express my heartfelt gratitude to Dr. Sushant. K. Raut for providing me useful informations regarding the simulations related to long baseline neutrino experiments and for helping me at various stages of my research work. I would like to thank Dr. Jennifer L Raaf for the various interesting discussions on neutrino physics at Fermilab. I thank Prof. Nita Sinha and Dr. Poonam Mehta and I have really enjoyed the discussion with them on NSIs. It is my great pleasure to thank Prof. Kaushik

Bhattacharya, who helped me at various stages. My thanks to Dr. Suprabh Prakash, Dr. Arnab Dasgupta, Dr. Monojit Gosh, Dr. Mehdi Masud for the useful discussions on current trends in neutrino physics and GLoBES. I also thank Mr. Newton Nath for helping me during my stay at PRL.

My sincere thanks to all the anonymous referees for their valuable comments and suggestions to improve the works that I have done.

I express my gratitude to UGC and SERB for the financial support during my research. The fund provided by Indo-US Science and Technology Forum during my visit at Fermilab is greatly acknowledged.

My thanks also go to the office staffs of School of Physics, especially Mr. Sekhar, Mr. Abraham, Mr. Sreenivas, Ms. Deepika, Mrs. Shailaja and Mr. Prasad, who were helped me in administrative activities.

I thank my senior-cum-collaborator K.N Deepthi for her motivational discussions and guidance as a sister. I have no words to thank my best friend Sruthilaya, who was always with me during my good and bad times of university life. My special thanks to Ali, Siraj and Manu, who always encouraged me to aim higher and gave me the confidence to go ahead with the research. I thank Anjana, Zuhair, Anoop, Sravan and Masroor for the nice group discussions and the funs that we had, and for the support during these years. I also thank all my colleagues and theory room mates especially Siva, Shankar, Sreenu, Sumen, Raju, Alu, Ahmed, Sanjeev, Monisha, Rasmita, Rasna, Luhluh, Naveen, Zuhail, Umalavanya, and Sivaprasad for always being so helpful and friendly. I also thank all juniors especially Suchismitha, Sivaramakrishna and Robertson for their help and support. My special thanks to my cousin Ashitha and her husband Salah for their care and support as local guardians.

Last but not the least, I would like to thank my family. I would like to extend my deepest gratitude to my parents, Mr. Ramachandran and Mrs. Sarojini for their unconditional love, care, support and constant encouragement to pursue my dreams. I also thank my sister Remya, brother-in law Anoop and nephew Rohan who have added new dimensions to the world of happiness in my life. Finally, I thank each and every persons of my family, who were there for me during the hardest time of my life.

Soumya C

To

My Beloved Parents

Abstract

Neutrino, one of the nature's elementary particle, has astounded physicists for past few decades by its peculiar properties like extreme lightness, no charge, and participates only in weak interaction. In addition to this, few years back scientists have discovered another fascinating nature of neutrino in which neutrino can change its flavor from one to other, so called neutrino oscillation. This discovery has firmly established that neutrinos are massive and thus new physics beyond the Standard Model (SM). Moreover this discovery has marked the beginning of many neutrino oscillation experiments. Furthermore, the neutrino oscillation data accumulated over many years allowed us to determine the solar and atmospheric neutrino oscillation parameters with very high precision. Thereafter, with the exciting discoveries of non-zero reactor mixing angle (θ_{13}) and non-maximal atmospheric mixing angle (θ_{23}), the focus of neutrino oscillation studies has been shifted towards the determination of other unknown parameters. These include the determination of mass hierarchy, octant of the atmospheric mixing angle θ_{23}, discovery of CP violation and the magnitude of the CP violating phase δ_{CP}. The main physics goal of current as well as future generation long baseline experiments is to unravel these unknowns in the neutrino oscillation sector. These experiments will take long time to collect the whole oscillation data. However, the phenomenological studies can make predictions on the sensitivity of these experiments, which ultimately help to extract improved oscillation data. In this regard, this thesis presents phenomenological studies towards unravelling the current unknowns in neutrino sector by looking at the sensitivity of current (T2K and NOνA) and future (T2HK and DUNE) generation long baseline experiments. As Neutrino Physics entered into precision era, it is crucial to understand the effect of sub-leading contributions such as non-standard interactions (NSIs) of neutrinos on the discovery potential of long-baseline neutrino oscillation experiments. In this regard, this thesis also presents a study on effect of lepton flavor violating propagation NSIs on the sensitivities of long baseline experiments in both model independent and model dependent approaches.

Contents

CHAPTER 1

Introduction

Neutrinos are the second most abundant elementary particles in the universe that were first created just after the Big Bang. They are always being created in the stars, supernovae and even on earth through the nuclear reactions. Hence, they can be found throughout our galaxy. Moreover, a hundred trillions of neutrinos are passing through our body in every second and we never even notice them. This elusive nature of neutrinos made them as least understood particles, though they are abundant in nature. Just before a couple of decades, scientists have found out that these particles do posses masses which completely conflicts the very well established theory of particle physics so called Standard Model (SM). Consequently, neutrino can be used as probe to understand the new physics beyond the SM and the mystery of the universe.

1.1 Brief History of Neutrinos

The idea of neutrino was born in 1930, when W. Pauli proposed a new particle in order to explain the continuous energy spectrum of electrons in beta decay process, which was discovered by Chadwick in 1914. Pauli was trying to find the source of missing energy in beta decay and as a result he introduced an electrically neutral and light fermion which participates only in weak interactions. He called this particle as neutron. Postulating a particle with low evidence for existence lead him to make the

statement “I have done a terrible thing. I have postulated a particle that can not be detected”. A while later, Fermi renamed this mysterious particle as neutrino (Italian meaning “the little neutral one”) in his theory of weak interaction in 1934.

In 1956, Reines and Cowan came up with an astonishing experiment, which could detect the antiparticle of neutrino [1–4]. They were looking for signals from inverse beta decay where anti-neutrino that is coming from nuclear reactor combines with proton in the target (water) and create positron and neutron. Thereafter, positron annihilates with an electron and emits photons. The neutron undergoes neutron capture with the cadmium atoms present in the water and emits another photon. The complete process is

$$\bar{\nu_e} + p \rightarrow n + e^+$$
$$e^+ + e^- \rightarrow 2\gamma$$
$$n + Cd^{108} \rightarrow Cd^{109} + \gamma$$

The presence of these photons in the observations are the signatures of neutrino interactions. This is the first reactor neutrino experiment. Later in 1995, Reines was honoured with the Nobel Prize for this work with Cowan in which they detected anti-neutrinos for the first time.

In 1957, Pontecorvo came up with the idea of neutrino oscillation in analogy with $K^\circ - \bar{K^\circ}$ mixing. However, during that period of time only one type of neutrino (ν_e) was known to exist and therefore he suggested the possibility of transition between neutrino and anti-neutrino. Later in 1962, Lederman, Schwartz, and Steinberger together discovered the second type of neutrino, so called muon neutrino and they won the Nobel Prize for this discovery in 1988. Soon after the discovery of muon neutrino, Maki, Nakagawa, and Sakata put forward the concept of mixing of ν_e and ν_μ. The third neutrino flavor ν_τ was discovered in 2000. Thereafter, Super Kamiokande and Subdhury Neutrino Observatory experiments provided the strong evidence for flavor transition of neutrino by looking at atmospheric neutrino and solar neutrino oscillations respectively. And McDonald and Kajita jointly won the Nobel Prize in the year 2015 for this excellent discovery of neutrino oscillation. Moreover, the three

flavor neutrino oscillation has become a complete picture of neutrino flavor transition after the determination of reactor mixing angle by reactor neutrino experiments in 2012 and neutrino physics entered into precision era.

1.2 Neutrinos in the Standard Model

The Standard Model [5–7] of particle physics is a very well established theoretical framework, which describes dynamics of elementary particles. This gauge theory deals with strong, weak and electromagnetic interactions of particles, which are governed by symmetry principle of local gauge invariance with a symmetry group $SU(3)_C \times SU(2)_L \times U(1)_Y$, where C, L and Y represent colour, left-handed chirality and hypercharge respectively. The strong, weak and electromagnetic interactions of particles in the SM are mediated by vector bosons, i.e., 8 gluons, $W^{\pm}$ and Z° bosons, and photon respectively. The fermions in the SM divided into quarks and leptons and they are of three generations as given in Table 1.2.1. The matter content of this model is listed in Table 1.2.2. Unlike other fermions, neutrino is a chargeless massless particle, which interacts only through weak force.

Generations	Quarks		Leptons	
I^{st}	u (up)	d (down)	ν_e (electron neutrino)	e (electron)
II^{nd}	c (charm)	s (strange)	ν_μ (muon neutrino)	μ (muon)
III^{rd}	t (top)	b (bottom)	ν_τ (tau neutrino)	τ (tau)

Table 1.2.1: The three generations of fermions in SM.

Particle	Notation	$SU(3)_C$	$SU(2)_L$	$U(1)_Y$	$U(1)_{em}$
Quarks	$Q_{1L} = \begin{pmatrix} u \\ d \end{pmatrix}_L$	3	2	1/6	$\begin{pmatrix} 2/3 \\ -1/3 \end{pmatrix}$
	$q_{uR} = u_R$	3	1	2/3	2/3
	$q_{dR} = d_R$	3	1	$-1/3$	$-1/3$
Leptons	$L_{eL} = \begin{pmatrix} \nu_e \\ e \end{pmatrix}_L$	1	2	$-1/2$	$\begin{pmatrix} 0 \\ -1 \end{pmatrix}$
	$l_{eR} = e_R$	1	1	-1	-1

Table 1.2.2: The weak isospin and hypercharge of leptons and quarks in SM.

The local gauge invariance is the basic principle on which SM is built. The local gauge

invariance of fermion field, which is described by the Lagrangian

$$\mathcal{L} = i\bar{\psi}\gamma^{\mu}\partial_{\mu}\psi - m\bar{\psi}\psi, \tag{1.2.1}$$

under the local phase transformation $\psi \rightarrow \psi' = e^{i\alpha(x)Q}\psi$, demands the interaction with a bosonic field A_{μ}, and this bosonic field has to transform as $A_{\mu} \rightarrow A_{\mu} + \frac{1}{e}\partial_{\alpha}$. This in turn gives rise to the Lagrangian for electromagnetic interaction,

$$\mathcal{L}_{QED} = \bar{\psi}(i\gamma^{\mu}\partial_{\mu} - m)\psi - e\bar{\psi}\gamma^{\mu}Q\psi A_{\mu} - \frac{1}{4}F_{\mu\nu}F^{\mu\nu}. \tag{1.2.2}$$

where $F_{\mu\nu} = \partial_{\mu}A_{\nu} - \partial_{\nu}A_{\mu}$. Now defining a covariant derivative $D_{\mu} = \partial_{\mu} - ieA_{\mu}$, the above equation becomes

$$\mathcal{L}_{QED} = \bar{\psi}(i\gamma^{\mu}D_{\mu} - m)\psi - \frac{1}{4}F_{\mu\nu}F^{\mu\nu}. \tag{1.2.3}$$

This is the local gauge invariant Lagrangian for electromagnetic interaction. It should also be noted that the addition of mass term for the boson A_{μ} is prohibited due to local gauge invariance, i.e, the term $\frac{1}{2}m^2A_{\mu}A^{\mu}$ is not invariant under the local gauge transformation. In a similar fashion, one can write the Lagrangian for strong interaction mediated by massless gauge boson as

$$\begin{aligned}\mathcal{L}_{QCD} &= \bar{q}(i\gamma^{\mu}\partial_{\mu} - m)q - g(\bar{q}\gamma^{\mu}T_a q)G^a_{\mu} - \frac{1}{4}G^a_{\mu\nu}G^{\mu\nu}_a \\ &= \bar{q}(i\gamma^{\mu}D_{\mu} - m)q - \frac{1}{4}G^a_{\mu\nu}G^{\mu\nu}_a \end{aligned} \tag{1.2.4}$$

where the quark q and bosonic field G^a_{μ} transform under the local phase transformation as

$$q \rightarrow e^{i\alpha_a(x)T_a}q \quad as \quad G^a_{\mu} \rightarrow G^a_{\mu} - \frac{1}{g}\partial_{\mu}\alpha_a - f_{abc}\alpha_b G^c_{\mu}.$$

Here T_a with $a = 1, 2, \cdots 8$ are the generators of $SU(3)_C$ symmetry group. The commutation relation of these generators is given by

$$[T_a, T_b] = if_{abc}T_c. \tag{1.2.5}$$

The covariant derivative is given by

$$D_{\mu} = \partial_{\mu} + igT_a G^a_{\mu}, \tag{1.2.6}$$

and the field strength tensor is given by

$$G^a_{\mu\nu} = \partial_\mu G^a_\nu - \partial_\nu G^a_\mu - g f_{abc} G^b_\mu G^c_\nu. \tag{1.2.7}$$

However, in the case of weak interaction it is impossible to construct a Lagrangian in this method, since the weak interaction is mediated by the massive gauge bosons $W^\pm$ ($W^\pm = \frac{1}{\sqrt{2}}(W^1 \pm iW^2)$), Z^0. As a solution for this, Glashow, Weinberg, and Salam came up with an idea of unification of electromagnetic and weak interaction, the so called electro-weak interaction. This gauge theory, which describes the electromagnetic and weak interactions on the same footing, is called Glashow-Weinberg-Salam model. It is based on the gauge group $SU(2)_L \times U(1)_Y$. The weak gauge bosons obtain masses by the spontaneous symmetry breaking of gauge group $SU(2)_L \times U(1)_Y$ into a symmetry group $U(1)_{em}$ through Higgs mechanism. The following subsection discusses about Higgs mechanism by which fermions and bosons in the SM get masses.

1.2.1 Higgs mechanism

The most effective way of the generation of mass of a particle by spontaneous symmetry breaking (SSB) is called Higgs mechanism. To understand this mechanism, let us consider a scalar field ϕ described by the Lagrangian

$$\mathcal{L}_\phi = \frac{1}{2}(\partial_\mu \phi)^2 - \left(\frac{1}{2}\mu^2\phi^2 - \frac{1}{4}\lambda\phi^4\right), \tag{1.2.8}$$

with $\lambda > 0$. This Lagrangian has a reflection symmetry, i.e., this Lagrangian is invariant under the transformation of $\phi \to -\phi$. To find the ground state of this field, one has to minimize the potential. The minimization conditions are $\frac{\partial V(\phi)}{\partial \phi} = 0$ and $\frac{\partial^2 V(\phi)}{\partial \phi^2}$ must be positive. The first derivative gives possible values of ground state as

$$\begin{aligned} \frac{\partial V(\phi)}{\partial \phi} &= \phi(\mu^2 + \lambda\phi^2) = 0, \\ \implies \phi &= 0 \quad \text{or} \quad \phi = \pm\sqrt{\frac{-\mu}{\lambda}} = \pm v. \end{aligned}$$

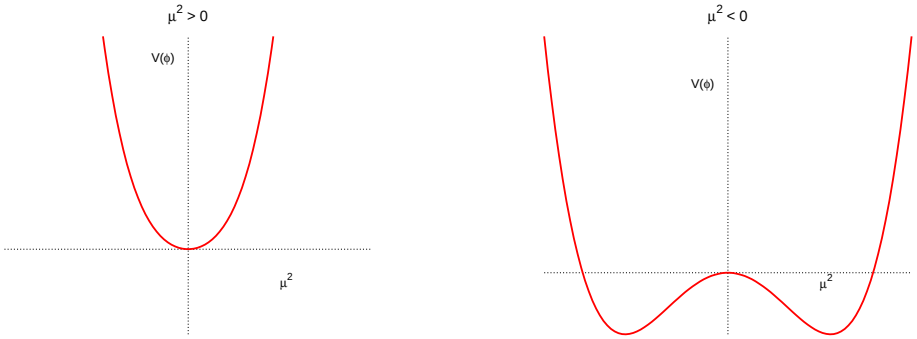

Figure 1.2.1: Higgs potential for two cases:i) $\mu^2 > 0$ is in left panel and ii) $\mu^2 < 0$ is in right panel.

Now the second derivative yields the actual minimum as

$$\frac{\partial^2 V(\phi)}{\partial \phi^2} = \mu^2 + 3\lambda\phi^2,$$
$$\text{for} \quad \phi = 0, \quad \frac{\partial^2 V(\phi)}{\partial \phi^2} = \mu^2 \quad \text{and}$$
$$\text{for} \quad \phi = \pm v, \quad \frac{\partial^2 V(\phi)}{\partial \phi^2} = -2\mu^2.$$

It should be noted that the parameter μ^2 can be either positive or negative. Therefore, there are two possibilities,

- For $\mu^2 > 0$: In this case the ground state is $\phi = 0$, which also has a reflection symmetry as shown in the left panel of Fig 1.2.1.

- For $\mu^2 < 0$: In this case there is two minima and they are $\phi = \pm v$, which is shown in right panel of the Fig 1.2.1.

The case of current interest is $\mu^2 < 0$, since the choice of ground state (either $\phi = +v$ or $-v$) break the reflection symmetry of the system. The quantum fluctuation around the minimum energy $\phi = +v$ is given by

$$\phi(x) = v + h(x). \tag{1.2.9}$$

Then the Lagrangian is modified as

$$\mathcal{L}' = \frac{1}{2}(\partial_\mu h)^2 - \lambda v^2 h^2 - \lambda v h^3 - \frac{1}{4}\lambda h^4 + ... \tag{1.2.10}$$

The first term in the Lagrangian corresponds to kinetic energy, the second term corresponds to mass and other terms correspond to self interaction. Thus, obtained a physical field h with mass $m_h = \sqrt{2\lambda v^2} = \sqrt{-2\mu^2}$ by spontaneously breaking the reflection symmetry of Lagrangian of an unphysical field ϕ. This is called Higgs mechanism. More details of Higgs mechanism can be seen in [8].

Gauge boson mass generation

The Higgs mechanism describes an elegant way to generate the mass for the elementary particle by breaking the electro-weak symmetry of the SM. The $SU(2)_L \times U(1)_Y$ invariant electro-weak Lagrangian is given by [8]

$$\begin{aligned} \mathcal{L}_{EW} &= \bar{L}_L \gamma^\mu \left[i\partial_\mu - g\frac{\tau}{2}.W_\mu - g'\frac{Y}{2}B_\mu \right] L_L \\ &+ \bar{e}_R \gamma^\mu \left[i\partial_\mu - g'\frac{Y}{2}B_\mu \right] e_R - \frac{1}{4}W_{\mu\nu}.W^{\mu\nu} - \frac{1}{4}B_{\mu\nu}B^{\mu\nu}, \end{aligned} \tag{1.2.11}$$

i.e., this Lagrangian is invariant under the local phase transformation of field $\psi \rightarrow e^{i\alpha(x)(T_3+\frac{Y}{2})}\psi$ where T_3 and Y are the generators of the symmetric group $SU(2)_L \times U(1)_Y$. The gauge field W_μ transform as $W_\mu \rightarrow W_\mu - \frac{1}{g}\partial_\mu\alpha - \alpha \times W_\mu$. The field tensors are given by

$$\begin{aligned} W_{\mu\nu} &= \partial_\mu W_\nu - \partial_\nu W_\mu - gW_\mu \times W_\nu, \\ B_{\mu\nu} &= \partial_\mu B_\nu - \partial_\nu B_\mu. \end{aligned} \tag{1.2.12}$$

In order to formulate the Higgs mechanism in such way that the weak bosons become massive and photon remains massless, one should add a scalar field, whose $SU(2)_L \times U(1)_Y$ gauge invariant Lagrangian is given by

$$\mathcal{L}_{scalar} = \left| \left(i\partial_\mu - gT.W_\mu - g'\frac{Y}{2}B_\mu \right) \phi \right|^2 - \underbrace{\left(\mu^2\phi^\dagger\phi + \lambda(\phi^\dagger\phi)^2 \right)}_{V(\phi)}, \tag{1.2.13}$$

where ϕ is an isospin doublet with weak hypercharge $Y = 1$ and it is of the form

$$\phi = \begin{bmatrix} \phi^+ \\ \phi^0 \end{bmatrix},$$

with $\phi^+ = (\phi_1 + i\phi_2)/\sqrt{2}$ and $\phi^0 = (\phi_3 + i\phi_4)/\sqrt{2}$. The Higgs potential $V(\phi)$ with $\mu^2 < 0$ and $\lambda > 0$ can be used to generate the mass for gauge bosons in a similar fashion as discussed earlier. One can choose the vacuum alignment of Higgs field in such a way that it breaks both $SU(2)_L$ and $U(1)_Y$ symmetry, and conserve $U(1)_{em}$ symmetry. Therefore, the best choice is field with $T = \frac{1}{2}$, $T_3 = -\frac{1}{2}$, and $Y = 1$. The fluctuation around v is given by

$$\phi = \frac{1}{\sqrt{2}} \begin{bmatrix} 0 \\ v + h(x) \end{bmatrix},$$

where $h(x)$ is the physical Higgs field. The expansion of Higgs potential upto second order in h^2 yields

$$V = V_0 + \frac{\mu^2}{2}(2vh + h^2) + \frac{\lambda}{4}(4v^3h + 6v^2h^2). \tag{1.2.14}$$

The coefficient of h^2 is the mass of the physical Higgs field, i.e., $M_h^2 = 2\lambda v^2 \implies M_h = \sqrt{2}\mu$, whereas other terms are the interaction terms of the Higgs field. The relevant term in the Lagrangian responsible for boson masses after the spontaneous symmetry breaking is given by

$$\begin{aligned}
\left|\left(i\partial_\mu - gT.W_\mu - g'\frac{Y}{2}B_\mu\right)\phi\right|^2 &= \frac{1}{8}\left|\begin{pmatrix} gW_\mu^3 + g'B_\mu & g(W_\mu^1 - iW_\mu^2) \\ g(W_\mu^1 + iW_\mu^2) & -gW_\mu^3 + g'B_\mu \end{pmatrix}\begin{pmatrix} 0 \\ v \end{pmatrix}\right|^2 \\
&= \frac{1}{4}v^2g^2\underbrace{\frac{1}{4}\left[\left(W_\mu^1\right)^2 + \left(W_\mu^2\right)^2\right]}_{W_\mu^+W^{-\mu}} + \frac{1}{8}v^2\overbrace{\left[gW_\mu^3 - g'B_\mu\right]^2}^{(g^2+g'^2)Z_\mu^2} + 0\underbrace{\left[g'W_\mu^3 + gB_\mu\right]^2}_{(g^2+g'^2)A_\mu^2}.
\end{aligned}$$

A comparison of the mass terms of gauge bosons yields

$$\begin{aligned}
&M_W^2W_\mu^+W^{-\mu} = \frac{1}{8}v^2g^2W_\mu^+W^{-\mu} \quad \implies \quad M_W = \frac{1}{2}vg, \\
&\frac{1}{2}M_Z^2Z_\mu^2 = \frac{1}{8}v^2(g^2 + g'^2)Z_\mu^2 \quad \implies \quad M_Z = \frac{1}{2}v\sqrt{g^2 + g'^2}, \\
&\frac{1}{2}M_A^2A_\mu^2 = 0A_\mu^2 \quad \implies \quad M_A = 0.
\end{aligned} \tag{1.2.15}$$

This is how weak gauge bosons in the SM get mass through the spontaneous symmetry breaking in the Higgs sector. In addition to this, from the relation between the Fermi coupling constant ($G = 1.16638 \times 10^{-5} GeV^{-2}$) and mass of the W boson, one can fix

the value of v as

$$\frac{G}{\sqrt{2}} = \frac{g^2}{8M_W^2} = \frac{1}{2v^2} \quad \Longrightarrow \quad v^2 = \frac{1}{\sqrt{2}G} \quad \Longrightarrow v \approx 246\ GeV. \tag{1.2.16}$$

Therefore, the vacuum expectation value of Higgs field in the SM is $\frac{v}{\sqrt{2}} = 174\ GeV$.

Fermion mass generation

The fermions in the SM get mass through the Yukawa interaction of fermion with Higgs field. The relevant $SU(2)_L \times U(1)_Y$ gauge invariant term in the Lagrangian to generate the mass for an electron is given by

$$\mathcal{L}_e = -G_e \left[\begin{pmatrix} \bar{\nu_e} & \bar{e} \end{pmatrix}_L \begin{pmatrix} \phi^+ \\ \phi^0 \end{pmatrix} e_R + \bar{e}_R \begin{pmatrix} \phi^- & \bar{\phi^0} \end{pmatrix} \begin{pmatrix} \nu_e \\ e \end{pmatrix}_L \right]. \tag{1.2.17}$$

The Lagrangian after the spontaneous symmetry breaking of Higgs field is given by

$$\begin{aligned} \mathcal{L}_e &= -\frac{G_e}{\sqrt{2}} v \left(\bar{e}_L e_R + \bar{e}_R e_L\right) \\ &= -m_e \bar{e} e \qquad \Longrightarrow \qquad m_e = \frac{G_e v}{\sqrt{2}}. \end{aligned} \tag{1.2.18}$$

In a similar way, one can generate mass for down quark, whereas to generate mass for up quark one has to construct a new Higgs doublet from ϕ such that up on SSB it should transform as

$$\tilde{\phi} = -i\tau_2 \phi^* = \begin{pmatrix} -\bar{\phi^0} \\ \phi^- \end{pmatrix} \rightarrow \frac{1}{\sqrt{2}} \begin{pmatrix} v \\ 0 \end{pmatrix}. \tag{1.2.19}$$

The relevent term in the Lagrangian is

$$\mathcal{L}_q = -G_d \begin{pmatrix} \bar{u} & \bar{d} \end{pmatrix}_L \begin{pmatrix} \phi^+ \\ \phi^0 \end{pmatrix} d_R - G_u \begin{pmatrix} \bar{u} & \bar{d} \end{pmatrix}_L \begin{pmatrix} -\bar{\phi^0} \\ \phi^- \end{pmatrix} u_R + h.c. \tag{1.2.20}$$

After the spontaneous symmetry breaking the above Lagrangian becomes

$$\mathcal{L}_q = -m_d \bar{d} d - m_u \bar{u} u. \tag{1.2.21}$$

This is how the fermions in the SM get their masses via Higgs mechanism. It is also to note that neutrino mass can not be generated in this way, since right handed neutrinos are absent in the SM. A discussion on the neutrino mass is given in next subsection.

1.2.2 Dirac and Majorana mass of neutrino

The fermions in the SM can have Dirac or Majorana mass. If a massive fermion is electrically charged then the charge conservation allows only Dirac type mass for such fermion. This is simply because of the structure of Dirac and Majorana mass terms, which are respectively given as

$$-\mathcal{L}_D = m_D \bar{\psi}\psi \quad \text{and} \tag{1.2.22}$$

$$-\mathcal{L}_M = m_M \bar{\psi^c}\psi, \tag{1.2.23}$$

where m_D is Dirac mass, m_M is Majorana mass, and ψ^c is the charge conjugate field. The fermion field consists of both left ($\psi_L = \frac{1}{2}(1-\gamma^5)\psi$) and right ($\psi_R = \frac{1}{2}(1-\gamma^5)\psi$) chiral projections. Therefore, the mass terms can be written as

$$-\mathcal{L}_D = m_D \bar{\psi_L}\psi_R + h.c \quad \text{and} \tag{1.2.24}$$

$$-\mathcal{L}_M = m_M \bar{\psi_L^c}\psi_L + h.c. \tag{1.2.25}$$

However, right handed neutrino and left handed anti-neutrino are absent in the SM. Therefore, neutrino can not have a Dirac mass term within the SM. Moreover, neutrino cannot have a Majorana mass term since it violates lepton number conservation, which is an accidental symmetry of the SM. In summary, the SM neutrinos do not have mass due to the following reasons:

- ν_R is absent in the SM.

- SM is a re-normalizable theory, in which interactions are described by dimension $d \leq 4$ operators.

Next section is mainly focussing on the various extensions of SM by which one can incorporate the observed neutrino mass.

1.3 Neutrinos Beyond Standard Model (BSM)

Although SM is a quite successful theory in describing particles and their interactions, it could not accommodate both Dark Matter (DM) and massive Neutrinos. This implies that SM is not the ultimate theory of particle physics and there should be New Physics beyond SM. Moreover, there are many other fundamental problems for which SM does not provide any satisfactory answer.

1.3.1 Neutrino mass and mixing

Neutrinos are considered as massless particles in the SM. However, the discovery of the phenomenon of flavour transition of neutrinos, the so called neutrino oscillation, which is a consequence of neutrino mixing, shows that neutrinos are massive particles. Therefore, one should find a mechanism to generate the masses for the neutrinos. In an effective Lagrangian approach, the New Physics effect can be parametrized at low energies by adding effective operators with dimension d>4 to SM Lagrangian as

$$\begin{aligned} \mathcal{L} &= \mathcal{L}_{SM} + \mathcal{L}_{eff}^{d=5} + \mathcal{L}_{eff}^{d=6} + ... \\ &= \mathcal{L}_{SM} + \sum_{n=5}^{\infty} \sum_{i} \left(\frac{C_i^n}{\Lambda^{n-4}} \mathcal{O}_i^n + h.c. \right) \end{aligned} \tag{1.3.1}$$

where C_i^n are coupling constants and Λ is the scale of New Physics. The operators ($\mathcal{O}^n$) are invariant under the SM gauge group. This approach is valid only if the new particles are much heavier than M_W (the electroweak scale). If the energy transfer E and the mass of new particle M much less than Λ then the effect of higher dimensional operators ($\mathcal{O}^n$) are suppressed by the powers of $\frac{E}{\Lambda}$ or $\frac{M}{\Lambda}$, which implies that the effect of New Physics is dominated by lowest dimension operator. The only possible operator at the lowest order in the expansion is the dimension five operator so-called Weinberg operator [9]

$$\mathcal{O}^{d=5} = \mathcal{O}^w = \left(\bar{L^c} \tilde{\phi}^* \right) \left(\tilde{\phi}^\dagger L \right) \tag{1.3.2}$$

This operator leads to Majorana masses of neutrino via spontaneous symmetry breaking (SSB) in the Higgs sector. At tree level, Weinberg operator can only be mediated

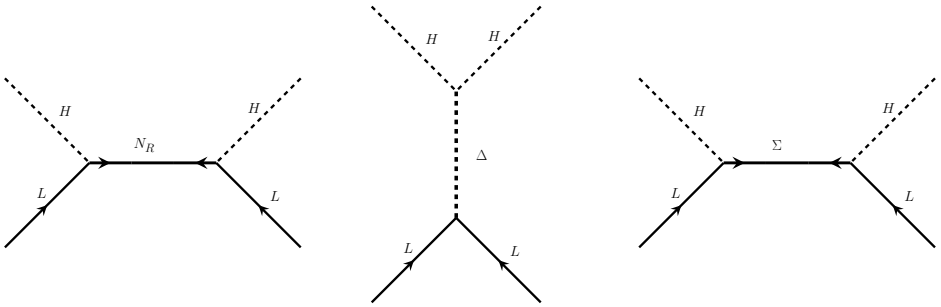

Figure 1.3.1: The generic realizations of seesaw mechanisms: type I is on the left, type II in the middle and type III on the right.

by a singlet fermion, a triplet scalar, or a triplet fermion [10–15]. This kind of most natural and viable mechanism of mass generation of neutrino is called seesaw mechanism [16–19]. As its name suggest, in this framework smallness of neutrino mass is explained by adding heavy particle to the SM. These mechanisms are of three types:

- Type I seesaw: Addition of singlet right handed neutrinos (ν_R) to SM.
- Type II seesaw: Addition of extra higgs triplet to SM.
- Type III seesaw: Addition of fermion triplet to SM.

Apart from these mass models, there are many other models, so called radiative neutrino mass models in which neutrino gets mass through loop corrections such as Zee model [21], Zee-Babu model [22], Ma model [23] etc. One of the interesting feature of these kind of mass models, is the prediction of mass of new particle within the reach of present or future experiments. However, this section discusses only about the seesaw models.

1.3.2 Seesaw mechanisms

Type I seesaw mechanism

The neutrino mass in Type I seesaw mechanism is generated at tree level by exchange of heavy $SU(2)_L \times U(1)_Y$ singlet right handed neutrino N_R. The most general gauge invariant renormalizable Lagrangian in this model is given by

$$\mathcal{L} = \mathcal{L}_{SM} + \mathcal{L}_{N_R}, \tag{1.3.3}$$

where new physics Lagrangian $\mathcal{L}_{N_R}$ is given by

$$\mathcal{L}_{N_R} = \overbrace{i\bar{N}_R \not{\partial} N_R}^{Kinetic\ term} - \underbrace{\left(\bar{L}_{lL}\tilde{\phi} Y_\nu N_R + h.c\right)}_{Yukawa\ interaction\ term} - \frac{Y_\nu}{\Lambda}\overbrace{(\bar{L^c}\tilde{\phi}^*)(\tilde{\phi}^\dagger L)}^{Weinberg\ operator} \tag{1.3.4}$$

where $\tilde{\phi} = i\tau_2\phi^*$ and Y_ν is the Yukawa coupling constant. Note that the covariant derivative D_μ is reduced to partial derivative ∂_μ, since the new field N_R is color and $SU(2)$ singlet with hyper charge zero. The Yukawa interaction term in the above equation gives rise to Dirac mass of neutrino via spontaneous symmetry breaking of Higgs field at electro weak scale, whereas the last term gives rise to Majorana mass of neutrino. Therefore, after symmetry breaking the gauge invariant Lagrangian mass term is given by

$$-\mathcal{L}_{mass} = \frac{1}{2}\left[M_D \bar{\nu}_L N_R + M_D \bar{N}^c_R \nu^c_L + M_m \bar{N}^c_R N_R + h.c.\right], \tag{1.3.5}$$

where the Dirac mass $M_D = \frac{Y_\nu v}{\sqrt{2}}$ and Majorana mass $M_m = \frac{Y_\nu^2 v^2}{2\Lambda}$. One can write the Lagrangian given above in a matrix form as

$$-\mathcal{L}_{mass} = \tfrac{1}{2}\begin{bmatrix} \bar{\nu}_L & \bar{N}^c_R \end{bmatrix}\begin{bmatrix} 0 & M_D \\ M_D^T & M_m \end{bmatrix}\begin{bmatrix} \nu^c_L \\ N_R \end{bmatrix} + h.c.$$

Then the neutrino mass matrix is given by

$$M_\nu = \begin{bmatrix} 0 & M_D \\ M_D^T & M_m \end{bmatrix}$$

Where M_D and M_m are $N \times N$ matrices for N generations of fermions. Then the neutrino mass matrix can be obtained by the block diagonalisation of mass matrix M_ν as in [24] and it is given by

$$M_\nu = -M_D^T M_R^{-1} M_D \tag{1.3.6}$$

This is known as Type I seesaw formula. For single generation (N=1), the mass matrix is

$$M_\nu = \begin{bmatrix} 0 & M \\ M & B \end{bmatrix}$$

where M is the Dirac mass and B is the Majorana mass. In this case M and B are just numbers and the mass matrix can be diagonalised by a rotation matrix

$$O = \begin{bmatrix} \cos\theta & -\sin\theta \\ \sin\theta & \cos\theta \end{bmatrix},$$

with $\tan 2\theta = 2M/B$. Then neutrino mass matrix is

$$m_\nu = O M_\nu O^T = \begin{bmatrix} -m_1 & 0 \\ 0 & m_2 \end{bmatrix},$$

which is a diagonal matrix with $m_{1,2} = \frac{1}{2}\left(\mp B + \sqrt{B^2 + 4M^2}\right)$. The diagonal elements in the neutrino matrix is negative which cannot be interpreted as a mass of physical fields. In order to make the diagonal matrix positive, one can rewrite the neutrino mass matrix as

$$m_\nu = \begin{bmatrix} -m_1 & 0 \\ 0 & m2 \end{bmatrix} = \begin{bmatrix} m_1 & 0 \\ 0 & m_2 \end{bmatrix} \begin{bmatrix} -1 & 0 \\ 0 & 1 \end{bmatrix} = mK^2,$$

which indicates that $M_\nu = O^T m K^2 O$. Suppose $B >> M$, then $m_1 \approx \frac{M^2}{B}$ and $m_2 \approx B$, which implies that $m_1 << M$. This way of explaining the lightness of left handed neutrino by making the right handed neutrino field too heavy is called seesaw mechanism.

Type II seesaw mechanism

The type II seesaw model contains a scalar triplet so-called Higgs triplet Δ with a hypercharge $Y = -2$ in addition to the SM Higgs doublet ϕ. In this mechanism, the Majorana mass of neutrino is generated by the spontaneous symmetry breaking in Higgs sector and the $SU(2)_L$ adjoint representation of Higgs triplet is

$$\Delta = \frac{\sigma_i \Delta_i}{\sqrt{2}} = \begin{bmatrix} \frac{\Delta^+}{\sqrt{2}} & \Delta^{++} \\ \Delta^0 & -\frac{\Delta^+}{\sqrt{2}} \end{bmatrix},$$

where $\Delta^{++} = \frac{(\Delta_1 - i\Delta_2)}{\sqrt{2}}$ and $\Delta^0 = \frac{(\Delta_1 + i\Delta_2)}{\sqrt{2}}$. The relevant term in Yukawa interaction Lagrangian is

$$\mathcal{L}_{Y_\Delta} = Y_\Delta \bar{L_L^c} i\tau_2 \Delta L_L + h.c. \tag{1.3.7}$$

This term yields the Majorana mass for neutrino by the spontaneous symmetry breaking of Higgs triplet, whose vacuum alignment is

$$\Delta = \begin{bmatrix} 0 & 0 \\ \frac{v_2}{\sqrt{2}} & 0 \end{bmatrix}.$$

This vacuum expectation value can be determined by the minimization of Higgs potential

$$V(\phi, \Delta) \;=\; m_\phi^2 \phi^\dagger \phi + M_\Delta^2 \Delta^\dagger \Delta + \frac{1}{2}\lambda_1 \left(\phi^\dagger \phi\right)^2 + \frac{1}{2}\lambda_2 \left(\Delta^\dagger \Delta\right)^2 + \lambda_3 \left(\phi^\dagger \phi\right)\left(\Delta^\dagger \Delta\right) + ..$$

Now arranging the parameters in the potential in such way that the vevs of Higgs fields at minimum

$$\langle \phi_0 \rangle = \frac{v_1}{\sqrt{2}}, \qquad \langle \Delta_0 \rangle = \frac{v_2}{\sqrt{2}}. \tag{1.3.8}$$

The spontaneous symmetry breaking yields the Majorana mass of neutrino as

$$M_\nu = \frac{v_2}{\sqrt{2}} Y_\Delta \tag{1.3.9}$$

The diagonalization of this mass matrix yeilds the neutrino masses. It is also note that Higgs triplet also couples to weak gauge bosons (W and Z). Therefore, the mass

of the gauge boson in this model is given by

$$\begin{aligned} M_W^2 &= \frac{1}{4}g^2\left(v_1^2+2v_2^2\right), \\ M_Z^2 &= \frac{1}{4}\left(g^2+g'^2\right)\left(v_1^2+4v_2^2\right), \\ \rho &= \frac{M_W^2}{M_Z^2\cos^2\theta_W} = \frac{1+2v_2^2/v_1^2}{1+4v_2^2/v_1^2}. \end{aligned}$$

Now using the experimental bounds on ρ parameter ($\rho = 0.998 \pm 0.0086$) one can obtain $\frac{v_2^2}{v_1^2} < 0.07$. Therefore, to explain the smallness of neutrino mass compare with corresponding charged lepton partner, the v_2 must be very smaller than its upper limit.

Type III seesaw mechanism

In type III seesaw mechanism, a triplet fermion Σ_R is added to SM. This fermion is singlet under $U(1)_Y$ and triplet under $SU(2)_L$, whose $SU(2)_L$ adjoint representation is given by

$$\Sigma_R = \begin{bmatrix} \frac{\Sigma_R^0}{\sqrt{2}} & \Sigma_R^+ \\ \Sigma_R^- & -\frac{\Sigma_R^0}{\sqrt{2}} \end{bmatrix},$$

where $\Sigma_R^{\pm} = \frac{(\Sigma_{R1} \mp i\Sigma_{R2})}{\sqrt{2}}$. Addition of this field introduces new terms in the Lagrangian. After the spontaneous breaking of gauge symmetry the SM higgs boson achieves a vev $\frac{v}{\sqrt{2}}$ and the Majorana mass of neutrino is given by

$$M_\nu = \frac{1}{2}Y_\Sigma \frac{v^2}{M_\Sigma} Y_\Sigma^T \tag{1.3.10}$$

From the above equation, it is clear that the smallness of neutrino mass is depend up on the mass of new field M_Σ. In this way of generation of mass of neutrino is called Type III seesaw mechanism.

1.3.3 Neutrinoless double beta decay

The discovery of neutrino oscillation, which shows neutrinos are massive particles, boosted the importance of neutrinoless double beta decay ($0\nu\beta\beta$). This section

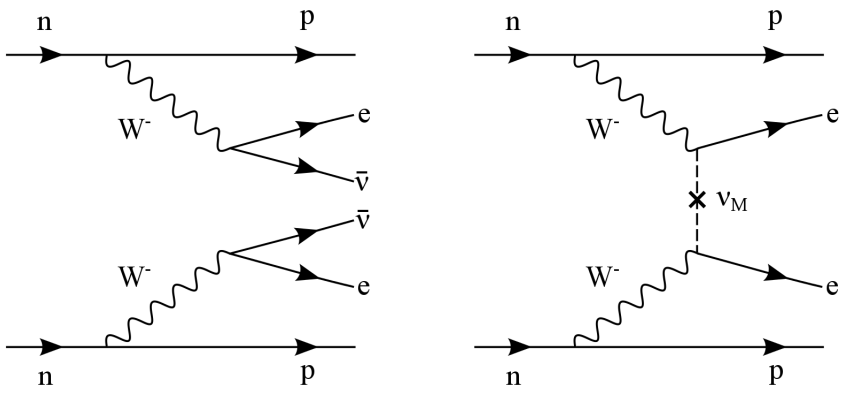

Figure 1.3.2: Feynman diagram for $2\nu\beta\beta$ process in the left panel and the $0\nu\beta\beta$ process in the right panel.

discusses the main features of neutrinoless double beta decay.

So far, there is no compelling evidence for the Majorana nature of neutrino. However, one can check whether neutrino is its own antiparticle by looking at the double beta decay process, where the created anti-neutrino in one beta decay process is annihilated and initiate the second beta beta decay process as shown in Fig. 1.3.2. The double beta decay process without the emission of neutrinos is called neutrinoless double beta decay. The life time of this process related to the effective Majorana neutrino mass, which is given by

$$\langle m_\nu \rangle = |\sum_k U_{ek}^2 m_k| = |\sum_k |U_{ek}|^2 m_k e^{i\alpha_k}|, \tag{1.3.11}$$

where m_k is neutrino mass, U_{ek} is the first row elements of neutrino mixing matrix so-called PMNS matrix, and α_k is the CP violating Majorana phase. The above equation can be rewritten in terms of three parameters m_{min} and the two Majorana phases, where $m_{min} = m_1$ for Normal mass Hierarchy ($m_1 < m_2 << m_3$) and $m_{min} = m_3$ for Inverted mass Hierarchy ($m_1 > m_2 >> m_3$). It is important to note that the observation of neutrinoless double beta decay process not only indicates that neutrino is a Majorana particle but also it indicates that the lepton number is not a fundamental symmetry of nature i.e, physics beyond the SM.

1.4 Outline of Thesis

The phenomenon of neutrino oscillation is the first ever confirmed new physics beyond the SM. The ultimate aim of the theories and experiments which are mainly focussing

on neutrinos is to construct a theoretical model which can explain both observed neutrino masses and lepton mixing pattern. Such a theoretical formulation requires the best knowledge of neutrino oscillation parameters especially neutrino mass hierarchy, octant of θ_{23}, and CP violating phase δ_{CP}. In other words, the theoretical models which predict wrong hierarchy, wrong octant or wrong CP phase can be ruled out. The long baseline neutrino oscillation experiments are capable of determining all these unknowns in neutrino sector. Though these experiments will take long time to collect the whole oscillation data, phenomenological studies can make predictions on the sensitivity of these experiments, which ultimately help to extract improved oscillation data. The main focus of this thesis is to unravel the unknowns in the neutrino oscillation sector by studying the sensitivities of long baseline experiment.

Chapter 2 of this thesis comprises all about the theory of neutrino oscillation, neutrino oscillation experiments and the current status of neutrino oscillation parameters. Further, chapter 3 presents a study towards extracting the best possible results from the NuMI Off-Axis ν_e Appearance (NOνA) experiment. Chapter 4 discusses a comprehensive study of the discovery potential of NOνA, T2K and T2HK experiments. The impact of Non-standard neutrino interactions (NSIs), which can be considered as sub-leading effects in neutrino oscillation, on the physics potential of long baseline experiments are discussed in chapter 5. Finally, the summary and conclusions of the entire thesis work and the future scope of research in this direction are discussed in chapter 6.

CHAPTER 2

Theory of neutrino oscillation

The phenomenon of flavor transition of neutrino from one to other as it propagates is called neutrino oscillation. This quantum mechanical phenomenon clearly shows that neutrino flavor state is not equal to mass eigenstate nevertheless it is a linear superposition of mass eigenstates. Therefore, neutrino state of definite flavor α is related to neutrino state of definite mass m_k as

$$|\nu_\alpha\rangle = \sum_{k=1}^{n} U_{\alpha k} |\nu_k\rangle , \tag{2.0.1}$$

where $|\nu_k\rangle$ is the mass eigenstate, n is the number of neutrinos and U is the unitary $n \times n$ mixing matrix, which is also known as Pontecorvo-Maki-Nakagawa-Sakata (PMNS) matrix. Neutrino is always produced as a flavor state along with its corresponding charged lepton through weak interactions. Moreover, there are three flavors of neutrino in SM namely electron neutrino (ν_e), muon neutrino (ν_μ) and tau neutrino (ν_τ). The charged current interaction Lagrangian of SM neutrino in flavor basis is given by

$$\begin{aligned} -\mathcal{L}_{CC} &= \frac{g}{2\sqrt{2}} \bar{l}_\alpha \gamma^\mu \left(1 - \gamma^5\right) \nu_\alpha W_\mu^- + h.c, \\ &= \frac{g}{\sqrt{2}} \bar{l}_{\alpha L} \gamma^\mu \nu_{\alpha L} W_\mu^- + h.c, \end{aligned}$$

where, g is the coupling strength. If there exists mixing of charged leptons $\left(l_{\alpha L} = \sum_i U^l_{\alpha i} l_{iL}\right)$ and neutral leptons ($\nu_{\alpha L} = \sum_k U^\nu_{\alpha k} \nu_{kL}$) then the Lagrangian in the mass basis becomes

$$\begin{aligned} -\mathcal{L}_{CC} &= \frac{g}{\sqrt{2}} \sum_i \sum_k \bar{l}_{iL} \left(U^l_{\alpha i}\right)^\dagger U^\nu_{\alpha k} \gamma^\mu \nu_{kL} W^-_\mu + h.c, \\ &= \frac{g}{\sqrt{2}} \sum_i \sum_k \bar{l}_{iL} \left(U_{PMNS}\right)_{ik} \gamma^\mu \nu_{kL} W^-_\mu + h.c, \end{aligned}$$

where $U_{PMNS} = \left(U^l\right)^\dagger U^\nu$ is the lepton mixing matrix. In the case of charged lepton the mass eigenstate is equal to its flavor state, which indicates that U^l is a unit matrix. Therefore, the matrix U_{PMNS} has only contribution coming from neutrino sector and it is known as neutrino mixing matrix. As time evolves, neutrino can change its flavor from one to other since its mass eigenstates evolve differently. Therefore, neutrino oscillation can be considered as a consequence of neutrino mixing. Many neutrino experiments have provided the strong evidences for oscillations of neutrinos and oscillation data imply that neutrino has nonzero mass and neutrino flavors mix with each other. This chapter discusses all about the theory of neutrino oscillation, its evidence, the various neutrino experiments, and the current status of neutrino oscillation parameter.

2.1 Neutrino oscillation in vacuum

This section starts with a derivation of generalised expression for oscillation probability in vacuum and it is followed by a discussion on vacuum oscillation in both two flavor and three flavor framework.

As neutrino propagates through vacuum, it is not bounded by any kind of potential and free to move. Therefore, the evolution equation of mass eigenstate (ν_k) is given by Schrödinger equation [25]

$$i\frac{d}{dt}\left|\nu_k\right\rangle = H\left|\nu_k\right\rangle = E_k\left|\nu_k\right\rangle, \tag{2.1.1}$$

where H is the Hamiltonian and $E_k = \sqrt{m_k^2 + p^2}$ is the energy of neutrinos with mass

m_k and momentum p. The solution of this plane wave equation is given by

$$|\nu_k(t)\rangle = e^{-iE_k t}\,|\nu_k(0)\rangle\,, \tag{2.1.2}$$

The corresponding evolution equation in flavor basis is given by

$$\begin{aligned} |\nu_\alpha(t)\rangle &= \sum_{k=1}^{n} U_{\alpha k} e^{-iE_k t}\,|\nu_k(0)\rangle \\ &= \sum_{k=1}^{n} U_{\alpha k} e^{-iE_k t} \sum_{\beta=e,\mu,\tau} U^*_{\beta k}\,|\nu_\beta(0)\rangle \\ &= \sum_{\beta=e,\mu,\tau} \sum_{k=1}^{n} U_{\alpha k} U^*_{\beta k} e^{-iE_k t}\,|\nu_\beta(0)\rangle\,. \end{aligned} \tag{2.1.3}$$

The amplitude of the flavor transition of neutrino from $\nu_\alpha \to \nu_\beta$ can be obtained as

$$A_{\nu_\alpha \to \nu_\beta}(t) \equiv \langle \nu_\beta \,|\, \nu_\alpha(t)\rangle = \sum_{k=1}^{n} U_{\alpha k} U^*_{\beta k} e^{-iE_k t}. \tag{2.1.4}$$

Therefore, the transition probability of neutrino from an initial flavor α to a final flavor β is given by

$$\begin{aligned} P_{\nu_\alpha \to \nu_\beta}(t) &= |A_{\nu_\alpha \to \nu_\beta}(t)|^2 \\ &= \sum_{k=1}^{n}\sum_{l=1}^{n} U_{\alpha k} U^*_{\beta k} U^*_{\alpha l} U_{\beta l} e^{-i(E_k - E_l)t} \\ &= \sum_{k=1}^{n}\sum_{l=1}^{n} U_{\alpha k} U_{\beta l} U^*_{\alpha l} U^*_{\beta k} e^{-i(E_k - E_l)t}. \end{aligned} \tag{2.1.5}$$

The energy of neutrino in the exponential term can be written as

$$\begin{aligned} E_k &= \sqrt{p^2 + m_k^2} = p\sqrt{1 + \frac{m_k^2}{p^2}} \\ &= p\Big(1 + \frac{m_k^2}{2p^2}\Big) = p + \frac{m_k^2}{2p}. \end{aligned} \tag{2.1.6}$$

Since the speed of neutrino is very close to speed of light, neutrino can be considered as an ultra relativistic particle. Moreover, the time (t) taken to travel is equal to the distance (L) travelled by the neutrino, i.e., $t = L$. Further, one can assume that the momentum of all neutrinos are the same and $|\vec{p}| \simeq E$. Then the exponential part of

Eqn (2.1.5) can be written as

$$\begin{aligned}(E_k - E_l)t &\simeq \Big(p + \frac{m_k^2}{2p} - (p + \frac{m_l^2}{2p}))L \\ &= \big(\frac{m_k^2 - m_l^2}{2p}\big)L \\ &= \frac{\Delta m_{kl}^2 L}{2E}. \end{aligned} \tag{2.1.7}$$

Therefore, the oscillation probability can be rewritten in terms of oscillation length L and neutrino energy E as

$$\begin{aligned}P_{\nu_\alpha \to \nu_\beta}(L,E) &= \sum_{k=1}^{n}\sum_{l=1}^{n} U_{\alpha k}U_{\beta l}U_{\alpha l}^* U_{\beta k}^* e^{-i\frac{\Delta m_{kl}^2 L}{2E}} \\ &= \sum_{k=l}^{n} |U_{\alpha k}|^2 |U_{\beta k}|^2 + \sum_{k=1}^{n}\sum_{l=1}^{n} U_{\alpha k}U_{\beta l}U_{\alpha l}^* U_{\beta k}^* e^{-i\frac{\Delta m_{kl}^2 L}{2E}}. \end{aligned} \tag{2.1.8}$$

It is very well known that

$$|\sum_{k=1}^{n} U_{\alpha k}U_{\beta k}^*|^2 = \sum_{k=l}^{n} |U_{\alpha k}|^2 |U_{\beta k}|^2 + \sum_{k\neq l}^{n} U_{\alpha k}U_{\beta l}U_{\alpha l}^* U_{\beta k}^* \tag{2.1.9}$$

and from unitarity relation

$$\sum_{k=1}^{n} U_{\alpha k}U_{\beta k}^* = \delta_{\alpha\beta} \tag{2.1.10}$$

Therefore Eqn (2.1.8) becomes

$$\begin{aligned}P_{\nu_\alpha \to \nu_\beta}(L,E) &= \delta_{\alpha\beta} - \sum_{k\neq l}^{n} U_{\alpha k}U_{\beta l}U_{\alpha l}^* U_{\beta k}^* + \sum_{k\neq l}^{n} U_{\alpha k}U_{\beta l}U_{\alpha l}^* U_{\beta k}^* e^{-i\frac{\Delta m_{kl}^2 L}{2E}} \\ &= \delta_{\alpha\beta} - \Big[\sum_{k<l}^{n} U_{\alpha k}U_{\beta l}U_{\alpha l}^* U_{\beta k}^* + \sum_{k<l}^{n} U_{\alpha k}^* U_{\beta l}^* U_{\alpha l}U_{\beta k}\Big] \\ &+ \Big[\sum_{k<l}^{n} U_{\alpha k}U_{\beta l}U_{\alpha l}^* U_{\beta k}^* e^{-i\frac{\Delta m_{kl}^2 L}{2E}} + \sum_{k<l}^{n} U_{\alpha k}^* U_{\beta l}^* U_{\alpha l}U_{\beta k} e^{i\frac{\Delta m_{kl}^2 L}{2E}}\Big]. \end{aligned}$$

Now using the properties of a complex number z ($z + z^* = 2\Re(z)$ and $z - z^* = 2\Im(z)$) and the Euler identity ($e^{i\theta} = \cos\theta + i\sin\theta$) the above equation can be written as

$$\begin{aligned}P_{\nu_\alpha \to \nu_\beta}(L,E) &= \delta_{\alpha\beta} - 2\sum_{k<l}^{n} \Re(U_{\alpha k}U_{\beta l}U_{\alpha l}^* U_{\beta k}^*) + 2\sum_{k<l}^{n} \Re(U_{\alpha k}U_{\beta l}U_{\alpha l}^* U_{\beta k}^*)\cos\left(\frac{\Delta m_{kl}^2 L}{2E}\right) \\ &+ 2\sum_{k<l}^{n} \Im(U_{\alpha k}U_{\beta l}U_{\alpha l}^* U_{\beta k}^*)\sin\left(\frac{\Delta m_{kl}^2 L}{2E}\right) \\ &= \delta_{\alpha\beta} - 2\sum_{k<l}^{n} \Re(U_{\alpha k}U_{\beta l}U_{\alpha l}^* U_{\beta k}^*)\left(1 - \cos\left(\frac{\Delta m_{kl}^2 L}{2E}\right)\right) \\ &+ 2\sum_{k<l}^{n} \Im(U_{\alpha k}U_{\beta l}U_{\alpha l}^* U_{\beta k}^*)\sin\left(\frac{\Delta m_{kl}^2 L}{2E}\right). \end{aligned}$$

The final expression of oscillation probability is given by

$$P_{\nu_\alpha \to \nu_\beta}(L,E) = \delta_{\alpha\beta} \quad - \quad 4\sum_{k<l}^{n} \Re(U_{\alpha k}U_{\beta l}U^*_{\alpha l}U^*_{\beta k}) \sin^2\left(\frac{\Delta m^2_{kl}L}{4E}\right) + \quad 2\sum_{k<l}^{n} \Im(U_{\alpha k}U_{\beta l}U^*_{\alpha l}U^*_{\beta k}) \sin\left(\frac{\Delta m^2_{kl}L}{2E}\right). \tag{2.1.11}$$

The anti-neutrino oscillation probability can be obtained by simply replacing U by U^*. In the case of survival probability $\alpha = \beta$ which implies that $U_{\alpha i}U^*_{\alpha i}U^*_{\alpha j}U_{\alpha j} = |U_{\alpha i}|^2|U_{\alpha j}|^2$ is real quantity and the last term in Eqn (2.1.11) becomes zero. Therefore, the expression of survival probability is given by

$$P_{\nu_\alpha \to \nu_\alpha}(L,E) = 1 \quad - \quad 4\sum_{k>l} |U_{\alpha k}|^2|U_{\alpha l}|^2 \sin^2\left(\frac{\Delta m^2_{kl}L}{4E}\right). \tag{2.1.12}$$

It should be noted that to happen neutrino oscillation, some of the non diagonal elements of PMNS matrix must be non-zero and neutrino masses should be non-degenerate i.e, the flavor state of neutrino must be a different superposition of its mass eigenstates with definite mass. If neutrinos are massless particles, then $\Delta m_{kl} = 0$ and oscillation probability $P_{\nu_\alpha \to \nu_\beta}(L,E) = \delta_{\alpha\beta}$. This implies that the observation of neutrino oscillation is a direct indication of massive neutrinos. However, neutrino oscillation can not probe the absolute mass of neutrino rather it probes the mass squared differences. In order to observe the effect of neutrino oscillation, the phase $\left(\Delta m^2 \frac{L}{E}\right)$ must be of the order of one. Therefore, the minimum length so called characteristic oscillation length below which neutrino oscillation does not develop is given by $L_{osc} \approx E/\Delta m^2$. However, if the baseline L (distance between source and detector) is too much greater than the characteristic oscillation length then one can observe only the average effect on the oscillation probability i.e, for $L >> L_{osc}$ the term in oscillation probability $\sin^2(\frac{\Delta m^2_{kl}L}{4E})$ averages out into half. A detailed discussion on this topic can be seen in the following subsections which cover all about two and three flavor oscillation of neutrinos in vacuum.

2.1.1 Two flavor neutrino oscillation

To understand flavor transition of neutrino in a simple way, one can consider the mixing of two neutrino flavors ($n = 2$), for example: ν_e and ν_μ mixing. In this case,

the mixing matrix is nothing but a orthogonal rotation matrix, which is parametrised by a mixing angle θ. Therefore, the mixing of neutrino flavor states can be represented as

$$\begin{pmatrix} \nu_e \\ \nu_\mu \end{pmatrix} = \begin{pmatrix} \cos\theta & \sin\theta \\ -\sin\theta & \cos\theta \end{pmatrix} \begin{pmatrix} \nu_1 \\ \nu_2 \end{pmatrix} \tag{2.1.13}$$

The transition probability of two flavor neutrino oscillation is given by

$$\begin{aligned} P_{\nu_e \to \nu_\mu} &= -4\Re(U_{e1}U_{\mu 2}U^*_{e2}U^*_{\mu 2}) \sin^2\left(\frac{\Delta m^2_{kl} L}{4E}\right) \\ &= 4\cos^2\theta \sin^2\theta \sin^2\left(\frac{\Delta m^2_{kl} L}{4E}\right) \\ &= \sin^2 2\theta \sin^2\left(\frac{\Delta m^2 L}{4E}\right), \end{aligned} \tag{2.1.14}$$

whereas, the survival probability is given by

$$\begin{aligned} P_{\nu_e \to \nu_e} &= 1 - P_{\nu_e \to \nu_\mu} \\ &= 1 - \sin^2 2\theta \sin^2\left(\frac{\Delta m^2 L}{4E}\right). \end{aligned} \tag{2.1.15}$$

This expression for probability is in natural unit (i.e, $c = \hbar = 1$), in which no one bother about the units of the quantities in the phase part. While reinserting the Planck constant ($\hbar$) and the velocity of light (c) in the phase part yields

$$\sin^2\left(\frac{\Delta m^2 L}{4E}\right) \implies \sin^2\left(\frac{\Delta m^2 c^3 L}{4\hbar E}\right). \tag{2.1.16}$$

If Δm^2 is measured in eV^2, E is in GeV and L is in kilometer, then the phase part becomes

$$\sin^2\left(\frac{\Delta m^2 c^3 L}{4\hbar E}\right) = \sin^2\left(1.27\frac{\Delta m^2 L}{E}\right). \tag{2.1.17}$$

Therefore, the oscillation probability equations becomes

$$P_{\nu_e \to \nu_\mu} = \sin^2 2\theta \sin^2\left(1.27\frac{\Delta m^2 L}{E}\right) \quad \text{and} \tag{2.1.18}$$

$$P_{\nu_e \to \nu_e} = 1 - \sin^2 2\theta \sin^2\left(1.27\frac{\Delta m^2 L}{E}\right). \tag{2.1.19}$$

The following points can be inferred from the equations 2.1.18 and 2.1.19

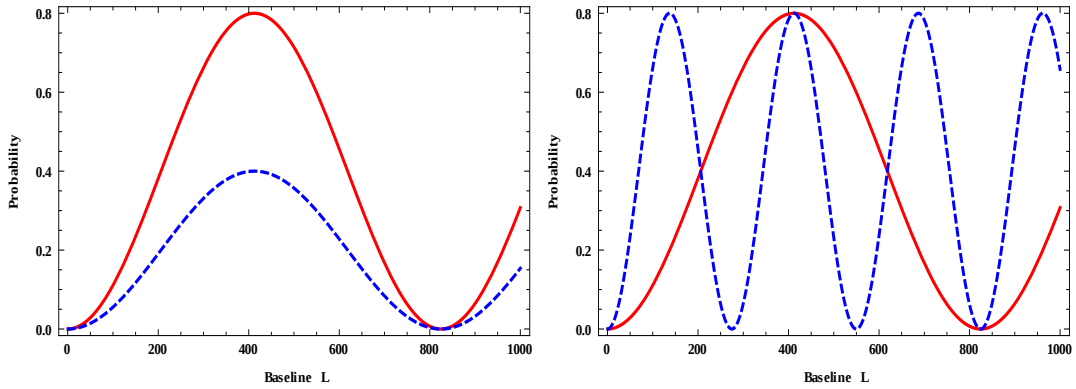

Figure 2.1.1: The transition probability as a function of baseline (L) for different values of mixing angle: $\sin^2 2\theta = 0.8$ (red solid curve) and $\sin^2 2\theta = 0.4$ (blue dashed curve) with $E = 1\text{GeV}$ and $\Delta m^2 = 3 \times 10^{-3}\text{eV}^2$ is given in the left panel. Whereas, the transition probability as a function of baseline (L) for different mass splitting: $\Delta m^2 = 3 \times 10^{-3}\text{eV}^2$ (red solid curve) or $\Delta m^2 = 9 \times 10^{-3}\text{eV}^2$ (blue dashed curve) with $E = 1\text{GeV}$ and $\sin^2 2\theta = 0.8$ is given in the right panel.

- **The mixing angle** θ: The parameter which gives idea about how the flavor state of neutrino different from mass eigenstate. If $\theta = 0$, then mass eigenstate is same as the flavor state. Therefore, for neutrino oscillation has to happen θ must be non-zero. Also note that the amplitude of neutrino oscillation is controlled by the mixing angle θ. As the value of $\sin^2 2\theta$ increases the amplitude of oscillation increases as one can see from the left panel of Fig 2.1.1.

- **Mass squared difference** Δm^2: It is clear that for neutrino oscillation to happen the mass of neutrino states must be non-degenerate i.e., $\Delta m^2 = m_2^2 - m_1^2 \neq 0$. The frequency of neutrino oscillation is controlled by this parameter. For a large value of Δm^2, the frequency of oscillation is large as one can see from the right panel of Fig 2.1.1.

- **L/E**: The pattern of neutrino oscillation is depend on the ratio of distance travelled by the neutrino and its energy (L/E). This is the parameter which can be controlled by an experimentalist to study the phenomenon of neutrino oscillation. The experiment which designed to look at transition probability should satisfy the condition

$$\begin{aligned} 1.27\Delta m^2 \frac{L}{E} &= \frac{\pi}{2}, \\ \implies \frac{L}{E} &= \frac{\pi}{2.54\Delta m^2}. \end{aligned} \tag{2.1.20}$$

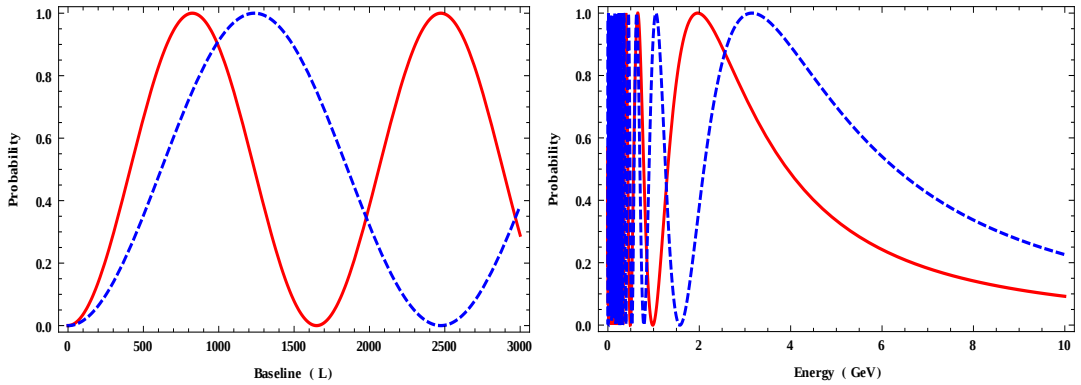

Figure 2.1.2: The transition probability as a function of baseline (L) for $\Delta m^2 = 3 \times 10^{-3} eV^2$, $\theta = \frac{\pi}{4}$, and $E = 2GeV$ (solid red curve) or $E = 3GeV$ (dashed blue curve) is given in the left panel. Whereas, the transition probability as a function of neutrino energy (E) for $\Delta m^2 = 3 \times 10^{-3} eV^2$, $\theta = \frac{\pi}{4}$, and $L = 810km$ (red solid curve) or $L = 1300km$ (blue dashed curve) is given in the right panel.

From the above equation, it is clear that one can probe very small Δm^2 by fixing $\frac{L}{E}$ of an experiment. It can be easily understood from the Fig 2.1.2 that to observe the maximum transition probability, the baseline of the experiment is set to $L \approx 800km$ ($\approx 1300km$), if the energy of neutrino beam is 2GeV (3GeV). Therefore, it is better to control the baseline L for a fixed energy E as it is very difficult to generate neutrino with high energy. However, in reality the neutrino beam has a spread out just as electric field from a point source, therefore one needs a detector with surface area L^2.

- **Types of Experiments**: The neutrino oscillation experiment is looking for either the appearance (transition probability) of a new flavor or the disappearance (survival probability) of the same flavor of neutrino that present at the source. Suppose the flavor of neutrino at the source is ν_α,

  1. ν_β appearance experiment: The experiment which is looking for the oscillation $P_{\nu_\alpha \to \nu_\beta}|_{\alpha \neq \beta}$, i.e, this experiment looking for appearance events of ν_β neutrinos at the detector which are coming from a ν_α neutrino beam.
  2. ν_α disappearance experiment: The experiment which is looking for the oscillation $P_{\nu_\alpha \to \nu_\alpha} = 1 - P_{\nu_\alpha \to \nu_\beta}$ is called the disappearance experiments, i.e, this experiment looking for disappearance events of ν_α neutrinos at the detector, which are coming from a ν_α neutrino beam.

The transition probability and survival probability as a function of baseline are given

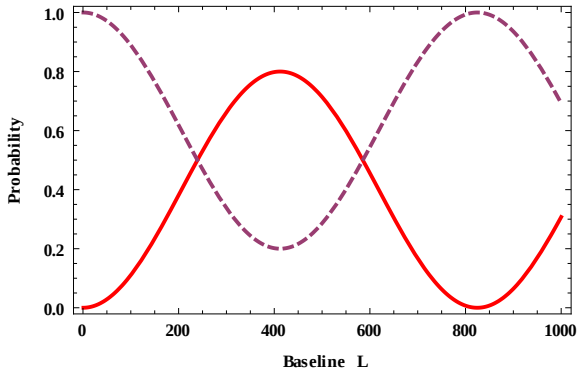

Figure 2.1.3: The transition probability (solid line) and survival probability (dashed line) as a function of baseline L with oscillation parameters $\sin^2 2\theta = 0.8, \Delta m^2 = 3 \times 10^{-3} eV^2$, and energy $E = 1GeV$.

in the Fig. 2.1.3. From the figure, one can see that at the source i.e, L=0, there exist only one type of neutrino say ν_e and as L increases the transition oscillation probability increases and reach a point where oscillation becomes maximum ($1.27\frac{\Delta m^2 L}{E} = \pi/2$ with $L = 400km$). At this point almost 80% of initial ν_e converted into ν_μ. As baseline increase further, the transition probability decreases and around $L = 800km$ all the neutrinos become ν_e. However, in general neutrino source is not mono-energetic beam, therefore the oscillation probability should be averaged over the energy spectrum.

2.1.2 Three flavor neutrino oscillation

This subsection is discussing about the mixing of three neutrino flavors, ν_e, ν_μ and ν_τ. In this case, the mixing matrix is a unitary 3×3 matrix. The mixing of three flavor neutrino can be represented as

$$\begin{pmatrix} \nu_e \\ \nu_\mu \\ \nu_\tau \end{pmatrix} = \begin{pmatrix} U_{e1} & U_{e2} & U_{e3} \\ U_{\mu 1} & U_{\mu 2} & U_{\mu 3} \\ U_{\tau 1} & U_{\tau 2} & U_{\tau 3} \end{pmatrix} \begin{pmatrix} \nu_1 \\ \nu_2 \\ \nu_3 \end{pmatrix}, \tag{2.1.21}$$

where U is the three flavor neutrino mixing matrix.

Parametrisation of PMNS matrix: Any general $n \times n$ unitary matrix has n^2 independent parameters. Out of these parameters, $\frac{n(n-1)}{2}$ are angles and $\frac{n(n+1)}{2}$ are phases. All these phases are not physical because one can reabsorb $(2n-1)$ phases in to $2n$ fields (n generations of fermions have n charged lepton fields and n neutrino fileds) in the Lagrangian. Finally, there left $\frac{(n-1)(n-2)}{2}$ phases. Therefore, the PMNS

matrix for three generations of neutrinos can be parametrised by three mixing angles (θ_{12}, θ_{13} and θ_{23}) and one phase so called Dirac CP violating phase (δ_{CP}). The standard parametrisation of PMNS matrix [26] is given by

$$\begin{aligned} U_{\text{PMNS}} &= R(\theta_{23})R(\theta_{13},\delta)R(\theta_{12}) \\ &= \begin{pmatrix} c_{12}c_{13} & s_{12}c_{13} & s_{13}e^{-i\delta} \\ -s_{12}c_{23} - c_{12}s_{23}s_{13}e^{i\delta} & c_{12}c_{23} - s_{12}s_{23}s_{13}e^{i\delta} & s_{23}c_{13} \\ s_{12}s_{23} - c_{12}c_{23}s_{13}e^{i\delta} & -c_{12}s_{23} - s_{12}c_{23}s_{13}e^{i\delta} & c_{23}c_{13} \end{pmatrix}, \end{aligned} \quad (2.1.22)$$

where $s_{ij} \equiv \sin\theta_{ij}$, $c_{ij} \equiv \cos\theta_{ij}$, the matrix $R(\theta_{ij})$ is the rotation matrix in the $ij-$plane and the rotation matrix $R(\theta_{ij},\delta)$ includes the CP-violating phase. Then the oscillation probability is given by

$$\begin{aligned} P_{\nu_\alpha\to\nu_\beta}(L,E) = \delta_{\alpha\beta} &- 4\sum_{k<l}^{3} \Re(U_{\alpha k}U_{\beta l}U^*_{\alpha l}U^*_{\beta k}) \sin^2\left(\frac{\Delta m^2_{kl}L}{4E}\right) \\ &+ 2\sum_{k<l}^{3} \Im(U_{\alpha k}U_{\beta l}U^*_{\alpha l}U^*_{\beta k}) \sin\left(\frac{\Delta m^2_{kl}L}{2E}\right). \end{aligned} \quad (2.1.23)$$

It should be noted from the above equation that the last term is depend on the CP violating phase δ_{CP}. The three flavor neutrino oscillation framework is most successful theoretical model which could accommodate all the observed oscillation data. However, one should also take care of the interaction of neutrino while it is propagating through matter. A discussion on this is given in the next section.

2.2 Neutrino oscillation in matter

As neutrinos propagate through matter, their propagation is significantly modified due to the coherent forward scattering of neutrinos on nucleons (protons and neutrons) and electrons present in the matter. The electron neutrinos (ν_e) can have both Charged Current (CC) and Neutral Current (NC) interactions with electrons present in the matter, whereas the other flavors of neutrinos have only NC interactions. The Feynman diagrams for both CC and NC interactions are given in the Fig. 2.2.1. The NC contributions appear as an effective phase factor and do not affect the oscillation probability. Whereas, the CC contribution comes only from ν_e and it modifies the oscillation probability. This is known as matter effect or Mikheyev Smirnov Wolfenstein (MSW) effect. The Hamiltonian density of CC interaction of electron neutrino on

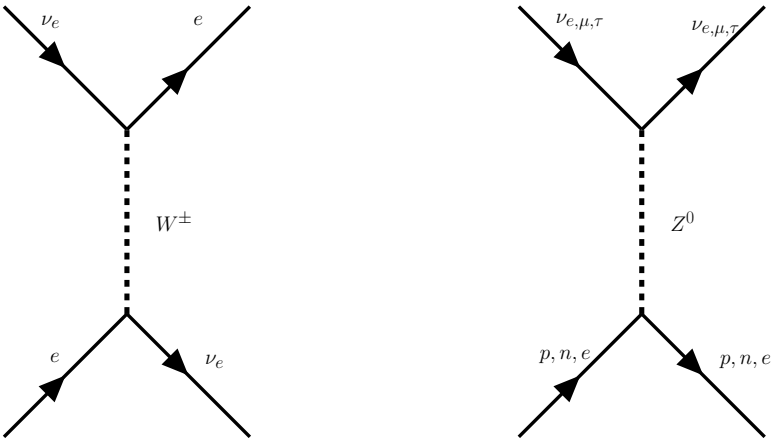

Figure 2.2.1: Feynman diagrams for weak CC and the NC interactions.

matter with Fermi coupling constant G_F and left chiral projection operator $P_L = \frac{(1-\gamma^5)}{2}$ is given by

$$\mathcal{H}_m = \sqrt{2} G_F \left[\bar{e}\gamma_\mu P_L \nu_e\right] \left[\bar{\nu_e}\gamma^\mu P_L e\right]. \tag{2.2.1}$$

The Fierz transformation yields

$$\begin{aligned} \mathcal{H}_m &= \sqrt{2} G_F \left[\bar{e}\gamma_\mu P_L e\right] \left[\bar{\nu_e}\gamma^\mu P_L \nu_e\right], \\ &= \sqrt{2} G_F \left(J_e\right)_\mu \left(J_\nu\right)^\mu. \end{aligned} \tag{2.2.2}$$

The interaction potential can be obtained by taking the average of effective Hamiltonian over the electron background in the matter

$$\mathcal{H}_m = \sqrt{2} G_F \left\langle J_e \right\rangle_\mu \left(J_\nu\right)^\mu. \tag{2.2.3}$$

In the non-relativistic limit, $\left\langle J_e \right\rangle_\mu$ has three components: $\langle \bar{e}\gamma_\mu\gamma^5 e\rangle$ related to spin, $\langle \bar{e}\gamma_i e\rangle$ related to the velocity, and $\langle \bar{e}\gamma_0 e\rangle$ related to electron density. Now assume that the matter is at rest and the medium is unpolarised, then the only nonzero component is the expectation value of electron density, which is given by, $\langle \bar{e}\gamma_0 P_L e\rangle = N_e$. Therefore,

the matter potential can be written as $V_e = \sqrt{2}G_F N_e$ and Hamiltonian becomes

$$\mathcal{H}_m = V_e \left(J_\nu\right)^0 = V_e \left[\bar{\nu_{eL}} \gamma^0 \nu_{eL}\right]. \tag{2.2.4}$$

Now replacing neutrino field with its conjugate field one should get the matter Hamiltonian for anti-neutrino as

$$\begin{aligned}
\mathcal{H}_m &= V_e \left[\bar{\nu_{eL}}^C \gamma^0 \nu_{eL}^C\right], \\
&= V_e \left[\bar{\nu_{eL}}^C \gamma^0 C \bar{\nu}_{eL}^T\right], && \left| \because \nu_{eL}^C = C\bar{\nu}_{eL}^T \right. \\
&= V_e \left[-\nu_{eL}^T C^{-1} \gamma^0 C \bar{\nu}_{eL}^T\right], && \left| \because \bar{\nu}_{eL}^C = -\nu_{eL}^T C^{-1} \right. \\
&= V_e \left[\nu_{eL}^T \left(\gamma^0\right)^T \bar{\nu}_{eL}^T\right], && \left| \because C^{-1}\gamma^0 C = -\left(\gamma^0\right)^T \right. \\
&= -V_e \left[\bar{\nu}_{eL} \gamma^0 \nu_{eL}\right].
\end{aligned} \tag{2.2.5}$$

It should be noted from the above equation that the matter potential for anti-neutrino is negative. In general, matter potential can be either constant or it can vary as the density of electron in the matter varies, for instance inside the Sun the electron density is not a constant. However, this section is mainly focus on the effect of constant matter on neutrino oscillation in a two and three flavor framework.

2.2.1 Two flavor neutrino oscillation in matter

A simple way to understand the role of matter effect on neutrino oscillation is by looking at two flavor oscillation. For simplicity, first of all rewrite the vacuum Hamiltonian in a convenient way. The evolution equation of neutrino mass eigenstate in vacuum is given by

$$i\frac{d}{dt}\left|\nu_i\right\rangle = H\left|\nu_i\right\rangle, \tag{2.2.6}$$

with vacuum Hamiltonian

$$H = \frac{1}{2E}\begin{bmatrix} m_1^2 & 0 \\ 0 & m_2^2 \end{bmatrix}. \tag{2.2.7}$$

One can write the evolution equation in flavor state as

$$i\frac{d}{dt}\left|\nu_\alpha\right\rangle = UHU^\dagger \left|\nu_\alpha\right\rangle. \tag{2.2.8}$$

Therefore, the Hamiltonian in flavor state is given by

$$\begin{aligned} H_f &= UHU^{\dagger}, \\ &= \begin{bmatrix} \cos\theta & \sin\theta \\ -\sin\theta & \cos\theta \end{bmatrix} \begin{bmatrix} \frac{m_1^2}{2E} & 0 \\ 0 & \frac{m_2^2}{2E} \end{bmatrix} \begin{bmatrix} \cos\theta & -\sin\theta \\ \sin\theta & \cos\theta \end{bmatrix}, \\ &= \frac{m_1^2+m_2^2}{4E} I + \frac{\Delta m_{21}^2}{4E} \begin{bmatrix} -\cos 2\theta & \sin 2\theta \\ \sin 2\theta & \cos 2\theta \end{bmatrix}, \\ &= H_0 + \frac{\Delta m^2}{4E} \begin{bmatrix} -\cos 2\theta & \sin 2\theta \\ \sin 2\theta & \cos 2\theta \end{bmatrix}. \end{aligned} \tag{2.2.9}$$

In two flavor framework, the evolution of neutrino state in presence of constant matter density is given by

$$i\frac{\partial}{\partial t}\left|\nu_\alpha\right\rangle = \mathcal{H}_{eff}\left|\nu_\alpha\right\rangle, \tag{2.2.10}$$

where the effective Hamiltonian is given by

$$\mathcal{H}_{eff} = H_f + \begin{pmatrix} V_e & 0 \\ 0 & 0 \end{pmatrix}. \tag{2.2.11}$$

An addition of $diag(-\frac{V_e}{2}, -\frac{V_e}{2})$ to the above Hamiltonian and removal of H_0 from the Hamiltonian do not affect the oscillation probability. Now defining a parameter $A = \pm\frac{2\sqrt{2}G_F N_e E}{\Delta m^2}$ the Hamiltonian becomes

$$\mathcal{H}_{eff} = \left(\frac{\Delta m^2}{4E}\right) \begin{pmatrix} -\cos 2\theta + A & \sin 2\theta \\ \sin 2\theta & \cos 2\theta - A \end{pmatrix}. \tag{2.2.12}$$

The Hamiltonian can be re-diagonalised by using a rotation matrix with mixing angle θ_m. To diagonalise a Hamiltonian of the form

$$H = \begin{bmatrix} A & Be^{iD} \\ Be^{-iD} & C \end{bmatrix}, \tag{2.2.13}$$

one can use a rotation matrix

$$R = \begin{bmatrix} \cos\theta_b & \sin\theta_b e^{iD} \\ -\sin\theta_b e^{-iD} & \cos\theta_b \end{bmatrix}, \tag{2.2.14}$$

with $\tan 2\theta_b = \frac{2B}{C-A}$. Therefore, the diagonalisation of $\mathcal{H}_{eff}$ gives

$$\tan 2\theta_m = \frac{\sin 2\theta}{(\cos 2\theta - A)}. \tag{2.2.15}$$

The final Hamiltonian will be of the form

$$\mathcal{H}_{eff} = \left(\frac{\Delta m^2_m}{4E}\right) \begin{pmatrix} -\cos 2\theta_m & \sin 2\theta_m \\ \sin 2\theta_m & \cos 2\theta_m \end{pmatrix}, \quad \text{and} \tag{2.2.16}$$

the oscillation probability is

$$P(\nu_\mu \to \nu_e) = \sin^2 2\theta_m \sin^2 \left(\frac{\Delta m^2_m L}{4E}\right), \tag{2.2.17}$$

where $\sin 2\theta_m$ and Δm^2_m are the effective mixing angle and the effective mass squared difference in presence of matter and they are given by

$$\begin{aligned} \sin 2\theta_m &= \frac{\sin 2\theta}{\sqrt{(\cos 2\theta - A)^2 + \sin^2 2\theta}} \\ \Delta m^2_m &= \Delta m^2 \sqrt{(\cos 2\theta - A)^2 + \sin^2 2\theta}. \end{aligned} \tag{2.2.18}$$

The consequences of matter effect can be understood from above set of equations and they are followings:

- To observe significant matter effect either long baselines or higher matter density is required. As $V_e \to 0$, the $\Delta m^2_m \to \Delta m^2$ and $\sin^2 2\theta_m \to \sin^2 2\theta$ i.e, vacuum oscillation can be achieved.

- $\sin^2 2\theta = 0 \implies \sin^2 2\theta_m = 0$, then there will not be any oscillation. This indicates that oscillation of neutrino in presence of matter is only possible if there exists vacuum oscillation.

- As $V_e \to \infty$, then $\sin^2 2\theta_m = 0$. This means that neutrino oscillation can not be possible in a very dense medium.

- If $\cos 2\theta = A$, then the mixing angle is always maximal $\sin 2\theta_m = 1$. Therefore, the oscillation probability is significantly enhanced irrespective of the value of vacuum mixing angle (θ). This is known as resonant condition or MSW resonance. Therefore, under the resonant condition, the effective probability can

be enhanced even for a small values of θ. Further, at resonance condition

$$L_{vac} = L_e \cos 2\theta, \tag{2.2.19}$$

where $L_{vac} = \frac{4\pi E}{\Delta m^2}$ is the vacuum oscillation length and $L_e = \frac{4\pi}{2\sqrt{2}G_F N_e}$ is the neutrino-electron interaction length.

- The matter potential V_e changes sign while go from neutrino to anti-neutrino. Therefore, the oscillation probability for neutrino and anti-neutrino are different in presence of matter effect.

- It should be noted that the value of Δm^2_m and $\sin^2 2\theta_m$ are different for different signs of Δm^2. As mentioned earlier, the parameter V_e also changes sign as one go from neutrino to anti-neutrino. For normal hierarchy, $A = 2EV_e$ is positive for neutrino and negative for anti-neutrino. Whereas for inverted hierarchy, A is negative for neutrino and positive for anti-neutrino. Therefore, the matter effect plays crucial role in the determination of neutrino mass hierarchy.

2.2.2 Three flavor neutrino oscillation in matter

This subsection discusses how the presence of matter affect the oscillation probability in three flavor framework. Since it is very difficult to obtain the exact analytical expression of probability in three flavor framework, one should use certain approximation to get the analytical expressions, for instance one mass scale dominance (OMSD) approximation. In three flavor framework, the effective Hamiltonian in presence of matter in the flavor basis is given by

$$\begin{aligned}
\mathcal{H}_{eff} &= \frac{1}{2E} U \begin{bmatrix} m_1^2 & 0 & 0 \\ 0 & m_2^2 & 0 \\ 0 & 0 & m_3^2 \end{bmatrix} U^\dagger + \begin{bmatrix} V_e & 0 & 0 \\ 0 & 0 & 0 \\ 0 & 0 & 0 \end{bmatrix}, \\
&= \frac{1}{2E} U \begin{bmatrix} 0 & 0 & 0 \\ 0 & \Delta m_{21}^2 & 0 \\ 0 & 0 & \Delta m_{31}^2 \end{bmatrix} U^\dagger + \begin{bmatrix} V_e & 0 & 0 \\ 0 & 0 & 0 \\ 0 & 0 & 0 \end{bmatrix},
\end{aligned} \tag{2.2.20}$$

where $\Delta m^2_{ij} = m^2_i - m^2_j$. The experimentally measured value of Δm^2_{21} ($\approx 10^{-5}\text{eV}^2$) is really small while comparing with that of Δm^2_{31} ($\approx 10^{-3}\text{eV}^2$). Therefore, one can neglect the contributions from Δm^2_{21} terms and this is known as the OMSD

approximation. It is also note that the effect of solar mixing angle and CP-violating phase are irrelevant under this approximation. Therefore, the PMNS matrix in the above equation becomes

$$U = \begin{bmatrix} 1 & 0 & 0 \\ 0 & c_{23} & s_{23} \\ 0 & -s_{23} & c_{23} \end{bmatrix} \begin{bmatrix} c_{13} & 0 & s_{13} \\ 0 & 1 & 0 \\ -s_{13} & 0 & c_{13} \end{bmatrix}. \tag{2.2.21}$$

Then the energy eigenvalues of $\mathcal{H}_{eff}$ are given by

$$E_1 = \frac{1}{4E}\left[\Delta m^2_{31} + A + \Delta m^2_{31}\sqrt{(\cos 2\theta_{13} - A)^2 + (\sin 2\theta_{13})^2}\right], \tag{2.2.22}$$

$$E_2 = 0, \tag{2.2.23}$$

$$E_3 = \frac{1}{4E}\left[\Delta m^2_{31} + A - \Delta m^2_{31}\sqrt{(\cos 2\theta_{13} - A)^2 + (\sin 2\theta_{13})^2}\right]. \tag{2.2.24}$$

It can be understood from a qualitative analysis that matter effect only changes the evolution equation of electron neutrino (ν_e) and the mixing of mass eigenstates of ν_e is independent of atmospheric mixing angle θ_{23}. Therefore, the modified mixing matrix in the OMSD approximation will be of the form

$$U_m = R_{23} R^m_{13}. \tag{2.2.25}$$

Moreover, the modified mixing angle θ^m_{13} in terms of the vacuum mixing angle θ_{13} can be obtained as

$$\tan 2\theta^m_{13} = \frac{\sin 2\theta_{13}}{\cos 2\theta_{13} - A}. \tag{2.2.26}$$

Then the oscillation probabilities for $\nu_e \to \nu_\mu$ is given by

$$P(\nu_\mu \to \nu_e) = \sin^2\theta_{23} \sin^2 2\theta^m_{13} \sin^2\left(\frac{\Delta m^m_{31} L}{4E}\right), \tag{2.2.27}$$

where

$$\Delta m^m_{31} = \Delta m^2_{31}\sqrt{(\cos 2\theta_{13} - A)^2 + (\sin 2\theta_{13})^2}. \tag{2.2.28}$$

It should be noted that the OMSD approximation is valid only if $\frac{\Delta m^2_{21} L}{E} \ll 1$, which means that the ratio of the baseline to energy of neutrino must be $L/E \ll 10^4 km/\text{GeV}$. Therefore, this approximation can be used to study the atmospheric neutrinos.

2.3 Evidence of neutrino oscillation

2.3.1 Solar neutrino problem

The Sun is a natural source of electron neutrinos. The fusion reaction of Helium nuclei produces lots of electron neutrinos, whose energies are in few MeV range. The chain reactions that are responsible for electron neutrino production are given in the left panel of Fig. 2.3.1. The Standard Solar Model (SSM), the very well verified theoretical framework based on Helioseismology observations, predicts that most of the electron neutrino flux is coming from the proton- proton chain reactions, which can be easily understood from the neutrino energy spectrum that given in the right panel of Fig 2.3.1. There are several experiments which are indented to measure the solar neutrino flux like Gallium experiment, Chlorine experiments, Super KamiokaNDE and SNO etc. It can be seen from the figure that the Gallium experiment is the most sensitive experiment among all the solar neutrino experiments, which can probe neutrino flux even below 0.4MeV.

John Bachall theoretically calculated the neutrinos flux that are coming from the fusion reactions at Sun based on SSM. However, there was a repeated mismatch between the theoretically predicted and experimentally observed neutrino flux, which is known as Solar neutrino problem. The average neutrino rate obtained by Ray Davi's Homestake experiment was

$$R_{experiment} = 2.56 \pm 0.25 \quad \nu_e \; cm^{-2}s^{-1} \tag{2.3.1}$$

which is well below the theoretically predicted neutrino flux by Bachall,

$$R_{theory} = 8.1 \pm 1.3 \quad \nu_e \; cm^{-2}s^{-1}. \tag{2.3.2}$$

This deficit in the neutrino flux confirmed by a series of solar neutrino experiments such as SAGE at the Baksan Laboratory in Russia and GALLEX based at Gran Sasso. These results lead to the suspicion that the neutrino can oscillate from one flavor to other. Later, this is confirmed by the Super-kamiokande and Subdhury Neutrino Observatory experiments.

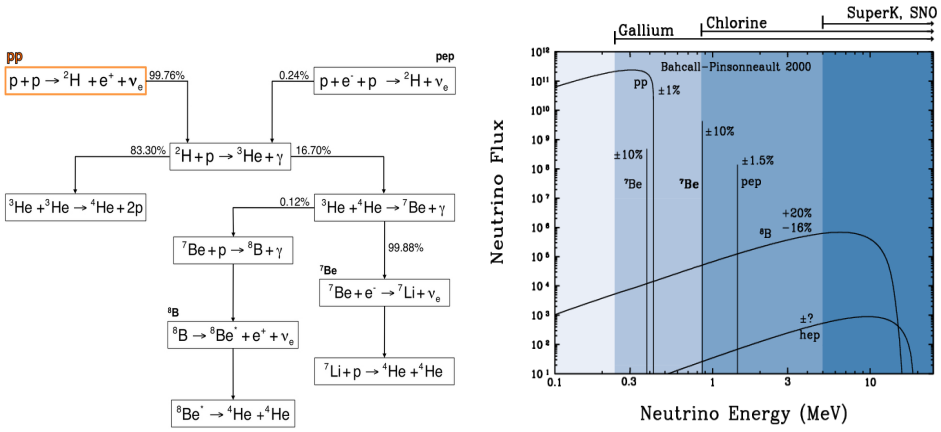

Figure 2.3.1: The chain reactions that produce electron neutrinos are on the left side and the neutrino energy spectrum is on the right side.

2.3.2 Atmospheric neutrino anomaly

The Earth's atmosphere is always being bombarded by cosmic rays which are coming from the outer space. The interaction of these high energy radiation, which composed of high energy protons, electrons, alpha particles and other heavy nuclei, with the atoms in the atmosphere produce a shower of mesons including charged pions. Further, these pions undergo decay and give both electron and muon neutrinos as

$$\pi^+ \rightarrow \mu^+ + \nu_\mu \quad \text{and} \quad \mu^+ \text{ decays as} \quad \mu^+ \rightarrow e^+ + \nu_e + \bar{\nu}_\mu,$$
$$\pi^- \rightarrow \mu^- + \nu_\mu \quad \text{and} \quad \mu^- \text{ decays as} \quad \mu^- \rightarrow e^- + \bar{\nu}_e + \nu_\mu.$$

It should be noted that the decay channel $\pi^+ \rightarrow e^+ + \nu_e$ is chiraly suppressed[1] From the decay pattern of charged pions, one can see that the ratio of number of muon type neutrinos to that of electron type neutrinos in each pion decay is 2. Therefore, if one considers all the interactions, even then the ratio must be

$$R_{theory} = \frac{[N(\nu_\mu) + N(\bar{\nu}_\mu)]}{[N(\nu_e) + N(\bar{\nu}_e)]} = \frac{N_\mu}{N_e} \approx 2. \tag{2.3.3}$$

However, the experimental observations is merely different from what is expected from the theory. In other words, the ratio of number of events $R = \frac{(N_\mu/N_e)_{observed}}{(N_\mu/N_e)_{predicted}}$ is always less than one. This discrepancy in the expected and observed number of

[1]The electron and the electron neutrino are left handed particles whose spins are always in a direction opposite to the direction of their momenta. In the center of mass frame (CM) of pion decay, there is no way of get back pion spin as 1 from these decay products. However, muon is much massive than that of electron.

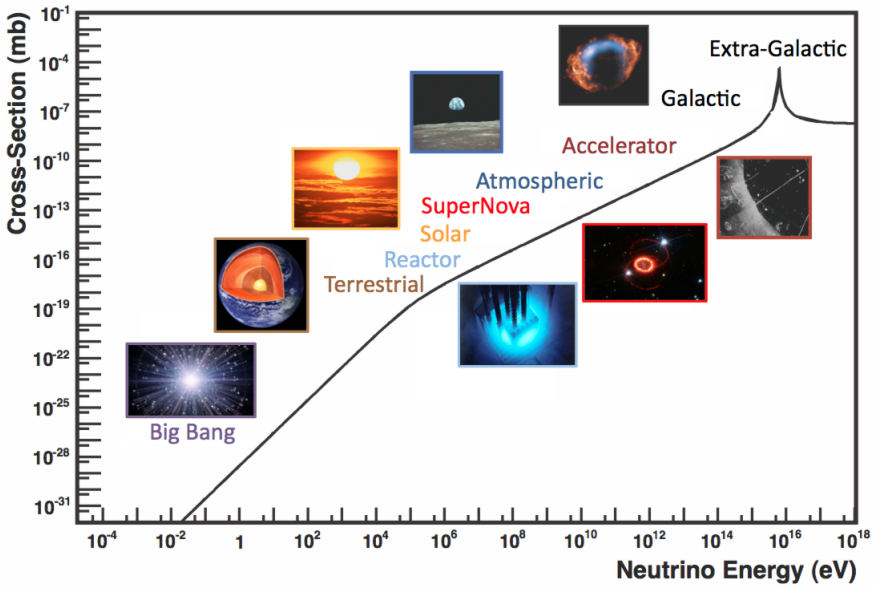

Figure 2.4.1: The neutrino sources with different energies.

neutrino is known as atmospheric neutrino anomaly. This missing of atmospheric neutrinos lead to the suspicion of oscillation of neutrino from one to other flavor. Later, Super-kamiokande obtained the zenith angle distribution of both muon-like and electron-like events. From these results, it is found that the observed electron-like events are well matched with the expectation, whereas observed muon-like events are significantly deviated from that of expected. All these results support the atmospheric neutrino oscillation.

2.4 Neutrino oscillation experiments

Neutrinos are present every where in the universe. All these neutrinos are produced through weak interactions from different sources (natural and man-made sources) with vast range of energies as shown in Fig 2.4.1. Therefore, there used different experimental technique to detect neutrino with different energies. This section discusses the various experiments that are used to study the phenomenon of neutrino oscillation. Each of these experiment probe neutrino with a definite energy range, so one should know all possible interactions of neutrino at the detector to avoid the misleading results. Therefore, this section starts with a brief discussion on neutrino interactions.

Interactions of neutrino at the detector

This subsection discusses about the type of neutrino interactions, which play crucial role in neutrino oscillation experiments. It is not possible to detect neutrinos directly and the detection of neutrino is usually done by looking at the charged lepton produced at the detector through the Charged Current interaction of neutrino with the target materials. Therefore, Neutral Currents are irrelevant for the detection of neutrino unless and until one needs to measure total neutrino flux irrespective of flavours. The interaction of neutrinos:

- **Neutrino-nucleon scattering**: The interaction of neutrino with the nucleon (proton or neutron) in the target is called neutrino-nucleon scattering. This process can be occurred in three different ways depending on the energy of the neutrino and they are:

  - Quasi-elastic scattering (QE) for $E_\nu \approx 1-10$MeV: In this scattering process the nucleon (Nu) converts into its isospin partner (Nu'), i.e.,

$$\nu + Nu \to l^- + Nu' \quad \text{and} \quad \bar{\nu} + Nu \to l^+ + Nu'. \tag{2.4.1}$$

  - Resonance scattering (RES) for $E_\nu \approx 1$GeV: As the name indicates, the nucleon excited to its resonance state in this process, i.e.,

$$\nu + Nu \to l^- + Nu^* \quad \text{and} \quad \bar{\nu} + Nu \to l^+ + Nu^*, \tag{2.4.2}$$

  - Deep inelastic scattering (DIS) for $E_\nu \gg 1GeV$: In this process, neutrino interact with the valence quark present in the nucleon, i.e.,

$$\nu + q \to l^- + X \quad \text{and} \quad \bar{\nu} + q \to l^+ + X. \tag{2.4.3}$$

- **Neutrino-nucleus scattering**: In this process, neutrino interacts with the nucleus (bound state of nucleons) in the target and neutrino excites the parent nucleus present in the detector, i.e.,

$$\nu_e + N(Z, A) \to e^- + N'(Z + 1, A). \tag{2.4.4}$$

- **Neutrino-electron scattering**: In this case electron neutrinos can have both CC and NC interactions, whereas other neutrinos (ν_μ or ν_τ) only have NC interaction, i.e.,

$$\nu_e + e^- \rightarrow \nu_e + e^- \qquad (CC) \tag{2.4.5}$$

$$\nu_x + e^- \rightarrow \nu_x + e^- \qquad (NC). \tag{2.4.6}$$

However,at high energy the interaction cross sections of neutrino-electron scattering is much lesser than that of neutrino-nucleon scattering as one can see from [27].

2.4.1 Solar neutrino experiments

The experiment which is indented to study the electron neutrinos that come from the Sun is known as solar neutrino experiment. They are of two types namely radiochemical and real time experiments.

- Radiochemical experiments:
  The radiochemical experiments make use of neutrino-nucleon scattering to detect the solar neutrino. This interaction converts the nucleus present in the detector to a new nucleus, i.e., $\nu_e + N(Z, A) \rightarrow e^- + N'(Z + 1, A)$ and the total count of those new nuclei (N') give the number of electron neutrino, which can be achieved by looking at the decay products of new nucleus N'. There are different types of radiochemical experiments which are using different target materials in the detector.

  - Chlorine Experiments:
    As the name indicates the target material used in this experiment is Chlorine atoms. The detector of this experiment is filled with tetrachloroetilene. Therefore, the observed reaction in this experiment is

$$\nu_e + Cl^{37} \rightarrow e^- + Ar^{37},$$

    The number of neutrino events are calculated by counting the Argon atoms in the detector. The energy threshold of this experiment is $0.813MeV$

and hence this experiment is less sensitive to Be^7 solar neutrino and more sensitive to B^8 solar neutrinos.

– Gallium experiments:

These experiments use gallium as target material and the corresponding neutrino interaction is

$$\nu_e + Ga^{71} \rightarrow e^- + Ge^{71}.$$

The number of neutrino events are determined by counting the number of germanium atoms produced in the detector. The energy threshold of this experiment is $0.223MeV$ and hence this experiment is mainly looking for neutrinos from proton-proton chain reactions. There are three types of gallium experiments and they are GALLEX, SAGE, and GNO.

- Real time experiments:

These experiments use water as target material and they are looking for the Cherenkov radiation emitted by the fast moving particle produced during the charged current neutrino interaction. These Cherenkov radiations are detected by the photomultipliers placed on the detector surface. The speciality of this kind of detector is that one can identify the flavor of neutrino by looking at the pattern of Cherenkov radiation, i.e, the Cherenkov radiation from a muon yields very well defined circular ring whereas that from a electron gives a fuzzy ring. Hence, a well defined ring in the detector corresponds to muon neutrino event and the fuzzy ring corresponds to electron neutrino event. Moreover, if one uses a magnetised iron detector, then it is possible to identify the charge on the lepton by looking at the path travelled by the particle. Kamiokande, Super-Kamiokande (SK), and Subdhury Neutrino Observatory (SNO) are the some examples of real time neutrino experiments.

– Kamiokande and Super-Kamiokande:

These experiments detect neutrino via neutrino electron scattering process i.e., $\nu_e + e^- \rightarrow \nu_e + e^-$, which indicates that these experiments are only sensitive to electron neutrinos. Moreover, these experiments, which use water as target material, have a energy threshold 7MeV and they are mainly sensitive to B^8 solar neutrinos. The neutrino event rate obtained

by Kamiokande is $\phi(\nu_e) = 2.80 \pm 0.19 \pm 0.33 \ \times 10^6 cm^{-2}s^{-1}$ with ratio $R = \frac{N_{obs}}{N_{SSM}} = 0.50 \pm 0.04 \pm 0.07$. Whereas the event rate for SK is $\phi(\nu_e) = 2.35 \pm 0.02 \pm 0.08 \ \times 10^6 cm^{-2}s^{-1}$ with ratio $R = \frac{N_{obs}}{N_{SSM}} = 0.47 \pm 0.04 \pm 0.014$. Both Kamiokande and SK confirmed the solar neutrino puzzle.

– Sudbury neutrino Observatory (SNO):
The SNO uses 1000 tons heavy water (D_2O) as target material. Further, the underground detector of this experiment is looking for the following type neutrino interactions

$$\begin{aligned} \nu_e + d &\rightarrow p + p + e^- \quad \text{(CC:only sensitive to } \nu_e) \\ \nu_x + e &\rightarrow \nu_x + e \qquad \text{(ES: sensitive to all } \nu) \\ \nu_x + d &\rightarrow p + n + \nu_x \qquad \text{(NC:sensitive to all } \nu). \end{aligned} \tag{2.4.7}$$

Since SNO can determine the NC events by looking at the signals for neutrons in the final states, it enables to determine the flavor independent neutrino flux from Sun unlike Superkamiokande. Moreover, the fluxes in the units of $10^6 cm^{-2} sec^{-1}$ are given by

$$\begin{aligned} \phi(CC) &= 1.76 \pm 0.06 \pm 0.09, \\ \phi(ES) &= 2.39 \pm 0.24 \pm 0.12, \\ \phi(NC) &= 5.09 \pm 0.44 \pm 0.46. \end{aligned}$$

Interestingly, the number of neutrinos observed via NC interaction is in agreement with that predicted by the SSM, whereas the number of electron neutrinos via CC interaction is only one-third of that predicted by the SSM. In this way SNO experiment provides a clear evidence of flavour transition of neutrino.

2.4.2 Atmospheric neutrino experiments

These experiments are indented to detect atmospheric neutrinos that is produced through the interaction of cosmic rays with the atoms in the atmosphere. The detector of this experiment is under-grounded to reduce the backgrounds due to cosmic rays. Moreover, the Super Kamiokande experiment is also looking for atmospheric neutrino oscillation and measured the upward and downward going muon neutrino fluxes. It has been seen that the number of muon neutrino which are coming in the downward direction is not equal to that is going in the upward direction, whereas the number of electron neutrinos are the same. This indicates the most of the muon neutrino which are going in the upward direction are oscillated to other kind of neutrinos. As these experiments are looking for the neutrinos which are travelling through a varying matter density like solar neutrinos, they are more sensitive to determine the mass hierarchy of neutrino, which is the one of the main goal of current and future generation oscillation experiment.

2.4.3 Reactor neutrino experiments

These man-made experiments are looking for the electron anti-neutrino coming from the nuclear reactors. Moreover, the anti-neutrinos are detected by Inverse Beta Decay (IBD) processes using liquid scintillator detector. These experiments can constrain both solar and atmospheric neutrino oscillation parameters by choosing appropriate baseline for the experiment. The KamLAND reactor experiment is very long baseline experiment looking for solar neutrino oscillation parameters, whereas the short baseline reactor experiments like RENO, Double CHOOZ, and Daya Bay constrain the atmospheric mass squared difference and the reactor mixing angle.

2.4.4 Accelerator neutrino experiments

The experiments which use accelerators to produce neutrino beam are called accelerator experiments. These experiments are categorised into two on the basis of baseline length: short baseline experiments and long baseline experiments. The short baseline

experiments like LSND, MiniBooNE, KARMEN etc are designed in such way that they can observe the neutrino oscillation driven by a mass squared difference of $1eV^2$ and some of them are indented to do the precision measurements of neutrino flux and the interaction crossection. Whereas long baseline experiment are mainly indented to observe the atmospheric neutrino oscillation, or in other words they are looking for the oscillation driven by mass squared difference of $2.4 \times 10^{-3}eV^2$. Moreover, the main objectives of long baseline experiments are both the precision measurements of neutrino oscillation parameters and the determinations of current unknowns in the neutrino oscillation sector, i.e., determination of neutrino mass hierarchy and CP-violating phase and resolutions of atmospheric mixing angle.

2.5 Current status of neutrino oscillation parameters

This section discusses the current status of oscillation parameters in the standard three flavor picture of neutrino oscillation. They are: three mixing angle ($\theta_{12}, \theta_{13}, \theta_{23}$), two mass squared differences (Δm^2_{21}, Δm^2_{31}) and one phase δ_{CP}. These parameters can be divided into mainly three categories:

- **Solar neutrino sector**: ($\sin^2 2\theta_{12}$, Δm^2_{21})

  The solar mixing angle and solar mass squared difference are constraint mainly by solar neutrino experiments (SNO, Super Kamiokande) and reactor experiment (KamLAND). The solar neutrino oscillation experiments are looking for electron neutrino disappearance events, whereas the reactor experiment is looking for electron anti-neutrino disappearance events. The oscillation parameters are constraint by using two flavor survival probability,

  $$P(\nu_e \to \nu_e) = 1 - \sin^2 2\theta_\odot \sin^2 \left(1.27 \frac{\Delta m^2_\odot L}{E}\right). \tag{2.5.1}$$

  The constraint on the parameters are obtained by comparing the experimental data with fit data in a $\sin^2 2\theta_\odot - \Delta m^2_\odot$ plane. The solar neutrino that is coming from the inner core of the Sun travels through a varying matter density.

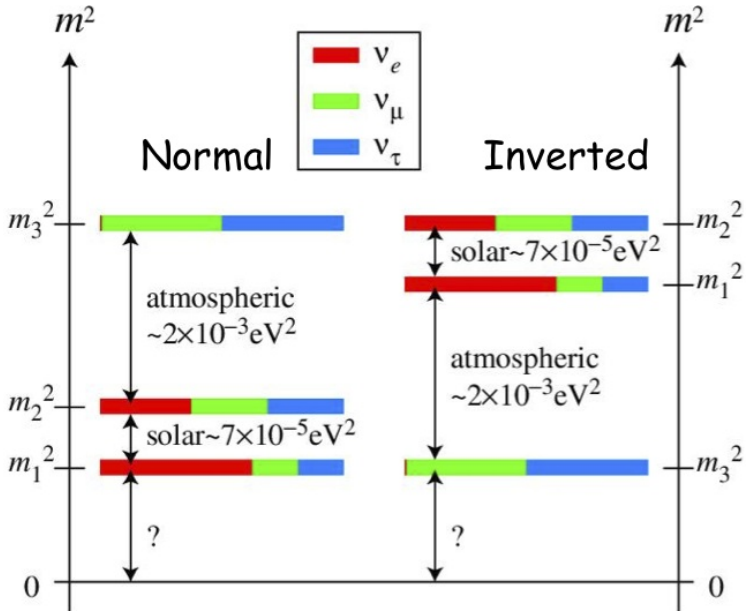

Figure 2.5.1: Neutrino mass ordering

- **Atmospheric neutrino sector**: $(\sin^2 2\theta_{23},\ \Delta m^2_{32} \approx \Delta m^2_{31})$

  The atmospheric mixing angle and atmospheric mass squared difference are constraint by the atmospheric neutrino experiments and long baseline accelerator experiments. The atmospheric experiments like K2K and MINOS are looking for the ν_μ survival probability,

$$P(\nu_\mu \to \nu_\mu) = 1 - \sin^2 2\theta_{atm} \sin^2 \left(1.27 \frac{\Delta m^2_{atm} L}{E}\right). \tag{2.5.2}$$

- **Reactor neutrino sector**: $(\sin^2 2\theta_{13})$

  The reactor experiments [30], which are looking for $\bar{\nu_e}$ disappearance events, are indented to determine the mixing angle θ_{13} by looking at the electron anti-neutrino survival probability,

$$P(\bar{\nu_e} \to \bar{\nu_e}) = 1 - \sin^2 2\theta_{13} \sin^2 \left(1.27 \frac{\Delta m^2_{atm}}{E}\right). \tag{2.5.3}$$

  Initially, these experiments did not observe any kind of oscillation and obtained an upper bound on θ_{13}. Later, the accelerator experiments like T2K [31] and MINOS [32] disfavoured the $\theta_{13} = 0$. Recently in 2012, Double Chooz [33], Daya Bay [34], and RENO [35] confirmed that $\theta_{13} \neq 0$ and obtained the value of $\theta_{13} \approx 9^\circ$.

Experiment	Dominant	Important
Solar Experiments	θ_{12}	Δm^2_{21}, θ_{13}
Reactor LBL (KamLAND)	Δm^2_{21}	θ_{12}, θ_{13}
Reactor MBL (Daya-Bay, Reno, D-Chooz)	θ_{13}	$\lvert\Delta m^2_{3\ell}\rvert$
Atmospheric Experiments	θ_{23}	$\lvert\Delta m^2_{3\ell}\rvert$, θ_{13}, δ_{CP}
Accelerator LBL ν_μ Disapp (Minos, NOνA, T2K)	$\lvert\Delta m^2_{3\ell}\rvert$, θ_{23}	
Accelerator LBL ν_e App (Minos, NOνA, T2K)	δ_{CP}	θ_{13}, θ_{23}, $sign(\Delta m^2_{3\ell})$

Table 2.5.1: Experiments contributing to the present determination of the oscillation parameters.

The experimental endeavours in the past few decades have firmly established the phenomenon of neutrino oscillations [38–40]. The experiments contributing to the present determination of the oscillation parameters are given in Table 2.5.1 and the present global fit values of oscillation parameters are given in Table 2.5.2.

Mixing Parameters	Best Fit value	3σ Range
$\sin^2\theta_{12}$	0.323	$0.278 \to 0.375$
$\sin^2\theta_{23}$ (NH)	0.567	$0.392 \to 0.643$
$\sin^2\theta_{23}$ (IH)	0.573	$0.403 \to 0.640$
$\sin^2\theta_{13}$ (NH)	0.0234	$0.0177 \to 0.0294$
$\sin^2\theta_{13}$ (IH)	0.0240	$0.0183 \to 0.0297$
$\Delta m^2_{21}/10^{-5}$ eV^2	7.6	$7.11 \to 8.18$
$\lvert\Delta m_{31}\rvert^2/10^{-3}$ eV^2 (NH)	2.48	$2.30 \to 2.65$
$\lvert\Delta m_{31}\rvert^2/10^{-3}$ eV^2 (IH)	2.38	$2.20 \to 2.54$

Table 2.5.2: The best-fit values and the 3σ ranges of the neutrino oscillation parameters from Ref. [28].

However, till now no one knows whether the third mass eigenstate of neutrino ν_3 is heavier or lighter than other two mass eigenstates ν_2 and ν_1. If ν_3 is heavier than other two mass eigenstates then neutrino masses in the order $m_1 < m_2 << m_3$ and it is called Normal Hierarchy (NH), whereas if ν_3 is lighter than other two mass eigenstates then neutrino masses in the order $m_1 > m_2 >> m_3$ and it is called Inverted Hierarchy (IH) as one can see from Fig. 2.5.1 . Further, the Super-kamiokande experimental result shows that the third neutrino mass eigenstate is composed of equal amount of ν_μ and ν_τ, i.e., experimental data prefers a maximal mixing of atmospheric mixing angle

($\theta_{23} = \pi/4$). However, disappearance measurements of MINOS [29] point towards non-maximal mixing, which contradicts the measurements of Super-Kamiokande. Therefore, there are two possibilities: θ_{23} can be less than $\pi/4$, so called Lower Octant (LO) or θ_{23} can be greater than $\pi/4$, so called Higher Octant (HO). Furthermore, the results from current generation long baseline neutrino oscillation experiments T2K [36] and NOνA [37] hint towards a maximal CP violation i.e., $\delta_{CP} = -90$.
The determination of neutrino mass hierarchy and the CP violating phase, and resolution of octant atmospheric mixing angle are the main challenging goals in the field of neutrino oscillation research, since all these unknown parameters play crucial role in neutrino mass model building.

2.6 Conclusions

This chapter started with a discussion on neutrino oscillation. Then obtained a general expression for oscillation probability. Thereafter, the discussion was on the vacuum oscillation and oscillation in the matter. This followed by a discussion on evidence of neutrino oscillation, various neutrino oscillation experiments and current status of neutrino oscillation parameters. It can be seen that there are still unknown parameters in the standard paradigm of neutrino oscillation such as neutino mass hierarchy, CP -violating phase and octant of atmospheric mixing angle. There are several neutrino oscillation experiments overall the world are taking part in the quest for the determination of these unknowns in the neutrino sector. Moreover, the proposed experiments to improve the oscillation data, which are under the construction. The following chapters discuss the physics potential of currently running experiments like T2K and NOνA and proposed experiments like T2HK and DUNE.

CHAPTER 3

Towards extracting the best possible results from NOνA

3.1 Introduction

The NuMI Off-Axis ν_e Appearance (NOνA) is the currently running leading long-baseline neutrino oscillation experiment, whose main physics goal is to explore the current issues in the neutrino sector, such as determination of the neutrino mass ordering, resolution of the octant of atmospheric mixing angle and to constrain the Dirac-type CP violating phase δ_{CP}. The determination of these parameters by an oscillation experiment like NOνA, which is mainly rely on the oscillation probability, is extremely difficult due to the parameter degeneracies, since various combination of these parameters give the same probability. The scheduled run period of NOνA is for a total of six years with first three years in neutrino mode followed by the next three years in antineutrino mode. Therefore, it is of great importance to study the ability to discriminate the degeneracies between different oscillation parameters of this experiment within a minimal time-span, since it leads to an early understanding of neutrino oscillation parameter space. A lot of work has been done in the literature to resolve these degeneracies among oscillation parameters [41–43]. Moreover, there was a suggestion for the need of an early anti-neutrino run to get a first hint of mass ordering

in NOνA [44]. There it has been shown that the sensitivity for the determination of mass hierarchy is above 2σ (i.e., $\chi^2 > 4$) only for δ_{CP} value around $\mp 90°$ for true hierarchy and octant as NH-LO or HO-IH, where the scheduled run time, i.e., (3 yrs in ν mode + 0 yr in $\bar{\nu}$ mode) gives almost null sensitivity. However, this chapter discusses about how to extract the best possible results from NOνA with shortest time-span by analysing its physics potential and degeneracy discrimination capability for a total of four years of runs, with two years in each neutrino and antineutrino modes.
Furthermore, this chapter also discusses whether there is any improvement in the sensitivities by adding data from T2K experiment for a total of five years run with 3.5 years in neutrino mode and 1.5 years in antineutrino mode.

This chapter starts with a detailed discussion on currently running experiments T2K and NOνA. This is followed by a discussion on the various degeneracies among the neutrino oscillation parameters. Subsequent sections contain the details of simulation of T2K and NOνA experiments and comparative study of NOνA experiment to determine the mass ordering and octant determination of θ_{23}. Finally, the conclusions of the sensitivity analysis are given in the last section of this chapter.

3.2 Current generation long baseline experiments

This section discusses the main objectives of current generation long baseline experiments. The discovery of neutrino oscillation by SK [45] is a milestone in the neutrino physics, which opens up a way to explore the basic nature of a fundamental particle neutrino and new physics beyond SM. The observed deficit in atmospheric neutrino flux can be interpreted as the flavor transition of muon neutrino to other flavors. However, the CHOOZ experimental data [46] excluded the possibility of the muon to electron neutrino flavor transition as the dominant flavor transition. Thereafter, the first generation long baseline experiments like K2K [47], MINOS [48], ICARUS [49] and OPERA [50] are introduced to observe the signals for muon neutrino to tau neutrino oscillations, which required a very high energy neutrino beam since the threshold energy for CC interaction of tau neutrino is about 3.5 GeV. Subsequently, the three

flavor mixing of neutrino becomes the standard picture of neutrino mixing, which also contains θ_{13} terms in the muon neutrino to electron neutrino oscillation probability. Moreover, the observation of muon neutrino to electron neutrino oscillation is a clear indication of nonzero θ_{13}. Therefore, the current generation long baseline experiments are designed in such way that to observe signals for muon neutrino to electron neutrino oscillation. The uniqueness of this oscillation channel is that it is also sensitive to current unknowns in the neutrino oscillation sector such as neutrino mass hierarchy, CP-violating phase and octant of atmospheric mixing angle. T2K [51] and NOνA [52, 53] are currently running long-baseline neutrino oscillation experiment and they are looking for:

- ν_e and $\bar{\nu_e}$ appearance events: To determine the value of θ_{13}, determination of the octant of θ_{23}, mass ordering and constrain the Dirac CP phase.
- ν_μ and $\bar{\nu_\mu}$ disappearance events: The precision measurement of atmospheric oscillation parameters, Δm^2_{23} and θ_{23}.

The T2K experiment uses muon neutrino beam with power 0.77MW, which is coming from Japan Proton Accelerator Research Complex (JPARC). JPARC produces mesons (pions and kaons) by colliding 30 GeV proton beam on a graphite target. These mesons direct towards the decay pipe, through which they under go decay and produce muon neutrinos. The polarity of current on the magnetic horns placed inside the decay pipe determines whether the produced beam contain neutrinos or antitneutrinos. The direction of muons produced from the meson decay determines the direction of neutrino beam. The neutrino beam is directed towards a water Cherenkov detector with fiducial mass 22.5 kiloton which is placed about 295km far away.
Whereas, NOνA uses an upgraded NuMI beam power of 0.7 MW at Fermilab. The Main Injector accelerator produces mesons by colliding 120GeV proton beam on carbon target. The produced neutrino beams is directed towards 14 kiloton totally active scintillator detector (TASD) placed about 810km away from Fermilab (near the Ash River). It also has a 0.3 kton near detector located at the Fermilab site to monitor the un-oscillated neutrino or anti-neutrino flux.
Moreover, both T2K and NOνA make use of off-axis technique to get neutrino energy spectrum with very narrow band as one can see from [54]. Further, this technique

enables the flux to peaks at low energies, which helps to suppress the high energy tail of neutrino energy spectrum and reduces the backgrounds due to NC interactions and tau productions. Moreover, the monochromatic neutrino beams enables to distinguish between the ν_e signals from the intrinsic ν_e background present in the muon neutrino beam. The far detector of NOνA experiment is placed 0.8° off-axis from the NuMI beamline, whereas that of T2K is kept 2.5° off-axis to the central line of neutrino beam.

One of the main objective of current generation experiments is the resolution of degeneracy among the oscillation parameters. Next section discusses about the various parameter degeneracies among the oscillation parameters.

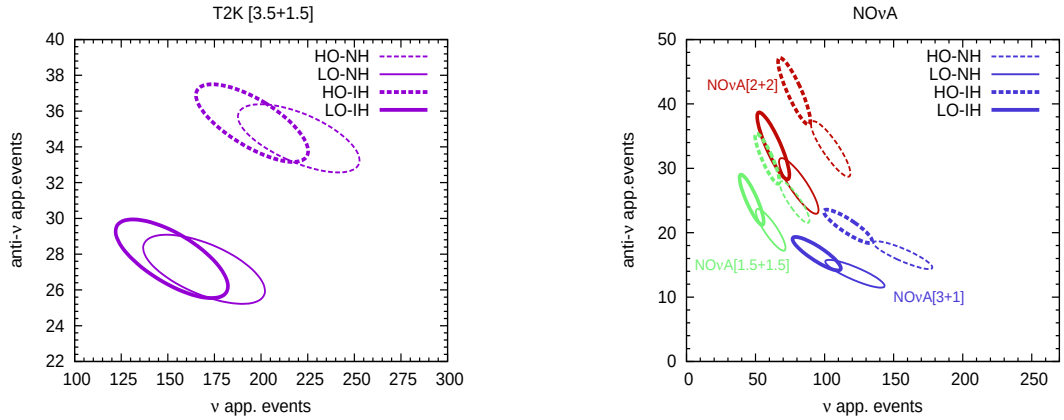

Figure 3.2.1: Neutrino and antineutrino appearance events for the $\nu_\mu \to \nu_e$ versus $\bar{\nu}_\mu \to \bar{\nu}_e$ channels by assuming both IH and NH and for lower and higher octants of θ_{23}.

3.3 Neutrino oscillation parameter degeneracies

The resolution of degeneracies among the oscillation parameters is one of the main challenge in neutrino physics. This section discusses the various degeneracies among the oscillation parameters and the best ways to analyse these degeneracies.

In general, the parameter degeneracies in neutrino oscillation sector are of mainly three types and they are: $(\delta_{CP}, \theta_{13})$, sign of Δm^2_{31} and $(\theta_{23}, \pi/2 - \theta_{23})$. Recently, the reactor experiments such as Daya Bay [34], Double Chooz [33] and RENO [35] have precisely measured the value of the reactor angle as $\sin^2 2\theta_{13} \approx 0.089 \pm 0.01$. Therefore, the eight fold degeneracy is reduced to four-fold degeneracy. Out of these degeneracies,

the degeneracy in which θ_{23} can't be distinguished from $(\pi/2 - \theta_{23})$ is called octant degeneracy and the degeneracy in the sign of Δm^2_{31} is called hierarchy ambiguity. So far left with four degeneracies and they are represented as NH-HO, NH-LO, IH-HO and IH-LO, where NH/IH (HO/LO) stands for Normal/Inverted ordering (Higher/Lower Octant). Resolution of these degeneracies are the main challenges of the present and future long-baseline neutrino oscillation experiments, which are mainly looking for oscillation from $\nu_\mu(\bar{\nu}_\mu) \to \nu_e(\bar{\nu}_e)$. The expression for the oscillation probability, which is up to first order in $\sin\theta_{13}$ and $\alpha \equiv \Delta_{21}/\Delta_{31}$ is given as [55–57]

$$\begin{aligned} P(\nu_\mu \to \nu_e) &\approx \sin^2 2\theta_{13} \sin^2\theta_{23} \frac{\sin^2(\hat{A}-1)\Delta}{(\hat{A}-1)^2} \\ &+ \alpha \cos\theta_{13} \sin 2\theta_{12} \sin 2\theta_{13} \sin 2\theta_{23} \frac{\sin \hat{A}\Delta}{\hat{A}} \frac{\sin(\hat{A}-1)\Delta}{(\hat{A}-1)} \cos(\Delta + \delta_{CP}), \end{aligned} \tag{3.3.1}$$

where $\Delta = \Delta m^2_{31} L/4E$ and $\hat{A} = 2\sqrt{2} G_F n_e E/\Delta m^2_{31}$, where G_F is the Fermi coupling constant and n_e is the electron number density. For neutrinos, $\hat{A}$ is positive for NH and negative for IH. For antineutrino, $\hat{A}$ and δ_{CP} reverse their sign, i.e, $\hat{A} \to -\hat{A}$ and $\delta_{CP} \to -\delta_{CP}$ for $P(\bar{\nu}_\mu \to \bar{\nu}_e)$.

The best way to express the degeneracies without any mathematical expression is simply by using bi-events curves. The bi-events plots for various octant-hierarchy combinations of T2K and NOνA are depicted in Fig. 1, which are obtained by computing the $\nu(\bar{\nu})$ appearance events for the full range of δ_{CP} with a particular octant-hierarchy combination. The detailed description of event simulation of a particular experiment is given in the next section. From the plots, it can be seen that the ellipses for two hierarchies overlap with each other for both T2K and NOνA for Lower Octant, which show that they have poor mass hierarchy discrimination capability. Whereas, the overlap is minimal for Higher Octant in the case of NOνA, which shows that NOνA has better degeneracy discrimination capability compared to T2K. However, the ellipses for HO and LO are very well separated and they have good octant resolution capability. Moreover, NOνA (2+2) has better capability to determine the octant of θ_{23} among all other combinations due to balanced ν and $\bar{\nu}$ runs.

3.4 Simulation details

The General Long Baseline Experiment Simulator (GLoBES) [128, 129], a magnificent software package, is used to do the numerical simulations. In GLoBES, the experimental set-ups are specified by using Abstract Experiment Definition Language (AEDL). Further, the simulation of events and sensitivity analysis are done by using C-user interface. The capability of an experiment to determine a parameter or resolve an ambiguity is known the sensitivity of that particular experiment. It is determined by performing the χ^2 analysis using the method of pulls [60–62]. The event rate (N) for an experiment with a particular set of oscillation parameters $\vec{p}$ is a function of the detector mass M, the energy resolution R of the detector, the run time T of that experiment, the cross section σ of neutrino at the detector, the efficiency ϵ of the detector, and the flux ϕ of neutrinos. It should be note that these characteristics are different for different experiments, which can be adjusted in a particular experiment in such a way that to achieve the best sensitivity (optimization of experiment).
In order to do χ^2 analysis, one simulate the true event rates with the present best fit value of the oscillation parameters and compare it with the event rate of the hypothesis (test event rate). Therefore, the statistical χ^2 is given by

$$\chi^2_{stat}(\vec{p}_{\rm true}, \vec{p}_{\rm test}) = \sum_{i \in \rm bins} \frac{(N_i^{\rm true} - N_i^{\rm test})^2}{N_i^{\rm true}}. \tag{3.4.1}$$

However, one should also take care of the uncertainties that are coming from both theoretical inputs and the experimental systematics. These uncertainties can be incorporated by using method of pulls as mentioned earlier. In this method, the χ^2 is defined as

$$\chi^2_{\xi}(\vec{p}_{\rm true}, \vec{p}_{\rm test}) = \min_{\xi} \left[\left(\sum_{i \in \rm bins} \frac{(N_i^{\rm true} - N_i^{\rm test}(\xi))^2}{N_i^{\rm true}} \right) + \frac{\xi^2}{\sigma^2_{\xi}} \right] , \tag{3.4.2}$$

where the parameter ξ is known as nuisance parameter and σ_ξ is the 1σ systematic error of corresponding nuisance parameter. The terms associated with nuisance parameter in the χ^2 expression are called pull terms and these parameters are minimized at each test point. The ξ^2 term is the penalty term that added to χ^2 in order to compensate the systematic effects as test rate $N_i^{\rm test}$ modified to $N_i^{\rm test}(\xi)$. The nuisance parameters do not have any direct involvement in the neutrino oscillation, but they vary with the

experiment that one consider for the analysis, for instance error associated with flux normalisation, cross section, fiducial mass of the detector etc.

Further, obtain minimum χ^2_{min} by doing marginalization over all oscillation parameter space. The shifting of a oscillation parameter from the true value can worsen the fit of the experiment which used to determine that particular parameter. Therefore, add penalty terms for the oscillation parameter so called priors to χ^2. Hence, the minimised χ^2 with a Gaussian prior on the oscillation parameter θ_{13} is given by

$$\chi^2_{min} = Min\left[\chi^2_{\xi}(\vec{p}_{\rm true}, \vec{p}_{\rm test}) + \left(\frac{\sin^2 2\theta^{true}_{13} - \sin^2 2\theta_{13}}{\sigma(\sin^2 2\theta_{13})}\right)^2\right]. \qquad (3.4.3)$$

Characteristics	T2K	NOνA
Beam power	0.77MW	0.7MW
Detector mass	22.5kt Water Cherenkov	14kt TASD
Baseline	295km	810km
Run time	5 yrs. (3ν+ $2\bar{\nu}$)	4 yrs. (3ν+ $1\bar{\nu}$) and (2ν+ $2\bar{\nu}$)
Flux peaks at	0.6 GeV	2GeV
$P_{\mu e} I^{st}$ oscillation maximum	0.55 GeV	1.5GeV

Table 3.4.1: The experimental specifications of T2K and NOνA .

The T2K and NOνA experiments are simulated by using GLoBES along with their auxiliary files [63]. The experimental specifications of NOνA are taken from [64] with the following characteristics:

- Signal efficiencies: 45% for electron neutrino and electron anti-neutrino signals, whereas 100% for both muon neutrino and muon anti-neutrino signals.
- Background efficiencies: There are mainly three backgrounds and they are
  1. Mis-ID muons acceptance: The mis-identified muons (anti-muons) at the detector are about 0.83% (0.22%).
  2. NC background acceptance: There exist almost 2% (3%) neutral current events at the detector, which resemble the muon neutrino (muon anti-neutrino) events.

3. Intrinsic beam contamination: The possibility of existence of electron neutrino (electron anti-neutrino) in the neutrino beam is about 26% (18%).

And assume that there exists 5% uncertainty on signal normalization and 10% on background normalization. The migration matrices for NC background smearing are taken from [64]. Other experimental specifications of both T2K [65] and NOνA are listed in the Table-3.4.1. Furthermore, the true values of oscillation parameters, which used in the simulation are listed in the Table-3.4.2. Moreover, one has to

$\sin^2\theta_{12}$	0.32
$\sin^2 2\theta_{13}$	0.1
$\sin^2\theta_{23}$	0.41 (LO), 0.59 (HO)
Δm^2_{atm}	2.4×10^{-3} eV^2 for NH -2.4×10^{-3} eV^2 for IH
Δm^2_{21}	7.6×10^{-5} eV^2
δ_{CP}	0°

Table 3.4.2: The true values of oscillation parameters considered in the simulations.

take into account the relation between the atmospheric parameters measured in the experiment ($\Delta m^2_{\rm atm}, \theta_{\mu\mu}$) and that are in standard oscillation framework ($\Delta m^2_{31}, \theta_{23}$), whose derivations can be seen in Appendix-A, while doing the simulation. These relations are given by [66–68]

$$\sin\theta_{23} = (\sin\theta_{\mu\mu}/\cos\theta_{13}) \qquad \text{and}$$
$$\Delta m^2_{31} = \Delta m^2_{\rm atm} + (\cos^2\theta_{12} - \cos\delta_{CP}\sin\theta_{13}\sin 2\theta_{12}\tan\theta_{23})\Delta m^2_{21}. \quad (3.4.4)$$

It is clear from the above relations that the observed value of moderately large θ_{13} significantly affects the oscillation parameters. Therefore, one should use corrected definitions of these parameters to analyze octant sensitivity. Hence, calculate oscillation probabilities in terms of Δm^2_{31} and θ_{23} by allocating the measured values of atmospheric oscillation parameters $\Delta m^2_{\rm atm}$ and $\theta_{\mu\mu}$.

Further, the next section discusses the sensitivity of NOνA experiment to determine mass hierarchy, octant of θ_{23} and the resolution capability of parameter degeneracies.

3.5 Mass hierarchy and Octant determination

This section discusses the potential of NOνA experiment to determine the mass hierarchy, octant of atmospheric mixing angle and the role of mass hierarchy-octant parameter degeneracy in the determination of these parameters.

3.5.1 Mass hierarchy determination

As discussed in previous chapter, the matter effect plays a significant role in the determination of neutrino mass hierarchy. The baseline length of NOνA experiment is about 810km and it ensures that neutrinos, which reach at the far detector significantly affected by the matter present on their path. This subsection discusses the MH sensitivity of NOνA experiment.

So far, no one knows the mass hierarchy of neutrino, i.e, hierarchy can be either normal or inverted. Therefore, one has to consider both case while doing a sensitivity analysis of an experiment. For the first case, assume that nature prefers Normal Hierarchy (NH) for neutrino and check with how much significance NOνA can exclude the Invert Hierarchy (IH) . In order to do this, simulate the true event rates by assuming hierarchy to be normal and test event rates by assuming hierarchy to be inverted. Further, calculate the χ^2 by comparing both event rates using GLoBES. Then the marginalisation over all other parameters and addition of a prior term for $\sin^2 2\theta_{13}$ yields minimum value of χ^2. Finally, obtain χ^2_{min} for each true value of δ_{CP} so that one can express obtained mass hierarchy sensitivity as a function of true value of δ_{CP}. In a similar fashion, it is possible to find the significance with which NOνA can exclude Normal Hierarchy if nature prefers Inverted Hierarchy for neutrino.
Since this chapter mainly focus on the resolution capability of degeneracies among the oscillation parameters, the MH sensitivity is calculated for various true values of $\sin^2\theta_{23}$ (i.e, $\sin^2\theta_{23} = 0.5$ for maximal mixing and $\sin^2\theta_{23} = 0.41$ (0.59) for LO (HO).

The Fig. 3.5.1 shows the minimised χ^2 as a function of δ_{CP} for maximal mixing of atmospheric mixing angle. The left panel corresponds to true NH and the right panel is for true IH. From these figures, one can see that the potential to determine mass

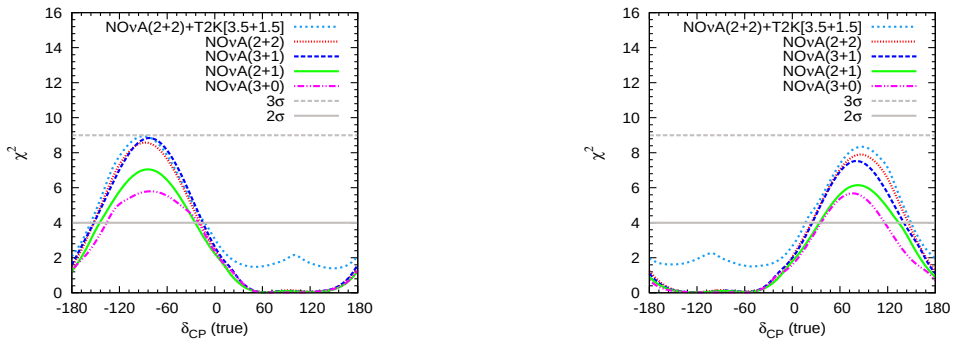

Figure 3.5.1: The potential of determination of mass hierarchy. NH is considered as true hierarchy in the left panel and IH considered as true hierarchy in right panel.

hierarchy for NOνA is above 2σ for less than half of parameter space of δ_{CP} and it also depends on the neutrino mass ordering. The mass hierarchy sensitivity of NOνA (2+2) is lower (higher) than that of NOνA (3+1) for true NH (IH) and maximal mixing of atmospheric mixing angle. Moreover, the sensitivity increases for a combined analysis of NOνA (2+2) and T2K (3.5+1.5) and has a 3σ significance in the case of true NH. Further, the mass hierarchy sensitivities for non-maximal atmospheric mixing angle are presented in Fig. 3.5.2. These are obtained by considering all possible combinations with $\sin^2\theta_{23} = 0.41$ (LO) and $\sin^2\theta_{23} = 0.59$ (HO), and different combinations of neutrino and antineutrino mode of runs like NOνA (2+1), NOνA (2+2), NOνA (3+0) and NOνA (3+1). It can be seen from the figure that the value of χ^2 is always above 6 for all cases of NOνA (2+2), whereas for NOνA (3+1) the χ^2 value is below 6 ($\sim 2.4\sigma$) for two combinations (NH-LO and IH-HO). Hence, NOνA (2+2) has a good mass hierarchy discrimination capability compared to the scheduled run of NOνA for four years. Thus, it is possible to get an early information about the nature of mass ordering if NOνA runs in $(2\nu + 2\bar{\nu})$ mode rather than its scheduled run of $(3\nu + 1\bar{\nu})$ years. Furthermore, if nature would be kind enough in the sense that the real mass ordering is inverted in nature and θ_{23} lies in the higher octant, then mass hierarchy can be determined with more than 2σ C.L. for values of δ_{CP} in the range $[0 : 180]^\circ$ with $(2\nu + 2\bar{\nu})$ years of run. Also if one compare the results of three years of run, the sensitivity for the determination of mass hierarchy is better for (2+1) combination than the scheduled (3+0) combination. This in turn implies that there would be better perspective if NOνA runs in antineutrino mode after completing two years of run in neutrino mode.

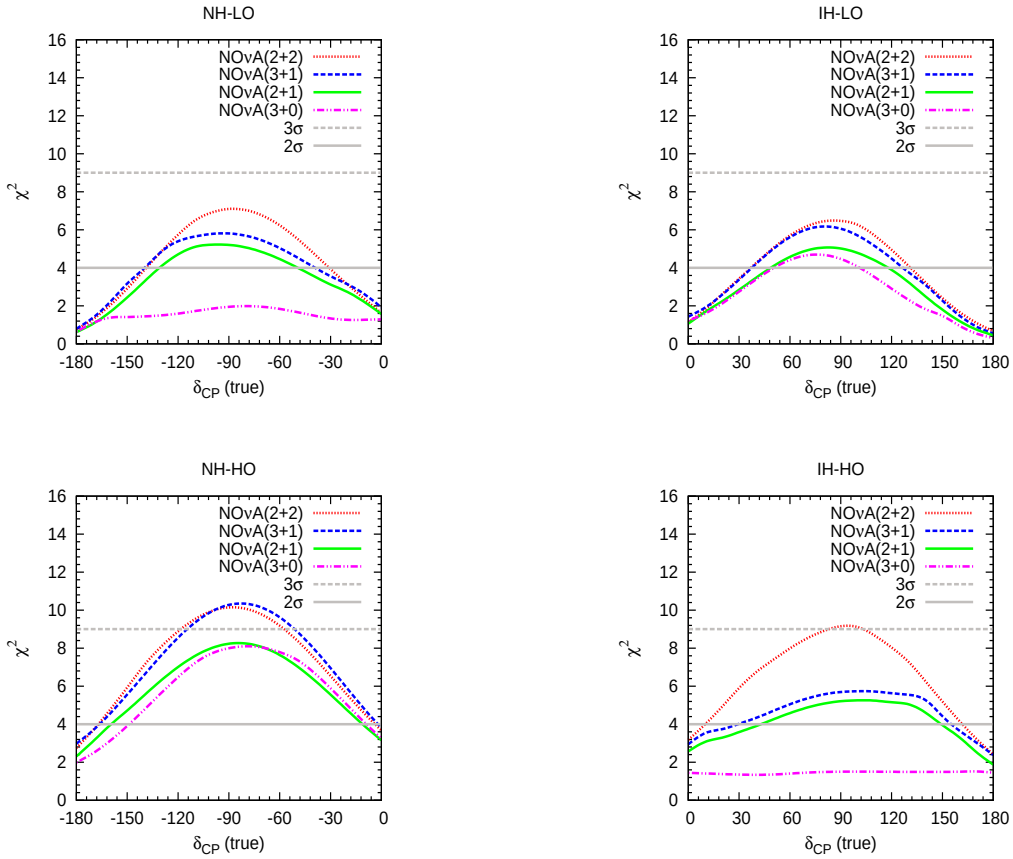

Figure 3.5.2: The mass hierarchy sensitivities. The top (bottom) panel is for LO (HO), where we have used $\sin^2\theta_{23} = 0.41$ (0.59) for LO (HO) and left (right) panel is for true NH (IH).

3.5.2 Octant of θ_{23} determination

The hint of non-maximal atmospheric mixing angle observed by the MINOS Collaboration [29] is one of the recent subject of interest in neutrino oscillation sector. The deviation of θ_{23} from maximal ends up with two solutions so called lower octant ($\sin^2\theta_{23} < 0.5$) and higher octant ($\sin^2\theta_{23} > 0.5$). For the determination of resolution of octant of θ_{23}, obtain the minimum χ^2 with which one can rule out the wrong octant from the true octant. In order to do this, simulate true events by taking LO (HO) as true octant and test events by taking HO (LO) as test octant. To obtain the minimum χ^2, compare the true events and test events by marginalizing over other parameters $\sin^2 2\theta_{13}$, Δm^2_{31}, and δ_{CP} within their allowed range, for true values of $\sin^2\theta_{23}$ in the range [0.32:0.68]. Also add a prior on $\sin^2 2\theta_{13}$ while calculating minimum χ^2 .

Furthermore, the obtained χ^2_{min} as a function of $\sin^2\theta_{23}$ is given in Fig. 3.5.3. The

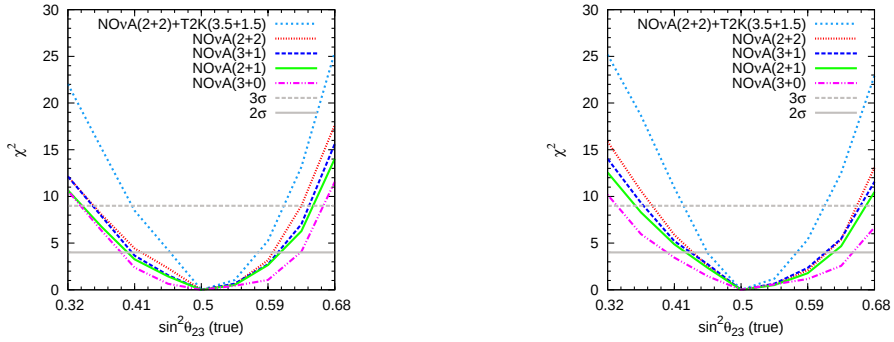

Figure 3.5.3: The potential of octant resolution. NH is considered as true hierarchy in the left panel and IH considered as true hierarchy in right panel.

left panel of the figure corresponds to NH and the right panel corresponds to IH as true hierarchies. From the plots, it is clear that the potential to determine the octant of atmospheric angle is better for NOνA (2+2) than that for NOνA (3+1). It can be seen that a combined analysis of NOνA (2+2) and T2K (3.5+1.5) has good octant resolution sensitivity.

3.5.3 Correlation between θ_{23} and Δm^2_{32}

The discovery reach of mass hierarchy and octant of atmospheric mixing angles are crucial because of the degeneracies between the oscillation parameters. Therefore, resolution of these degeneracies is very important to have a clear understanding of the neutrino mixing phenomenon.

This subsection focuses on the θ_{23} and Δm^2_{32} degeneracy. First of all, one can check how does the hierarchy ambiguity affect $\sin^2\theta_{23}$ - Δm^2_{32} parameter space. In order to do this, simulate the true events for maximal value of $\sin^2\theta_{23}$ ($\sin^2\theta_{23} = 0.5$) and test events for allowed values of $\sin^2\theta_{23}$ ([0.32:0.68]) and Δm^2_{32} ($[2.05 : 2.75] \times 10^{-3}$ eV^2). Then obtain the minimum χ^2 by comparing true events and test events by doing marginalization over both $\sin^2 2\theta_{13}$ and δ_{CP} with a prior on $\sin^2 2\theta_{13}$. The Fig. 3.5.4 shows the obtained χ^2 as a function of $\sin^2\theta_{23}$ and Δm^2_{32}. From the figure, it can be seen that there is small difference in the allowed parameter space for NH and IH. However, there is no difference in the allowed parameter space for (2+2) and (3+1) years of NOνA running as far as the determination of Δm^2_{32} is concerned.

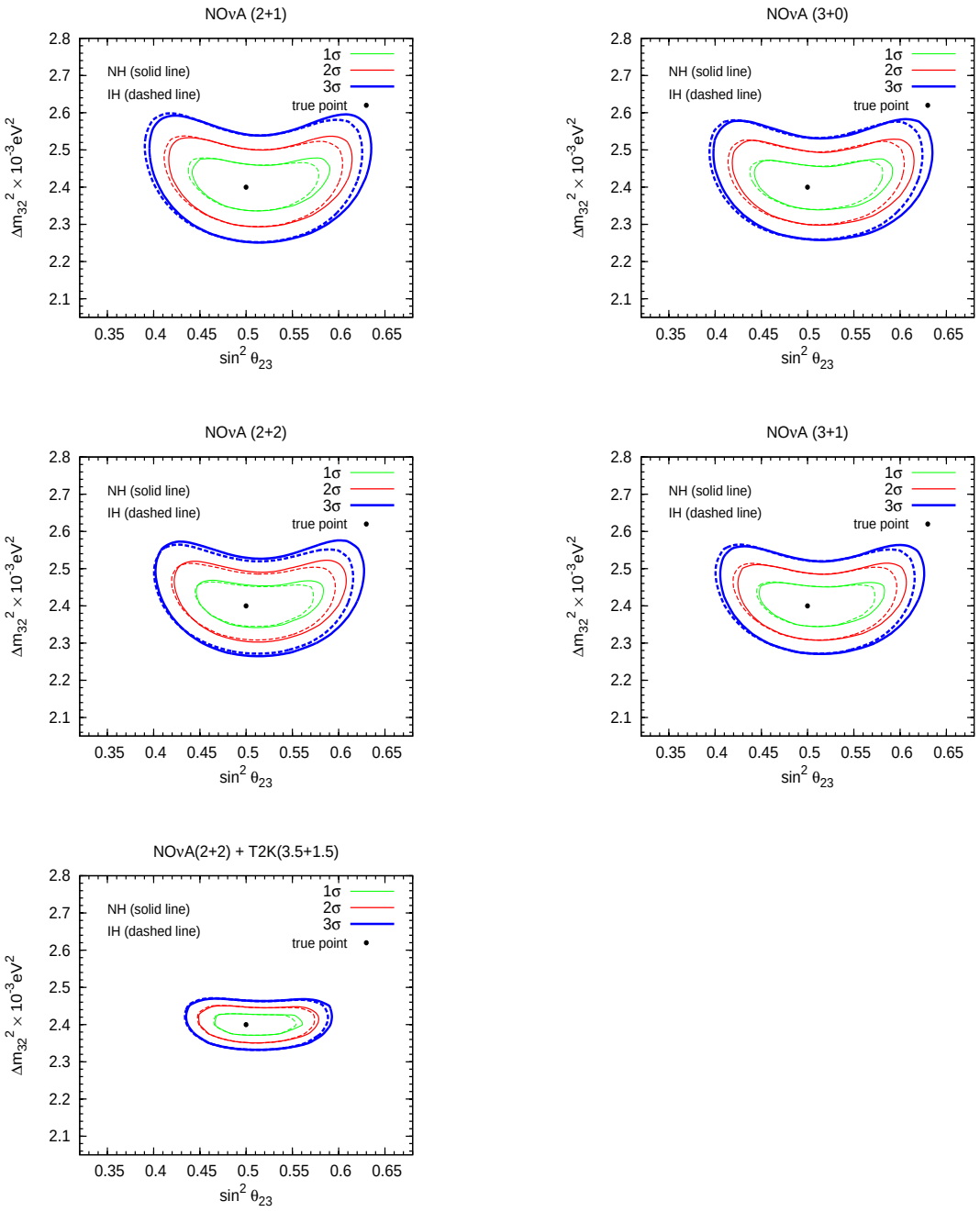

Figure 3.5.4: The $\sin^2\theta_{23} - \Delta m^2_{32}$ contour plots with true $\sin^2\theta_{23} = 0.5$.

Moreover, similar kind of results can be obtained if one compare the parameter space for both NOνA (2+2) and NOνA (3+1), and as expected such parameter spaces are significantly reduced when compared with NOνA (2+1) and NOνA (3+0). It should also be noted from the figure that the parameter space is substantially reduced for a combined analysis of T2K and NOνA. Therefore, if one combine the (2+2) years of NOνA results with (3.5+1.5) T2K results, the significance of the atmospheric mass square determination will improve significantly.

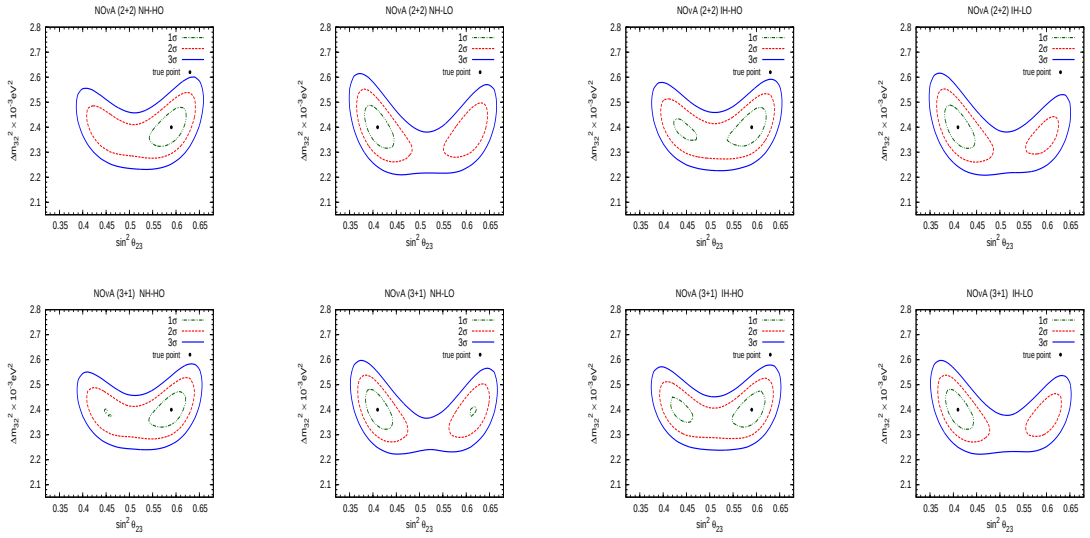

Figure 3.5.5: The 1σ (green), 2σ (red), and 3σ (blue) C.L. regions for $\sin^2\theta_{23}$ vs. Δm^2_{32} with true $\sin^2\theta_{23} = 0.41$ (0.59) for LO (HO) and true δ_{CP}= 0.

It is also possible to obtain $\sin^2\theta_{23}$ - Δm^2_{32} parameter space for non-maximal mixing of atmospheric mixing angle by considering deviation from maximal mixing with $\sin^2\theta_{23}$ = 0.41 (0.59) for Lower Octant (Higher Octant). Fig 3.5.5 shows the $\sin^2\theta_{23}$ - Δm^2_{32} parameter space for NH-HO, NH-LO, IH-HO, IH-LO combinations. It is clear from the figures that, in this case also there is no significant difference between the allowed parameter space for (2+2) and (3+1) years of NOνA run period. Therefore, the expected results on θ_{23} and Δm^2_{32} degeneracy discrimination would not be deteriorated if NOνA switches to antineutrino mode after completion of 2 years of neutrino run.

3.5.4 Correlation between δ_{CP} and $\sin^2\theta_{23}$

Another way to understand the degeneracies among the oscillation parameters by looking at $\sin^2\theta_{23}$ - δ_{CP} plane. This subsection shows the 1σ, 2σ, and 90% C.L. regions for $\sin^2\theta_{23}$ vs. δ_{CP} for both NOνA(2+2) and NOνA(3+1). Fig. 3.5.6 shows the C.L. regions for NOνA with true $\sin^2\theta_{23} = 0.41$ (0.59) for LO (HO) and true δ_{CP}= 0, whereas Fig. 3.5.7 corresponds to true δ_{CP}= $\pi/2$. Further, the true hierarchy is assumed to be Normal Hierarchy and the C.L. regions are obtained both for correct hierarchy (NH-LO and NH-HO) and wrong hierarchy (IH-LO and IH-HO) combinations. The black dots in these figures correspond to the assumed true values. From these figures, we can see that NOνA(2+2) has better degeneracy discrimination

capability than that of NOνA(3+1).

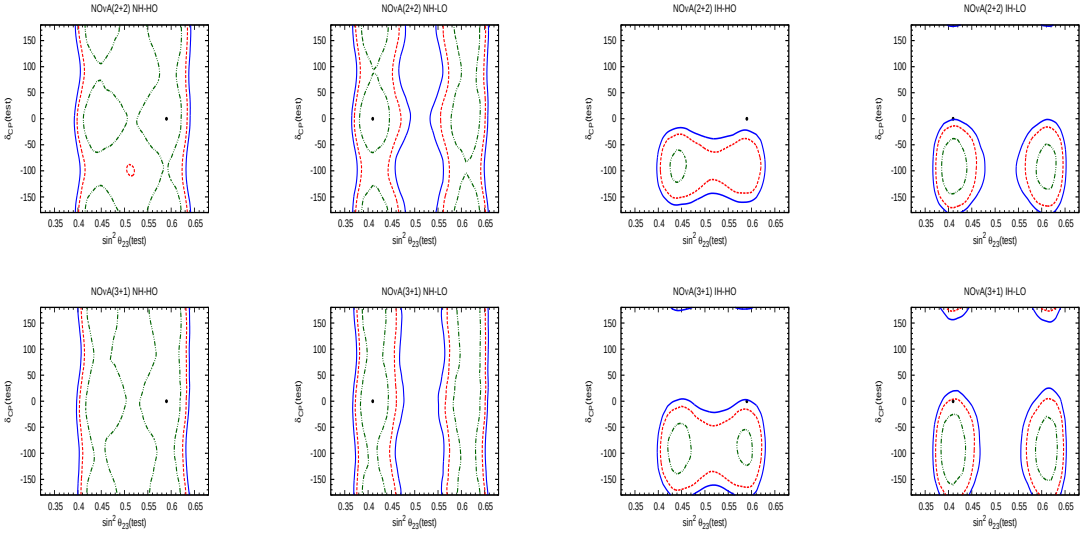

Figure 3.5.6: The 1σ (green), 2σ (red), and 90% (blue) C.L. regions for $\sin^2\theta_{23}$ vs. δ_{CP} with true $\sin^2\theta_{23} = 0.41(0.59)$ for LO(HO) and true $\delta_{CP}= 0$.

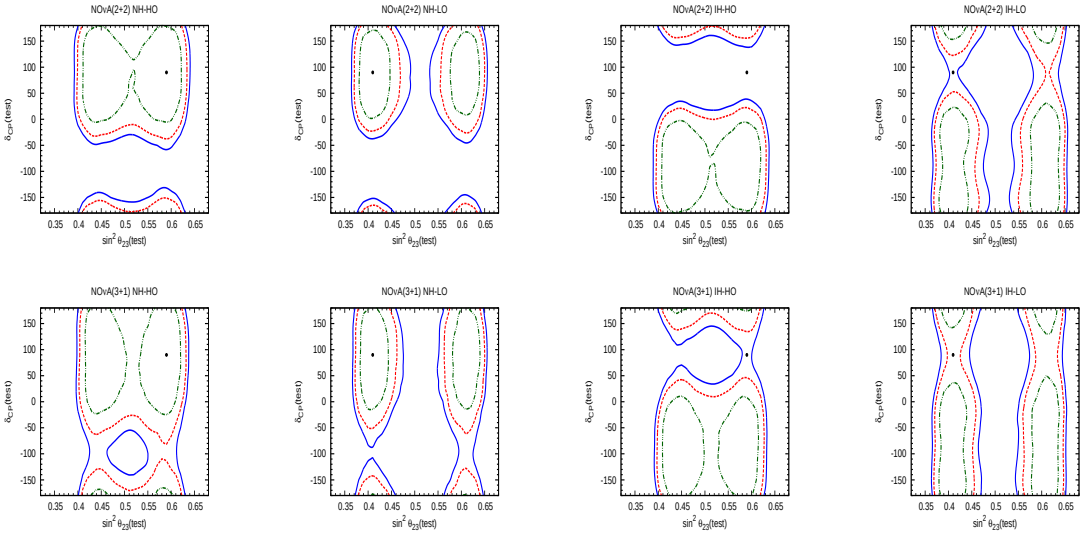

Figure 3.5.7: The 1σ (green), 2σ (red), and 90% (blue) C.L. regions for $\sin^2\theta_{23}$ vs. δ_{CP} with true $\sin^2\theta_{23} = 0.41(0.59)$ for LO(HO) and true $\delta_{CP}= \pi/2$.

3.6 Summary and Conclusions

At this point of time, where NOνA experiment already started taking data, it is crucial to analyze how to extract the best results from this experiment with shortest time span for a complete understanding of oscillation parameters. This chapter discussed

the physics potential as well as the role of parameter degeneracies in the determination of oscillation parameters of NOνA experiment with a total of four years of runs with (2ν+$2\bar{\nu}$) mode. It is found that the parameter degeneracy discrimination capability of NOνA (2+2) is quite good when compared with NOνA (3+1). Looking all these results from these analysis, it is strongly urged that after two years of neutrino running, NOνA should run for two years in antineutrino mode to provide better information about the determination of neutrino mass ordering and the octant of atmospheric mixing angle.

CHAPTER 4

A comprehensive study of the discovery potential of NOνA, T2K and T2HK experiments

4.1 Introduction

The discovery of neutrino oscillations has firmly established that neutrinos are massive. It has marked the beginning of many neutrino oscillation experiments. Moreover, with the exciting discoveries of non-zero θ_{13} and non-maximal θ_{23}, the focus of neutrino oscillation studies has now been shifted towards the determination of other unknown parameters such as determination of the neutrino mass ordering, resolution of the octant of atmospheric mixing angle and to constrain the Dirac-type CP violating phase δ_{CP}. Many dedicated experiments are proposed for instance DUNE and T2HK to determine these parameters which may take at least 10 years from now to become operational. It is therefore very crucial to use the results from the existing experiments to see whether one can get even partial answers to these questions. This chapter investigate the prospects of addressing these issues with the off-axis long-baseline experiments T2K, NOνA and T2HK with updated experimental specifications.

T2HK (Tokai-to-Hyper-Kamiokande) is a future long baseline experiment which is

expected to be operational around 2023. It can be considered as a natural advancement to the ongoing T2K experiment. It has same baseline and off-axis angle as T2K experiment. It uses J-PARC's neutrino experimental facilities with an improved beam power (7.5 MW) and 1 Mt volume water Cherenkov detector, Hyper-Kamiokande (Hyper-K). The other specifications of this experiment can be seen in [69]. It should be noted that the fiducial volume is about 0.56 Mt, therefore T2HK will have high statistics of neutrino events compared to T2K. These features of T2HK make it as one of the most sensitive experiment to probe neutrino CP violation.

The primary objective of T2K, NOνA and T2HK is to unravel the unknowns in the neutrino oscillation sectors. Therefore, these experiments use ν_μ beam and also run in antineutrino mode, which enable them to study the appearance ($\nu_\mu \to \nu_e$) and the disappearance channels ($\nu_\mu \to \nu_\mu$) along with their antineutrino counterparts. Moreover, the leading term in the appearance channels $\nu_\mu \to \nu_e$ ($P_{\mu e}$) and the corresponding antineutrino mode $\bar{\nu}_\mu \to \bar{\nu}_e$ ($P_{\bar{\mu}\bar{e}}$) is proportional to $\sin^2 2\theta_{13} \sin^2 \theta_{23}$ and with the observation of moderately large value of θ_{13}, these experiments are well-suited for the determination of mass hierarchy and the octant of θ_{23}.

This chapter is mainly focussing on

- whether the combination of T2K (3+2) and NOνA (3+3) provide more quantitative answer on the above posed questions than each one of these experiments.

- how the sensitivity on δ_{CP}, mass hierarchy and θ_{23} octant will improve if NOνA runs for 10 years in the (5+5) and (7+3) combination of modes.

- the sensitivities of T2HK experiment for its scheduled run of 3 years in neutrino and 7 years in anti-neutrino mode.

The chapter is organized as follows. The section 4.2 briefly describes the physics reach of these experiments. The prospect of octant resolution and mass hierarchy determination are discussed in section 4.3 and 4.4. Section 4.5 presents the CP violation discovery potential and the correlations between the CP violating phase δ_{CP} with θ_{13}, and θ_{23}. Finally, summary of various results are given in Section4.6.

4.2 Physics reach

As discussed before, determination of the neutrino mass ordering, resolution of the octant of atmospheric mixing angle and to constrain the Dirac-type CP violating phase δ_{CP} in the neutrino sector are the important physics goals of the current and future oscillation experiments. A simple way to achieve the above three goals is to measure the oscillation probabilities $P(\nu_\mu \to \nu_e)$ and $P(\bar{\nu}_\mu \to \bar{\nu}_e)$. This can be seen from the expression for probability of oscillation from $\nu_\mu(\bar{\nu}_\mu) \to \nu_e(\bar{\nu}_e)$ upto first order in $\sin\theta_{13}$ and $\alpha = \Delta m^2_{21}/\Delta m^2_{31}$ [55–57]

$$\begin{aligned} P(\nu_\mu \to \nu_e) &\approx \sin^2 2\theta_{13} \sin^2\theta_{23} \frac{\sin^2(\hat{A}-1)\Delta}{(\hat{A}-1)^2} \\ &+ \alpha \cos\theta_{13} \sin 2\theta_{12} \sin 2\theta_{13} \sin 2\theta_{23} \frac{\sin\hat{A}\Delta}{\hat{A}} \frac{\sin(\hat{A}-1)\Delta}{(\hat{A}-1)} \cos(\Delta + \delta_{CP}), \end{aligned} \tag{4.2.1}$$

where $\Delta m^2_{ij} = m^2_i - m^2_j$, $\Delta = \Delta m^2_{31} L/4E$ and $\hat{A} = 2\sqrt{2} G_F n_e E/\Delta m^2_{31}$. G_F is the Fermi coupling constant and n_e is the electron number density. The transition probability can be enhanced or suppressed depending on the oscillation parameters θ_{13}, θ_{23}, mass hierarchy, i.e., the sign of Δm^2_{31} and CP violating phase δ_{CP}. Parameters α, Δ and $\hat{A}$ are sensitive to neutrino mass ordering. For neutrinos, $\hat{A}$ is positive for normal hierarchy (NH) and negative for inverted hierarchy (IH), while going from neutrino to anti-neutrino mode its sign changes. Moreover, sign of δ_{CP} is reversed for anti-neutrinos. It should be noted from Eq. (4.2.1) that the leading term in the transition probability $P(\nu_\mu \to \nu_e)$ is proportional to $\sin^2 2\theta_{13} \sin^2\theta_{23}$. Therefore, the observed moderately large value of θ_{13} makes it possible for the current generation long-baseline experiments to address the problems of hierarchy and the octant of θ_{23} determination. The second term in Eq. (4.2.1) shows the prominence of matter effect on the oscillation probability. The dependency of all the terms on a moderately large reactor neutrino mixing angle θ_{13} suggests that NOνA detector will be able to collect a good number of $\nu_\mu(\bar{\nu}_\mu) \to \nu_e(\bar{\nu}_e)$ events. Therefore, one can check whether the energy spectrum information will help in resolving the octant degeneracy and mass hierarchy. Moreover, the GLoBES package [128, 129] can be used to obtain the energy spectra. For the simulation, the experimental specifications of currently running experiments T2K and

NOνA are the same as described in the previous Chapter, whereas the input files of T2HK are taken from GLoBES package [70–72]. Futher, the true values of the oscillation parameters that considered in the simulation are provided in Table 4.2.1.

Fig. 4.2.1, shows the energy spectrum of the appearance probabilities $P(\nu_\mu \to \nu_e)$

$\sin^2\theta_{12}$	0.32
$\sin^2 2\theta_{13}$	0.1
$\sin^2\theta_{23}$	0.41 (LO), 0.59 (HO)
Δm^2_{atm}	2.4×10^{-3} eV^2 for NH -2.4×10^{-3} eV^2 for IH
Δm^2_{21}	7.6×10^{-5} eV^2
δ_{CP}	0°

Table 4.2.1: The true values of oscillation parameters considered in the simulations.

for neutrino (left panel) and $P(\bar{\nu}_\mu \to \bar{\nu}_e)$ for antineutrino (right panel) for NOνA experiment, where the value δ_{CP} is varied within the range $-\pi$ to π. In each panel the red (blue) band is for NH (IH). Furthermore, in each band the probability for $\delta_{CP} = 90^\circ$ and $\delta_{CP} = -90^\circ$ cases are shown explicitly by the magenta and green lines. Due to matter effect the probability $P_{\mu e}$ increases for NH and decreases for IH and vice versa for $P_{\bar{\mu}\bar{e}}$. Thus, for δ_{CP} lying in the lower half plane (LHP) i.e., $-180^\circ \leq \delta_{CP} \leq 0$, $P_{\mu e}$ is larger and for δ_{CP} in the upper half plane (UHP) ($0 \leq \delta_{CP} \leq 180^\circ$), $P_{\mu e}$ is much lower. The situations reverse for the antineutrino probability $P_{\bar{\mu}\bar{e}}$. Thus, LHP is the favorable half-plane for NH and UHP is for IH for neutrino mode. However, the most unfavorable condition is (NH, $\delta_{CP} = 90^\circ$) and (IH, $\delta_{CP} = -90^\circ$) as the bands almost overlap with each other for the entire energy range.

The lower panels of Fig. 4.2.1 show the energy spectrum of $P_{\mu e}$ and $P_{\bar{\mu}\bar{e}}$ for two different values of θ_{23} assuming NH to be true hierarchy. The blue band in both the panels is for θ_{23} in the LO and red band is for θ_{23} in the HO. It can be seen from the figures that the two bands overlap with each other for some values of δ_{CP} and distinct for others. The overlap regions are the unfavorable ones for the determination of the θ_{23} octant.

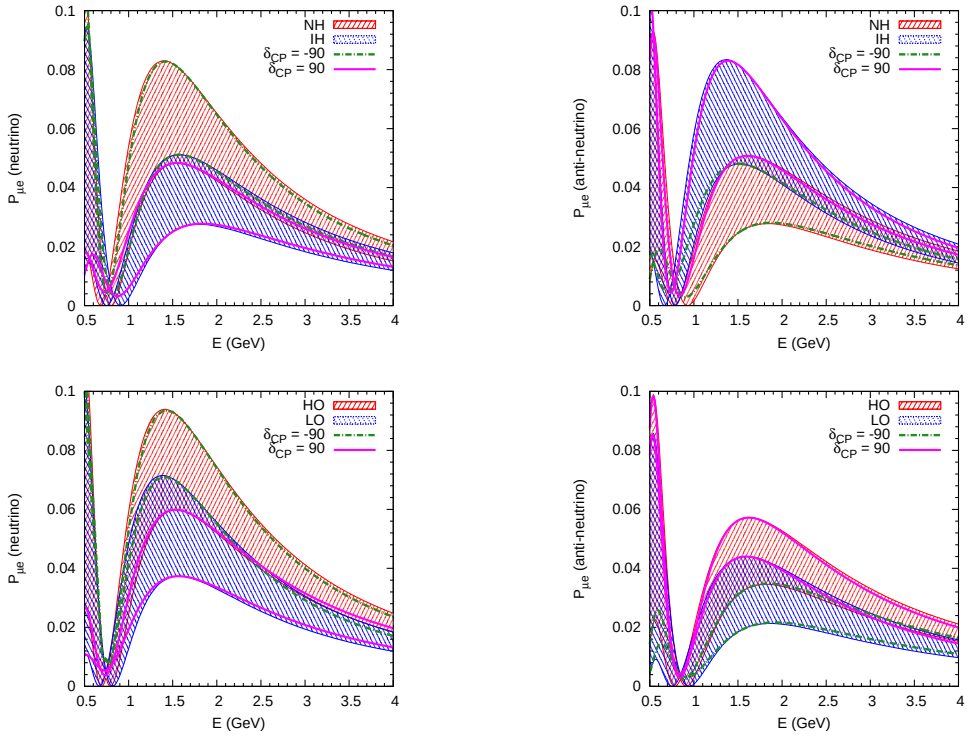

Figure 4.2.1: $P_{\mu e}$ energy spectrum for NOνA experiment. The left (right) panel is for neutrino (antineutrino). The red (blue) band in the top panel corresponds to NH (IH) with $\theta_{23} = 45°$, $\theta_{13} = 9°$, baseline $L = 810$ km and vary δ_{CP} between ($-\pi$ to π). The red (blue) band in the bottom panel is for HO (LO), where we have used $\sin^2\theta_{23} = 0.41$ (0.59) for LO (HO) and keep the hierarchy as normal. Inside each band the probability for $\delta_{CP} = 90°(-90°)$ case is shown by magenta (green) line.

4.3 Octant Resolution as a function of θ_{23}

This section presents the results of both individual and combined octant sensitivities of T2K, NOνA and T2HK experiments. Although the octant sensitivity of various long baseline experiments has been discussed extensively in the literature [73–75], this section is devoted to revisit the octant resolution potential of these experiments with the updated specification details. Therefore, obtain both individual and combined sensitivities for the scheduled run of these experiments, i.e, NOνA with $(3\nu + 3\bar{\nu})$ years of run, T2K with $(3\nu + 2\bar{\nu})$ years of run and for T2HK $(3\nu + 7\bar{\nu})$ years of run. Also obtain the sensitivity for the situation if NOνA continues to run for next 10 years with $(5\nu + 5\bar{\nu})$ as well as $(7\nu + 3\bar{\nu})$ years of running.

The indistinguishability of θ_{23} and $(\pi/2 - \theta_{23})$ is known as octant degeneracy. Moreover,

the relevant oscillation probability expressions for long baseline experiments NOνA, T2K and T2HK with negligible matter effects are given as

$$\mathrm{P}_{\mu\mu} = 1-\sin^2 2\theta_{23}\sin^2\left(1.27\ \frac{\Delta m^2_{31}L}{E}\right)+4\sin^2\theta_{13}\sin^2\theta_{23}\cos 2\theta_{23}\sin^2\left(1.27\ \frac{\Delta m^2_{31}L}{E}\right), \tag{4.3.1}$$

$$\mathrm{P}_{\mu\mathrm{e}} = \sin^2\theta_{23}\sin^2 2\theta_{13}\sin^2\left(1.27\ \frac{\Delta \mathrm{m}^2_{31}\mathrm{L}}{\mathrm{E}}\right). \tag{4.3.2}$$

It should be noted that the leading order term in the ν_μ survival probability ($\mathrm{P}^{\mathrm{v}}_{\mu\mu}$) depends on $\sin^2 2\theta_{23}$ and one can't distinguish between $\mathrm{P}^{\mathrm{v}}_{\mu\mu}(\theta_{23})$ and $\mathrm{P}^{\mathrm{v}}_{\mu\mu}(\pi/2-\theta_{23})$. This kind of degeneracy that comes from the inherent structure of neutrino oscillation probability is called intrinsic octant degeneracy. Whereas in the case of $\mathrm{P}^{\mathrm{v}}_{\mu\mathrm{e}}$ the degeneracy of the octant with the parameter θ_{13} comes into play, since it depends on the parameter combination $\sin^2\theta_{23}\sin^2 2\theta_{13}$. The values of θ_{23} in opposite octant for different values of θ_{13} and δ_{CP} can have the same probabilities, *i.e*, $\mathrm{P}^{\mathrm{v}}_{\mu\mathrm{e}}(\theta_{23},\theta_{13},\delta_{CP}) = \mathrm{P}^{\mathrm{v}}_{\mu\mathrm{e}}(\pi/2-\theta_{23},\theta'_{13},\delta'_{CP})$. This also gives rise to octant degeneracy and known as extrinsic octant degeneracy.

Before presenting the main results, it is possible to check what one can expect about the determination of mass hierarchy and octant of θ_{23} from the bi-event rate plots i.e., neutrino-antineutrino appearance event rates. These event rates can be simulated by using GLoBES package with true values oscillation parameters as given in Table 4.2.1 .

Fig.4.3.1 shows ν versus $\bar{\nu}$ events for all octant-hierarchy combinations. The blue curves are obtained by considering inverted hierarchy mass ordering with $\sin^2\theta_{23} = 0.41(0.59)$ for LO (HO). The red curves are obtained by considering normal hierarchy mass ordering with LO/HO values of $\sin^2\theta_{23}$. These ellipses are plotted by obtaining event spectra of an experiment for different octant-hierarchy combinations with all possible values of δ_{CP}. Each point on x-axis (y-axis) represents the number of events measured by the respective experiments in neutrino (anti-neutrino) mode. The top panel represents the ellipses for (3+2), (5+5) and (7+3) years of running in neutrino and antineutrino modes for T2K, the second panel of the figure represents the NOνA event rates for (3+3), (5+5) and (7+3) years of runs and the bottom panel represents the T2HK event rates for (3+7) years of run. For T2K and T2HK experiments the ellipses of both normal as well as inverted mass orderings overlap with each other for

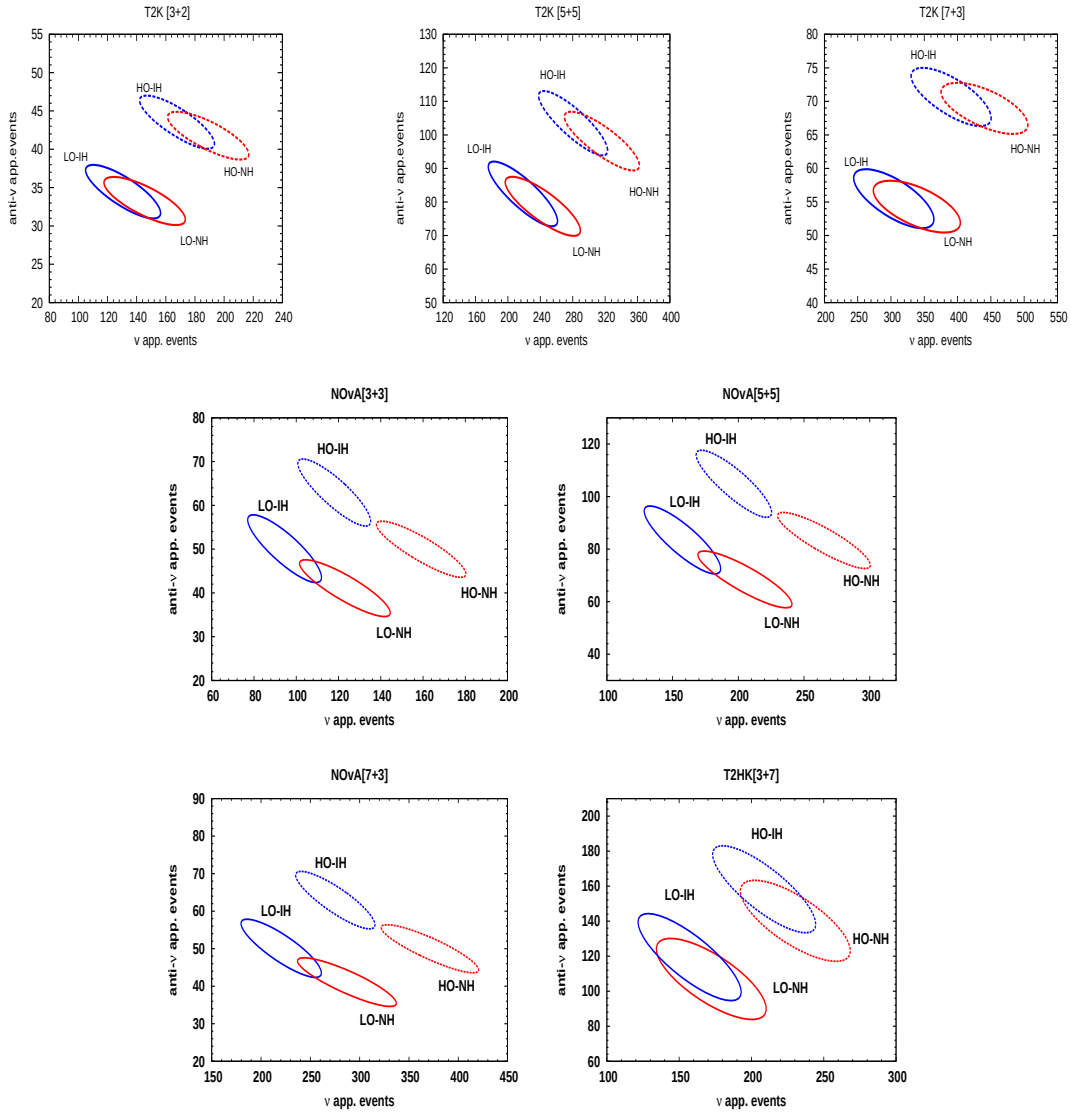

Figure 4.3.1: Neutrino and antineutrino appearance events for the $\nu_\mu \to \nu_e$ versus $\bar{\nu}_\mu \to \bar{\nu}_e$ channels by assuming both IH and NH and for lower and higher octants of θ_{23}.

both the octants whereas for NOνA the overlap region is less (marginal) for LO (HO). Thus, it is very likely that the mass hierarchy and octant degeneracy could be probed better with the NOνA experiment.

In order to obtain the octant sensitivity as a function of true values of $\sin^2\theta_{23}$, calculate the χ^2 for each true value of $\sin^2\theta_{23}$ in the allowed range $[0.32 : 0.68]$ and the true values of other oscillation parameters are kept as in Table 4.2.1. This χ^2 is calculated by using GLoBES gives the significance with which one experiment can distinguish θ_{23} from $\frac{\pi}{2} - \theta_{23}$. Therefore, the test value of $\sin^2\theta_{23}$ must be varied in the lower octant (higher octant) if the true value of $\sin^2\theta_{23}$ is in higher octant (lower octant). Further, the minimum χ^2 is calculated by doing marginalisation over other parameters

($\Delta m^2_{atm} \in [2.05 : 2.75] \times 10^{-3}$ eV^2, $\sin^2 2\theta_{13} \in [0.07 : 0.13]$ and $\delta_{CP} \in [\pi : -\pi]$) and by adding a prior for $\sin^2 2\theta_{13}$. The Fig. 4.3.2 illustrates the ability of NOνA experiment

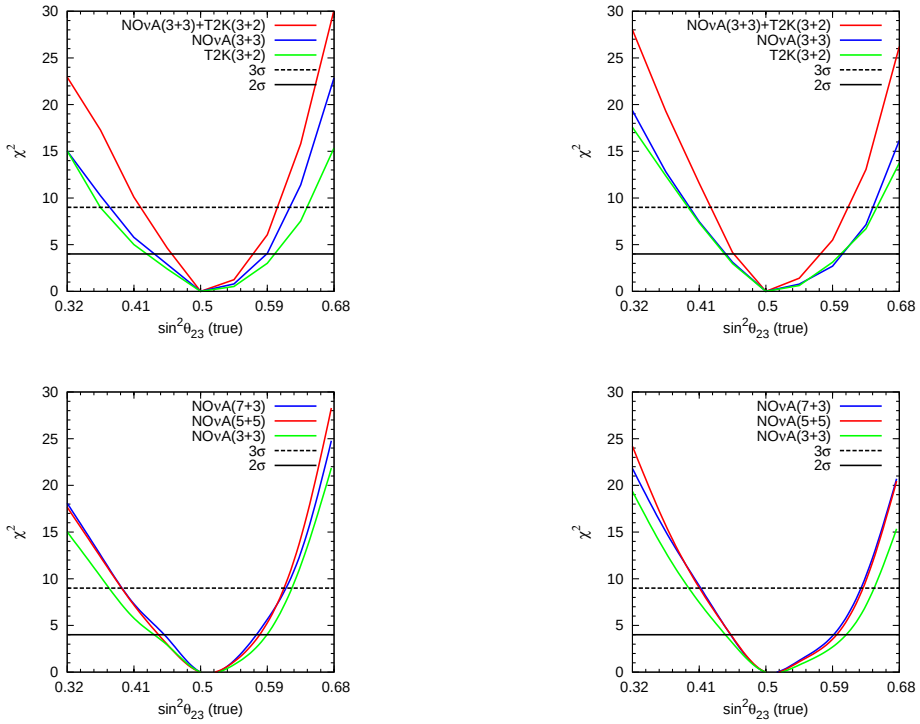

Figure 4.3.2: Octant sensitivity for a combination of T2K and NOνA for the case of Normal (left panel) and Inverted (right panel) hierarchy.

to determine the octant as a function of the true value of θ_{23}. The green, red and blue curves (in the bottom panel) represent the octant resolution of NOνA with $(3+3)$, $(5+5)$ and $(7+3)$ yrs of runs in ν and $\bar{\nu}$ modes respectively. From Fig. 4.3.2, it can be seen that with only T2K data of (3+2) years of run, it is possible to resolve the octant degeneracy with 2σ significance if the true $\sin^2\theta_{23}$ will lie around 0.41 (LO) or 0.59 (HO) and one can have a better sensitivity for NOνA experiment with (3+3) yrs of run period. The significance increases significantly if one combine the data from both T2K and NOνA as seen from the top panels. For ten years of runs of NOνA, although it is possible to get a better sensitivity than that of (3+3) yrs of run, there is no significant difference between (5+5) yrs and (7+3) years of running.

4.4 Mass Hierarchy Determination

Determination of neutrino mass hierarchy is one of the outstanding issues in neutrino oscillation physics. The conventional method to achieve this is by using matter effects in very long baseline neutrino oscillation experiments, as the matter effects enhance the separation between oscillation spectra, and therefore, the event spectra between the normal and inverted hierarchy. This section describes the capabilities of T2K, NOνA and T2HK experiments for the determination of mass hierarchy.

The value of χ^2 has been obtained by using the true parameters as listed in Table 4.2.1, except that of $\sin^2\theta_{23}$, which is taken to be 0.5. In order to get χ^2 as a function of true value of δ_{CP}, it is varied within its full range, i.e., between $[-\pi, \pi]$ and test value of Δm^2_{atm} is varied in IH (NH) range if the true hierarchy is NH (IH). The minimum χ^2 is obtained by doing marginalization over $\sin^2 2\theta_{13}$ and $\sin^2\theta_{23}$ in their 3σ ranges and by adding prior for $\sin^2 2\theta_{13}$ with $\sigma(\sin^2 2\theta_{13}) = 0.01$.

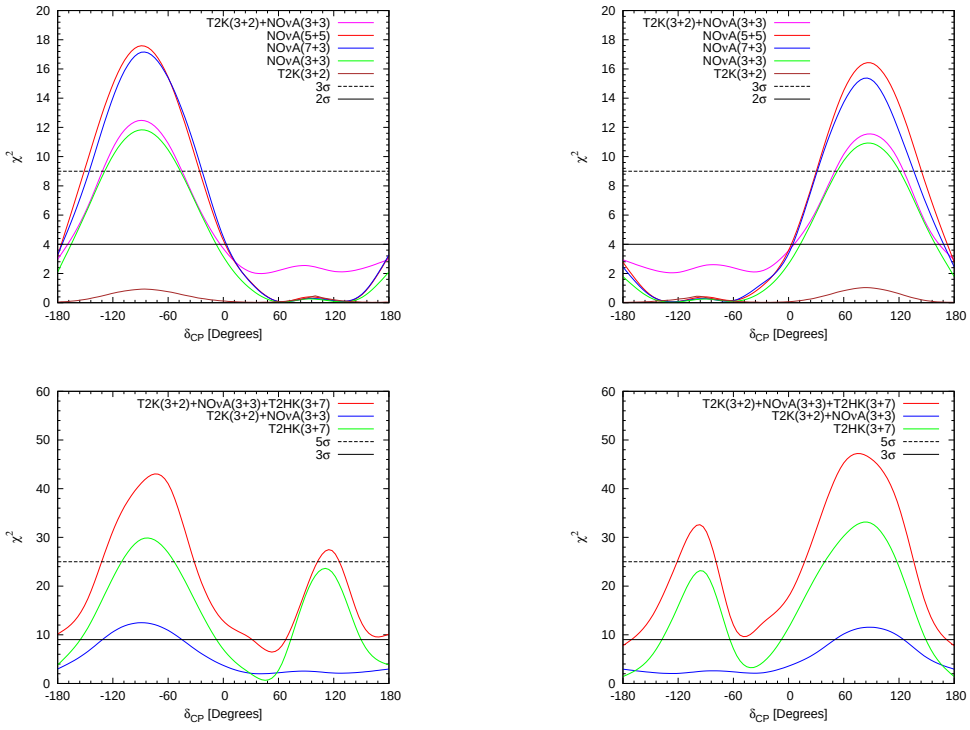

Figure 4.4.1: Mass hierarchy significance as a function of true δ_{CP}. In the left panel Normal hierarchy is considered as true hierarchy and inverted is taken as test hierarchy and in the right panel Inverted hierarchy is considered as true hierarchy and normal is taken as test hierarchy

The Fig. 4.4.1, presents the hierarchy determination sensitivity of T2K, NOνA and

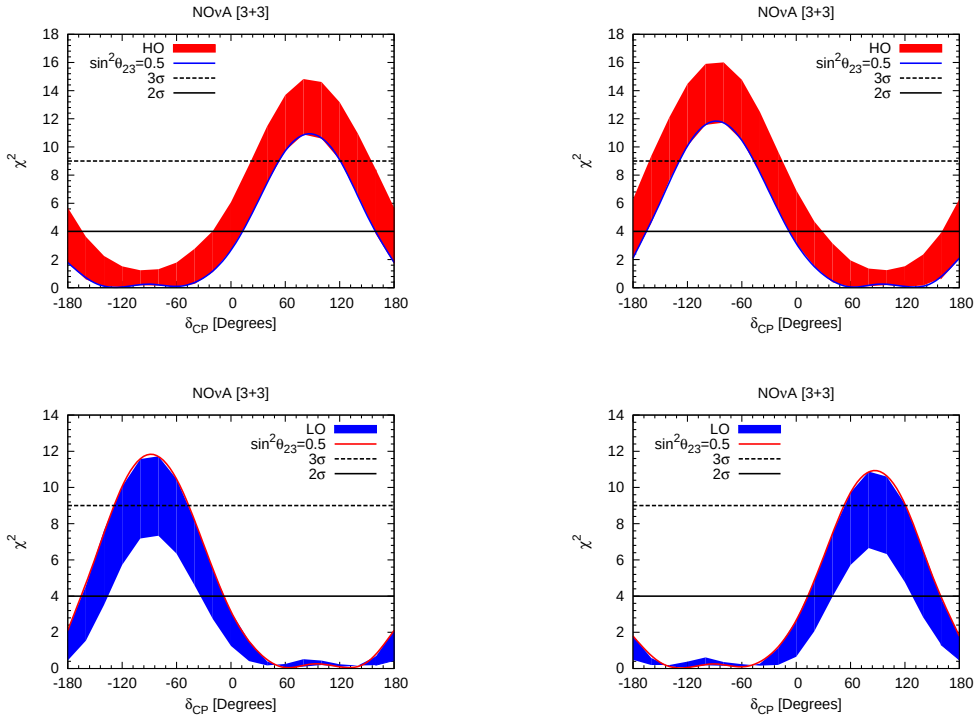

Figure 4.4.2: Mass hierarchy significance with the octant of θ_{23} for the scheduled run of NOνA experiment.

T2HK as a function of true value of δ_{CP}. The left panel corresponds to MH sensitivity with true hierarchy to be NH, whereas right panel corresponds to MH sensitivity with true hierarchy to be IH. It can be seen from the figure that the wrong hierarchy can be ruled out quite effectively in the LHP (UHP) for NH (IH), which is basically the favourable half plane and in the other half plane the mass hierarchy cannot be determined effectively for T2K and NOνA experiments. However, the combined data from these two experiments (T2K (3+2) and NOνA (3+3)) improves the situation significantly and the sensitivity increases to more than 1σ for all values of δ_{CP}. The mass hierarchy significance above 3σ, has a δ_{CP} coverage of 75% for T2HK experiment alone and 90% for combined data of T2K, NOνA and T2HK experiments. One can also to study the effect of θ_{23} octant on the MH sensitivity. In this case, to obtain the MH sensitivity by vary the true value of $\sin^2\theta_{23}$ in LO (HO) which has been shown in Fig.4.4.2 where the red (blue) band in the top (bottom) panel corresponds to HO (LO). It is clear from the figure that the MH sensitivity is significantly large if the value of $\sin^2\theta_{23}$ is in higher octant.

4.5 CP Violation Discovery Potential

Accelerator based long-baseline neutrino oscillation experiments can address CP-violation problem through the appearance channels of $\nu_\mu \to \nu_e$ and $\bar{\nu}_\mu \to \bar{\nu}_e$. From Eq. (4.2.1) one can see that the CP violating effects due to δ_{CP} are modified by all the three mixing angles and their combinations, thus resulting in an eight fold parameter degeneracy. In order to obtain the significance of CP violation sensitivity, one can simulate the true event spectrum by keeping the true values of oscillation parameters as in Table 4.2.1 except for $\sin^2\theta_{23} = 0.5$ and vary the true value of δ_{CP} in its allowed range ($[-\pi, \pi]$). To obtain the χ^2 compare those with test event spectrum for δ_{CP}=0 or π. In order to get minimum χ^2, one has to do marginalization over both hierarchy (to take care of the sign degeneracy of Δm^2_{31}) in its 3σ ranges, $\sin^2 2\theta_{13}$ and $\sin^2\theta_{23}$ in their 3σ and add a prior for $\sin^2 2\theta_{13}$.

The Fig. 4.5.1 presents the sensitivity to rule out the CP conserving scenario, as

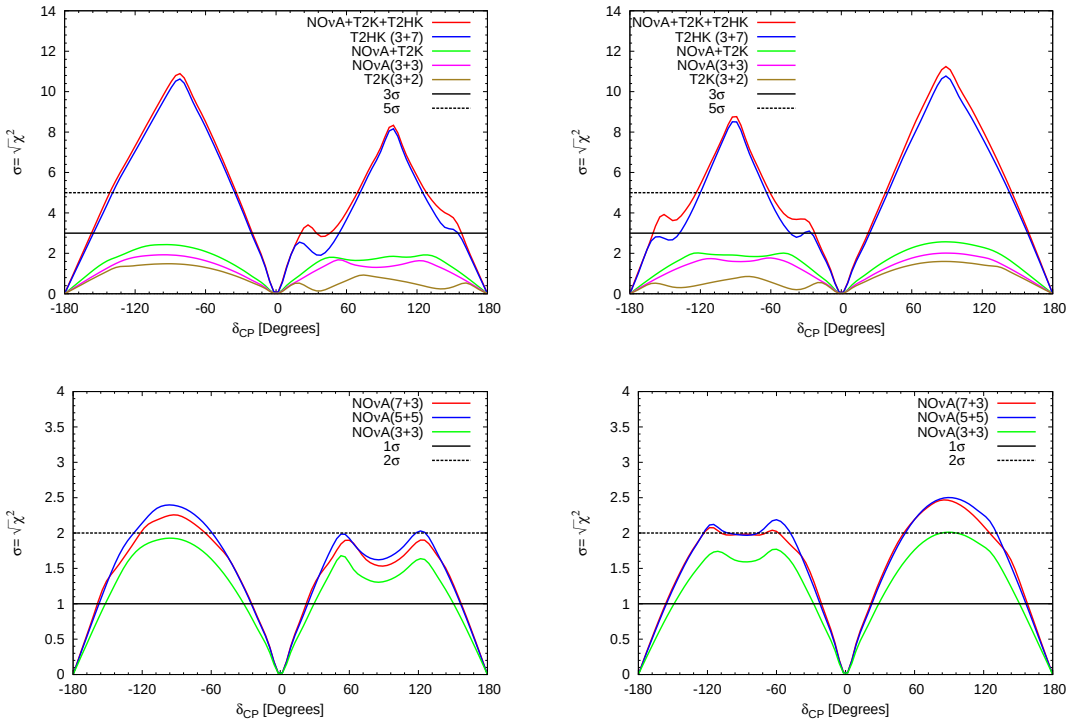

Figure 4.5.1: CP violation sensitivity for different combinations of run time of T2K, NOνA and T2HK experiment for NH (IH) in the left (right) panel.

a function of true δ_{CP} assuming NH (IH) as the true hierarchy in the left panel (right panel). From the figure one can notice that T2K by itself has no CP violation

sensitivity at 2σ C.L.. For NOνA with (3+3) years of running, there will be CP violation sensitivity above 1.5σ level for about one-third of the CP violating phase δ_{CP} space. Furthermore, the synergistic combination of NOνA and T2K leads to much better CP violation sensitivity compared to the individual capabilities. Even the combination of NOνA (3+3) and T2K (3+2) has comparable sensitivity as for 10 years running of NOνA. Owing to the fact that main goal of T2HK experiment is to determine CP violation, one can see that T2HK has a significance of above 5σ C.L. for a fraction of two-fifth values of the CP violating phase δ_{CP} space. This in turn boosts up the sensitivity when its data is added to NOνA (3+3) yrs and T2K (3+2) yrs. From the plots in the lower panel, it can be seen that the sensitivity of NOνA increases slightly for 10 years of run time, with $(5\nu + 5\bar{\nu})$ combination has better sensitivity than that of $(7\nu + 3\bar{\nu})$ combination. The drop in the half planes of δ_{CP} i.e, in the region [0,180]° ([-180,0]°) for NH (IH) is due to the fact that the hierarchy sensitivity is highly sensitive to δ_{CP}. As a result, of marginalization over hierarchy causes the CPV sensitivity to drop for unfavourable values of δ_{CP}.

The left panel of Fig.4.5.2 shows the 1σ uncertainty of δ_{CP} as a function of running

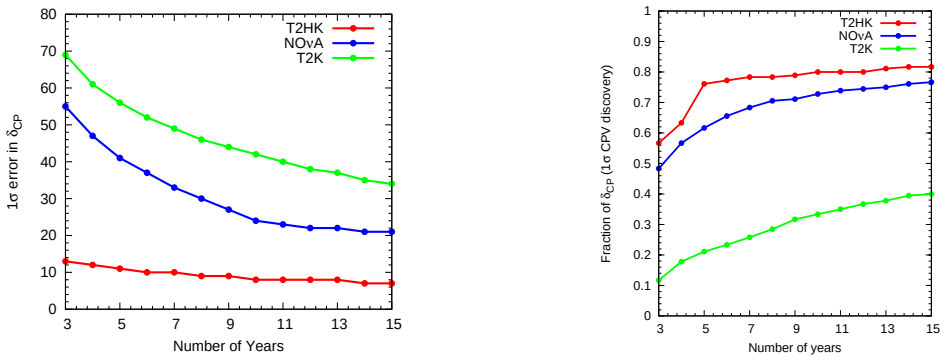

Figure 4.5.2: Sensitivity vs running time: 1σ error in δ_{CP} as a function of running time in years for true value of δ_{CP}=0 (left panel). The fraction of δ_{CP} for which δ_{CP} =0°, 180° is excluded with 1σ as a function of running time.

time (in years) for true value of δ_{CP}=0 and the right panel shows the CP violation sensitivity as a function of running time. In both cases, the ratio of neutrino and antineutrino modes is fixed to 1:1 for T2K and NOνA and 3:7 for T2HK. In this analysis, mass hierarchy is assumed to be unknown, which indicates that the marginalization is done over both the hierarchies. The result shown in Fig. 7 corresponds to true normal hierarchy. From the left panel of the figure, it can be seen that the values of δ_{CP} can be determined to better than 35° (21°) for all values of δ_{CP} for T2K (NOνA). In the

case of T2HK the values of δ_{CP} can be determined to better than 9° for all values of δ_{CP}. From the right panel, it can be seen that CP violation can be observed with more than 1σ significance for 40 (75)% of the possible values of δ_{CP} for T2K (NOνA). Whereas for T2HK, CP violation can be observed with more than 1σ significance for 80% of the possible values of δ_{CP}.

4.5.1 Correlation between δ_{CP} and θ_{13}

The knowledge of reactor mixing angle θ_{13} plays a crucial role in the discovery potential of δ_{CP}. The recent discovery of large value of θ_{13} has boosted the need of study to understand the dependency between δ_{CP} and θ_{13}. This subsection discusses the correlation between the oscillation parameters θ_{13} and δ_{CP}.
In obtaining the confidence region, the true values of parameters are fixed as in Table 4.2.1 and considered true $\sin^2\theta_{23} = 0.59$ for Higher Octant and true $\sin^2\theta_{23} = 0.41$ for Lower Octant, since the octant of θ_{23} is not known. Whereas, the test value of $\sin^2 2\theta_{13}$ is varied in its 3σ range. The χ^2 is calculated by comparing the two event spectra by assuming hierarchy to be normal. Fig. 4.5.3, shows the confidence regions in the $\sin^2 2\theta_{13}$ - δ_{CP} plane for different combinations of T2K and NOνA experiments. One can see from these figures that at the 2σ confidence level, the uncertainty in the knowledge of θ_{23} octant has a noticeable effect on the correlation between δ_{CP} and θ_{13}.

4.5.2 Correlation between δ_{CP} and θ_{23}

From the previous subsection, it can be seen that the uncertainty in θ_{23} has a very large impact on determination of neutrino oscillation parameters. Thus, it is important to understand the exclusive correlation between δ_{CP} and θ_{23} while keeping the true values of rest of the oscillation parameters to be fixed. This subsection discusses the correlation between the oscillation parameters θ_{23} and δ_{CP}. In this analysis, the true events are generated with values of oscillation parameters as in Table 4.2.1. Whereas, the test events are generated by varying the test values of $\sin^2\theta_{23}$ and δ_{CP} in their 3σ ranges. Then obtained the χ^2 by comparing two event spectra and the results are

shown $\sin^2\theta_{23}$ - δ_{CP} plane as in Figs. 4.5.4 and 4.5.5 for all combinations of NOνA experiment.

4.6 Summary and Conclusion

With the recent discovery of the last unknown reactor mixing angle θ_{13}, the mechanism of three flavor neutrino mixing pattern is now well established. But still there are several issues related to neutrino oscillation parameters that remain open, namely the determination of the neutrino mass ordering, resolution of the octant of atmospheric mixing angle and to constrain the Dirac-type CP violating phase δ_{CP}. Therefore, the main focus of the current and future oscillation experiments is to provide answers to some of these unsolved questions.

This Chapter presented an investigation of the prospects of the determination of mass hierarchy, the octant of θ_{23} and the observation of CP violation in the neutrino sector due to δ_{CP} with the currently running accelerator based neutrino experiments NOνA and T2K and the forthcoming T2HK experiment. As the reactor mixing angle θ_{13} is now known to be significantly large, the oscillation probability $P(\nu_\mu \to \nu_e)$ and its corresponding antineutrino counterpart are sensitive for the determination of mass hierarchy and θ_{23} octant.

It is found that T2K experiment with $(3\nu + 2\bar{\nu})$ years of running can resolve the octant degeneracy with nearly 2σ C.L. if the true value of θ_{23} to be around $\sin^2\theta_{23} = 0.41$ (LO) or $\sin^2\theta_{23} = 0.59$ (HO). The sensitivity increases to nearly 3σ with $(3\nu + 3\bar{\nu})$ years running of NOνA. However, if one combine the data from these two experiments the sensitivity increases significantly than the sensitivities of individual experiments. Furthermore, if one assume that NOνA continues data taking for 10 years then octant degeneracy can be resolved with NOνA experiment alone with more than 3σ significance.

For the determination of mass hierarchy, it is also possible to rule out nearly one-third of the δ_{CP} space at 3σ C.L. if one use the synergy between NOνA and T2K experiments. In this case the sensitivity increases significantly for ten years of running of NOνA with $(5 + 5)$ combination is found to be more suitable than the combination of (7+3) years.

Measuring CP violation in the lepton sector is another important challenging problem today. Although the current long-baseline experiments T2K and NOνA are not planned to study leptonic CP violation, one should analyze the synergies between these set-ups which may aid in CP violation discovery by constraining the value of δ_{CP}. Although dedicated long-baseline experiments like DUNE, T2HK are planned to study CP violation in neutrino sector, the analyses discussed in this chapter may have the the first hand information on δ_{CP} from these experiments much before those dedicated facilities are operational. It is found that T2K by itself has marginal CP violation sensitivity at 1σ CL. For NOνA with (3+3) years of running there will be CP violation sensitivity above 1.5σ level for about one-third of the CP violating phase δ_{CP} space. The sensitivity increases slightly for 10 years of run time, with $(5\nu + 5\bar{\nu})$ combination having sensitivity than that of $(7\nu + 3\bar{\nu})$ combination. The data from T2HK experiment will improve the CPV sensitivity significantly. It is also found that the CP violating phase δ_{CP} can be determined to be better than 35°, 21° and 9° for all values of δ_{CP} for T2K, NOνA and T2HK experiments.

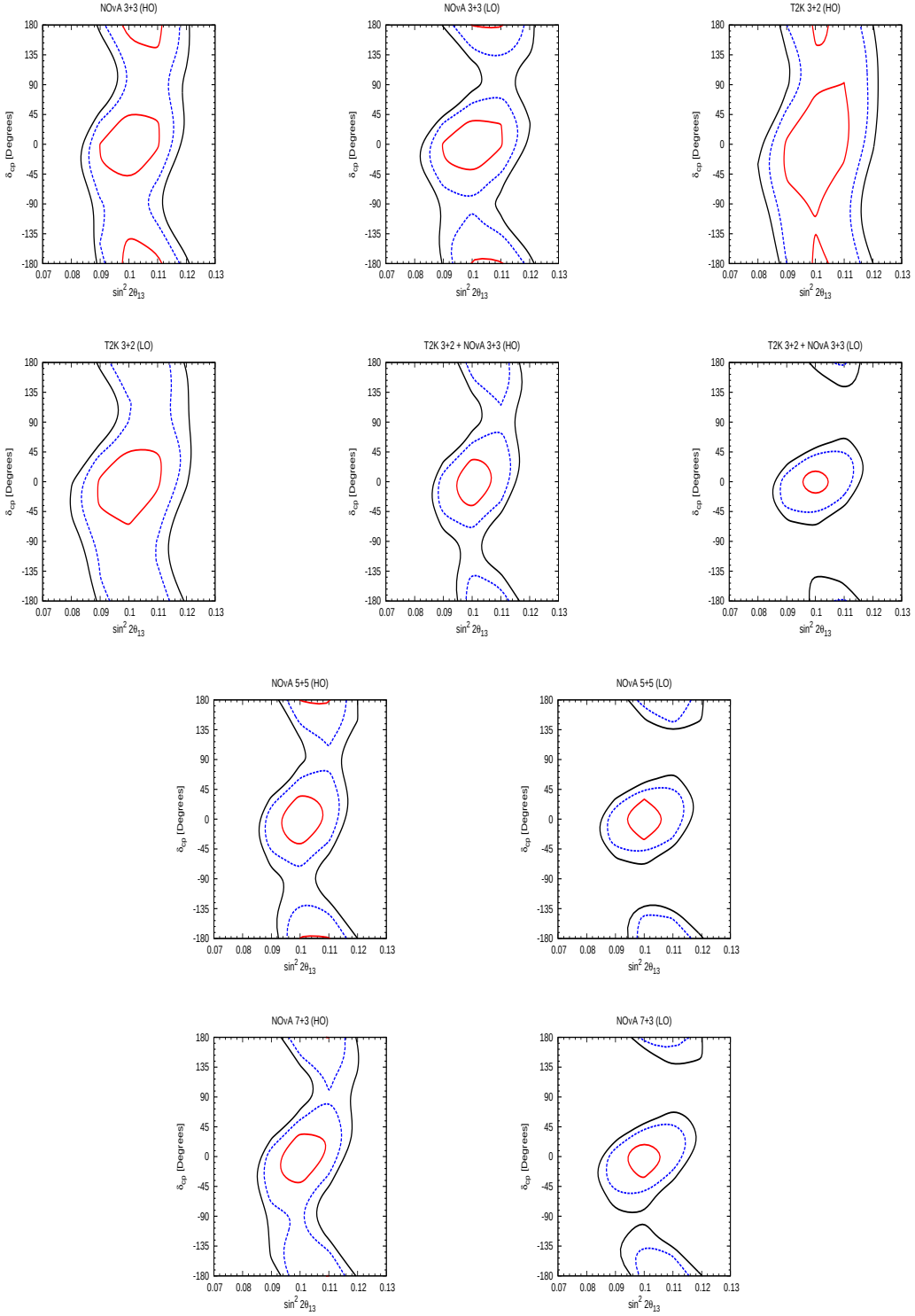

Figure 4.5.3: Confidence region in $\sin^2 2\theta_{13} - \delta_{CP}$ plane for $\delta_{CP} = 0$ and for different run combinations of T2K and NOνA experiments, where the red, blue and black contours represent the 1σ (68.3% C.L.), 1.64σ (90% C.L.) and 2σ (95.45% C.L.) values respectively for two degrees of freedom.

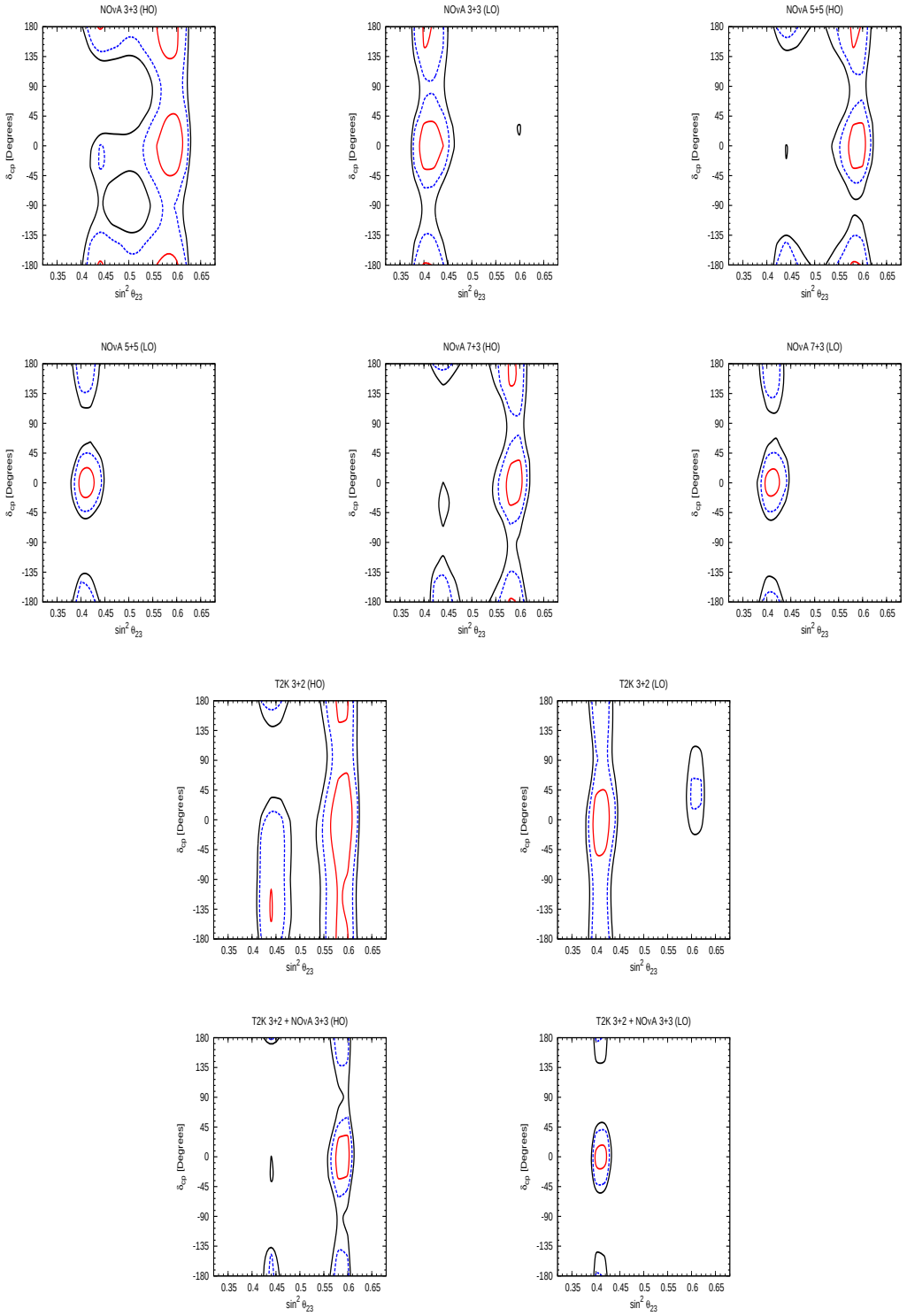

Figure 4.5.4: Confidence region in $\sin^2\theta_{23} - \delta_{CP}$ plane for true $\delta_{CP} = 0$, where red, blue and black contours represent the 1σ (68.3% C.L.), 1.64σ (90% C.L.) and 2σ (95.45% C.L.) values respectively for two degrees of freedom. Here hierarchy is assumed to be IH.

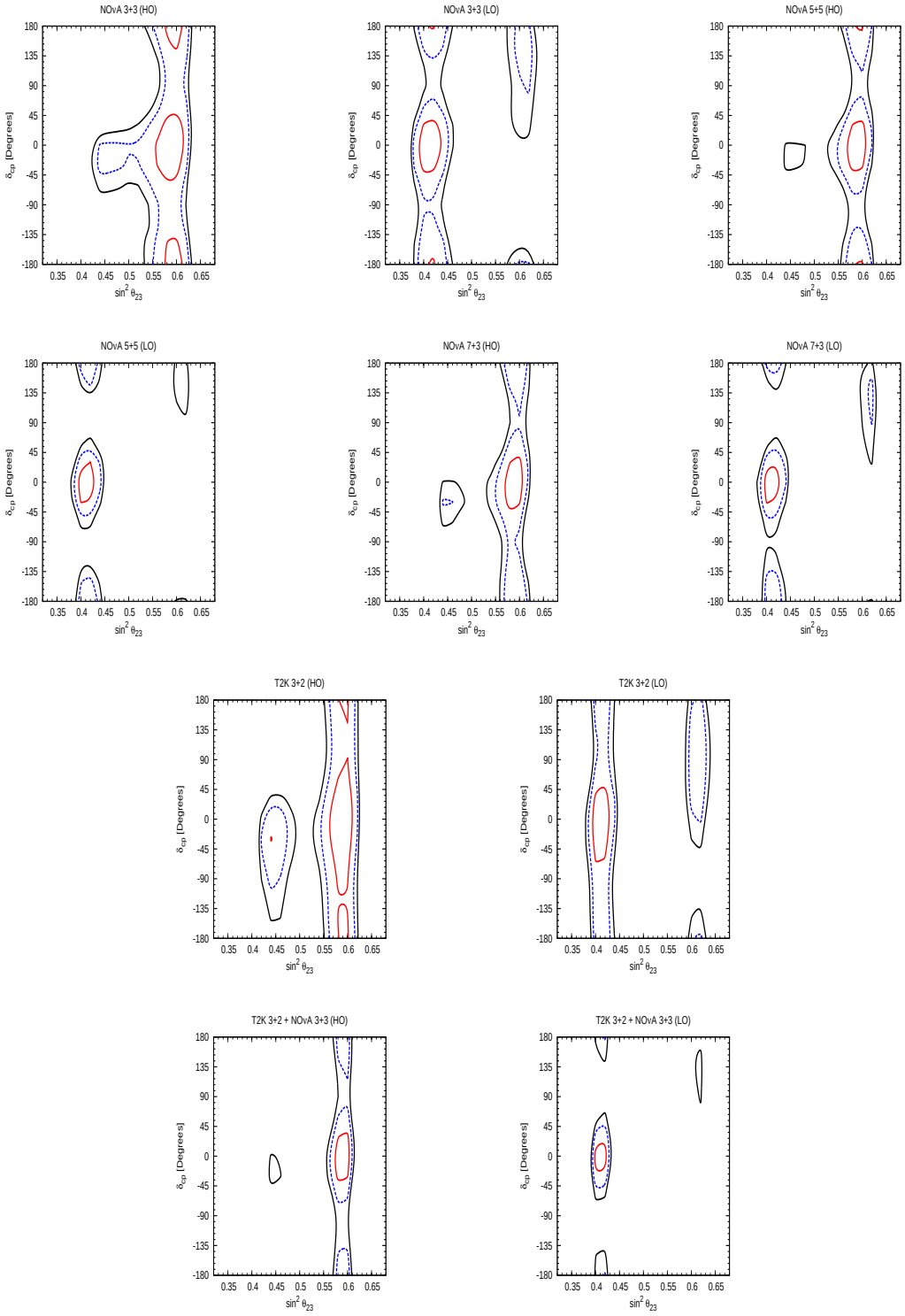

Figure 4.5.5: Confidence region in $\sin^2\theta_{23} - \delta_{CP}$ plane for true $\delta_{CP} = 0$, where red, blue and black contours represent the 1σ, 1.64σ and 2σ values respectively for two degrees of freedom. Here hierarchy is assumed to be NH.

CHAPTER 5

Impact of lepton flavour violating NSIs on the physics potential of long baseline neutrino oscillation experiments

The physics potentials of long baseline experiments to determine the unknowns parameters in the neutrino oscillation are discussed in the previous chapters. As neutrino oscillation physics already entered into its precision era, one should also take care of various sub-leading effects such as Non-standard neutrino interactions (NSIs) in the oscillation physics. This chapter devoted to study the effect of the lepton flavor violating NSIs on the determination of oscillation parameters.

5.1 Introduction

NSIs [76, 77] can be considered as sub-leading effects in the neutrino oscillations, which arise from various new physics scenarios beyond the SM. The NSIs, which come from Neutral Current (NC) interactions can affect the propagation of neutrino, whereas NSIs coming from the Charged Current (CC) interactions of neutrinos with quarks and leptons can affect the production and detection processes of neutrinos. However, this

chapter focuses on the NSIs which affect the propagation of neutrinos. The Lagrangian corresponds to NSIs during the propagation is given by [78],

$$\mathcal{L}_{\rm NSI} = -2\sqrt{2}G_F\varepsilon^{fC}_{\alpha\beta}(\overline{\nu}_\alpha\gamma^\mu P_L\nu_\beta)(\overline{f}\gamma_\mu P_C f)\,, \tag{5.1.1}$$

where G_F is the Fermi coupling constant, $\varepsilon^{fC}_{\alpha\beta}$ are the new coupling constants, so called NSI parameters, f is fermion and $P_C = (1 \pm \gamma_5)/2$ are the right ($C = R$) and left ($C = L$) chiral projection operators. The NSI contributions which are relevant as neutrino propagate through the earth are those coming from the interaction of neutrino with e, u and d because the earth matter is made up of these fermions only. Therefore, the effective NSI parameter is given by

$$\varepsilon_{\alpha\beta} = \sum_{f=e,u,d} \frac{n_f}{n_e}\varepsilon^f_{\alpha\beta}\,, \tag{5.1.2}$$

where $\varepsilon^f_{\alpha\beta} = \varepsilon^{fL}_{\alpha\beta} + \varepsilon^{fR}_{\alpha\beta}$, n_f is the number density of the fermion f and n_e the number density of electrons in earth. For earth matter, one can assume that the number densities of electrons, protons and neutrons are equal, i.e, $n_n \approx n_p = n_e$, which implies that $n_u \approx n_d = 3n_e$.

NSIs and their consequences have been studied quite extensively in the literature both in model dependent (mass models) and independent ways. Furthermore, there are studies, which have been done to investigate the effect of NSIs on atmospheric neutrinos [79–81], solar neutrinos [82–86], accelerator neutrinos [87–97] and supernova neutrinos [98–100]. However, it is very crucial to understand the implications of new physics effects at the long baseline experiments like T2K, NOνA and DUNE. In this regard, there are many recent works which have been discussed the various aspects of NSIs at long baseline experiments [101–103], for instance in [104], the authors have obtained the constraints on NSI parameters using long baseline experiments and in [105] the authors have discussed the degeneracies among the oscillation parameters in presence of NSIs. However, this chapter is mainly focussing on the effect of the lepton flavour violating NSIs on the determination of various unknowns at long baseline experiments.

This chapter is organized as follows. Section 5.2, discusses the basic formalism of

neutrino oscillation including NSI effects. The model-dependent and -independent bound on the NSI parameters are respectively given in section 5.3 and 5.4. Section 5.5 presents the effect of NSI parameters on ν_e appearance oscillation probability and event spectra. The effect of LFV NSI on Physics potential of long baseline experiments are discussed in section 5.6. Section 5.7 discusses the parameter degeneracies among the oscillation parameters in presence of NSIs. Finally, section 5.8 contains the summary and conclusions.

5.2 Neutrino oscillation with NSIs

In the standard oscillation (SO) paradigm, the propagation of neutrino through matter is described by the Hamiltonian

$$\begin{aligned} H_{SO} &= H_0 + H_{matter} \\ &= \frac{1}{2E} U \cdot \mathrm{diag}(0, \Delta m^2_{21}, \Delta m^2_{31}) \cdot U^\dagger + \mathrm{diag}(V_{CC}, 0, 0) \ , \end{aligned} \tag{5.2.1}$$

where the H_0 is the Hamiltonian in vacuum, $\Delta m^2_{ji} = m^2_j - m^2_i$ is neutrino mass squared difference, H_{matter} is the Hamiltonian responsible for matter effect, $V_{CC} = \sqrt{2} G_F n_e$ is the matter potential and U is the PMNS mixing matrix.The NSI Hamiltonian, which is coming from the interactions of neutrinos as they propagate through matter is given by

$$H_{NSI} = V_{CC} \begin{pmatrix} \varepsilon_{ee} & \varepsilon_{e\mu} & \varepsilon_{e\tau} \\ \varepsilon^*_{e\mu} & \varepsilon_{\mu\mu} & \varepsilon_{\mu\tau} \\ \varepsilon^*_{e\tau} & \varepsilon^*_{\mu\tau} & \varepsilon_{\tau\tau} \end{pmatrix}, \tag{5.2.2}$$

where $\varepsilon_{\alpha\beta} = |\varepsilon_{\alpha\beta}| e^{i\delta_{\alpha\beta}}$ are the complex NSI parameters, which give the coupling strength of non-standard interactions. The off-diagonal elements of the NSI Hamiltonian ($\varepsilon_{e\mu}, \varepsilon_{e\tau}$ and $\varepsilon_{\mu\tau}$) are the lepton flavor violating NSI parameters, which are our subject of interest. Then the neutrino oscillation probability in presence of NSI is given by

$$P_{(\nu_\alpha \to \nu_\beta)} = \left| \langle \nu_\beta e^{-i(H_{SO} + H_{NSI})L} \rangle \nu_\alpha \right|^2 . \tag{5.2.3}$$

The following two sections present the bounds on the NSI parameters in a model -dependent and -independent approaches.

5.3 Model-dependent bound on NSI parameter from B-meson decays

The recent experimental results on lepton flavor universality (LFU) violation in B meson decays are indications of new physics beyond the Standard Model. Many theoretical models, which are introduced in the literature as an extension of SM to explain these observed deviations in LFU, lead to NSIs between the elementary particles. Therefore, one can consider a model with an additional Z' boson (which is quite successful in explaining the observed LFU anomalies) and analyze its effect in the lepton flavour violating (LFV) $B_d \to \tau^{\pm} e^{\mp}$ decay modes. From the present upper bound of the $B_d \to \tau^{\pm} e^{\mp}$ branching ratio, one can obtain the constraints on the new physics parameters, which are related to the corresponding NSI parameters in the neutrino sector by $SU(2)_L$ symmetry.

In order to see the possible interplay of new physics in the τ-lepton sector, we first consider the leptonic decay channel $B^- \to \tau^- \bar{\nu}$. During the last few years, there has been a systematic disagreement between the experimental and SM predicted value for the branching ratio of $B \to \tau\nu$ mode. The branching ratio for $B^- \to \tau\nu_\tau$ is given as

$$\mathrm{Br}(B^- \to \tau\bar{\nu}_\tau) = \frac{G_F^2}{8\pi}|V_{ub}|^2 \tau_{B^-} f_B^2 m_B m_\tau^2 \left(1 - \frac{m_\tau^2}{m_B^2}\right)^2 . \tag{5.3.1}$$

This mode is very clean and the only non-perturbative quantity involved in the expression for branching ratio (5.3.1) is the decay constant of B meson. However, there is still a tension between the exclusive and inclusive value of V_{ub} at the level of 3σ. This mode has been precisely measured [106] with a value

$$\mathrm{Br}(B^- \to \tau^- \bar{\nu}_\tau) = (1.14 \pm 0.27) \times 10^{-4} . \tag{5.3.2}$$

The latest result from Belle Collaboration [107]

$$\mathrm{Br}(B^- \to \tau^- \bar{\nu}_\tau) = (1.25 \pm 0.28 \pm 0.27) \times 10^{-4} , \tag{5.3.3}$$

also in the line of the previous measurements. Since there is an uncertainty between the $|V_{ub}|$ values extracted from exclusive and inclusive modes, one should use the SM

fitted value of its branching ratio from UTfit collaboration [108]

$$\mathrm{Br}(B^- \to \tau^- \bar{\nu}_\tau) = (0.84 \pm 0.07) \times 10^{-4} \,. \tag{5.3.4}$$

This value agrees well with the experimental value (5.3.2). However, the central values of these two results differ significantly. One can eliminate the V_{ub} dependence completely by introducing the LFU probing ratio

$$R^{\pi}_{\tau/l} = \frac{\tau_{B^0}}{\tau_{B^-}} \frac{\mathrm{Br}(B^- \to \tau^- \bar{\nu}_\tau)}{\mathrm{Br}(B^0 \to \pi^0 l^- \bar{\nu}_l)} = 0.73 \pm 0.15 \,, \tag{5.3.5}$$

which has around 2.6σ deviation from its SM prediction of $R^{\pi,SM}_{\tau/l} = 0.31(6)$ [109]. Thus, these deviations may be considered as the smoking gun signal of new physics associated with the tauonic sector. The following subsection discusses the bound on the lepton flavor violating new physics parameter associated with the τ lepton from the decay mode $B_d \to \tau^{\pm} e^{\mp}$.

5.3.1 Extraction of the NP parameter from the lepton flavour violating decay process $B_d \to \tau^{\pm} e^{\mp}$

The violation of lepton flavour universality in principle can induce lepton flavour violation. Therefore, one can consider the lepton flavour violating decay process $B_d \to \tau^{\pm} e^{\mp}$, which is induced by flavour changing neutral current interactions. As an example, it is very convenient to consider a simple and well-motivated model, the model with an additional Z' boson, which would induce lepton flavour violating interactions at the tree level. Many SM extensions often involve the presence of an extra $U(1)'$ gauge symmetry and the corresponding gauge boson is generally known as the Z' boson. Here it is possible to consider the model which can induce the lepton flavour violating decays both in the down quark sector and the charged lepton sector [110, 111] at the tree level. Thus, in this model the coupling of Z' boson to down type quarks and charged leptons can be written generically as

$$\mathcal{L} \supset g' \left[\eta^L_{db} \bar{d} \gamma^\mu P_L b + \eta^R_{db} \bar{d} \gamma^\mu P_R b + \eta^L_{e\tau} \bar{e} \gamma^\mu P_L \tau + \eta^R_{e\tau} \bar{e} \gamma^\mu P_R \tau \right] , \tag{5.3.6}$$

where g' is the new $U(1)'$ gauge coupling constant, $\eta^{L/R}_{db}$ are the vector/axial vector FCNC couplings of $\bar{d}b$ quark-antiquark pair to the Z' boson and $\eta^{L,R}_{e\tau}$ are the LFV

parameters.

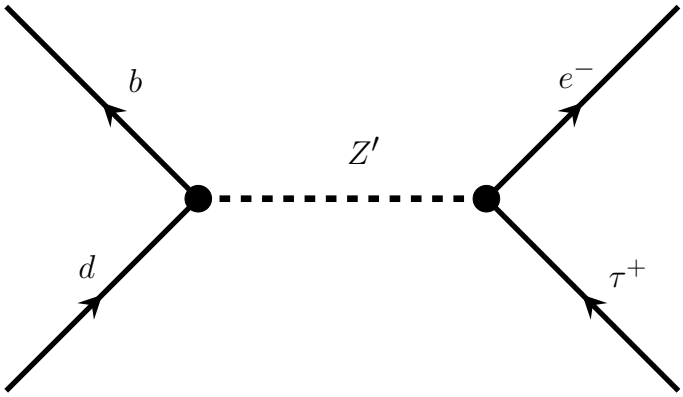

Figure 5.3.1: Feynman diagram for $B_d \to e^-\tau^+$ in the model with Z' boson, where the blobs represent the tree level FCNC couplings of Z' boson.

The constraint on the LFV coupling $\eta_{e\tau}$ can be obtained from the lepton flavour violating B decay mode $B_d \to \tau^\pm e^\mp$. In the SM this decay mode is loop-suppressed with tiny neutrino mass in the loop. However, in the Z' model it can occur at tree level, described by the quark level transition $b \to d\tau^\pm e^\mp$ and is expected to have significantly large branching ratio. The Feynman diagram for this process in the Z' model is shown in Fig. 5.3.1, where the blobs represent the tree level FCNC coupling of Z' boson. The present upper limit on its branching ratio is 2.8×10^{-5}. The effective Hamiltonian describing this process in the Z' model can be given as

$$\mathcal{H}_{eff} = \frac{G_F}{\sqrt{2}} \left(\frac{g' M_Z}{g M_{Z'}}\right)^2 [\bar{d}\gamma^\mu(\eta^L_{db} - \eta^R_{db}\gamma_5)b][\bar{e}\gamma_\mu(\eta^L_{e\tau} - \eta^R_{e\tau}\gamma_5)\tau] \,, \tag{5.3.7}$$

where $M_{Z'}$ is the mass of Z' boson. Further, the transition amplitude is evaluated by using the following matrix element

$$\langle 0|\bar{d}\gamma^\mu(1-\gamma_5)b|B_d\rangle = -if_B p_B^\mu \,, \tag{5.3.8}$$

where f_B is the decay constant of B meson and p_B its momentum. Thus, with eqns. (5.3.7) and (5.3.8), one can obtain the transition amplitude for the process $B_d \to \tau^- e^+$ as

$$\mathcal{M}(B_d \to \tau^- e^+) = -\frac{G_F}{\sqrt{2}} \left(\frac{g' M_Z}{g M_{Z'}}\right)^2 i f_B \eta^R_{db}\, p^\mu_B [\bar{e}\gamma_\mu(\eta^L_{e\tau} - \eta^R_{e\tau}\gamma_5)\tau] \,, \tag{5.3.9}$$

and the corresponding branching ratio is given as

$$\mathrm{Br}(B_d \to \tau^\pm e^\mp) = \frac{G_F^2 \tau_B}{16\pi} \left(\frac{g' M_Z}{g M_{Z'}}\right)^4 |\eta^R_{db}|^2 (|\eta^L_{e\tau}|^2 + |\eta^R_{e\tau}|^2) f_B^2 m_\tau^2 m_B \left(1 - \frac{m_\tau^2}{m_B^2}\right)^2 \tag{5.3.10}$$

where τ_B is the lifetime of B meson. In order to find out the bound on the LFV couplings $\eta^{L,R}_{e\tau}$, one need to know the value of the parameter η_{db}, which can be obtained from the decay process $B_d \to \mu^+\mu^-$. The branching ratio for this decay mode has been recently measured by the LHCb [112] and CMS [113] collaborations and the present world average value [114] is given as

$$\mathrm{Br}(B_d \to \mu^+\mu^-) = \left(3.9^{+1.6}_{-1.4}\right) \times 10^{-10} \,. \tag{5.3.11}$$

The corresponding SM value has been precisely calculated including the corrections of $\mathcal{O}(\alpha)$ and $\mathcal{O}(\alpha_s^2)$ with value [115]

$$\mathrm{Br}(B_d \to \mu^+\mu^-)|_{\mathrm{SM}} \;=\; (1.06 \pm 0.09) \times 10^{-10} \,. \tag{5.3.12}$$

Although the SM predicted value is in agreement with the experimental result but it does not exclude the possible existence of new physics as the central values of these two results differ significantly. The effective Hamiltonian describing this process is given as

$$\mathcal{H}_{eff} = -\frac{G_F}{\sqrt{2}} \frac{\alpha}{2\pi} V_{tb} V^*_{td} C_{10} [\bar{d}\gamma^\mu(1-\gamma_5)b][\bar{\mu}\gamma_\mu\gamma_5\mu], \tag{5.3.13}$$

where C_{10} is the Wilson coefficient and its value at the m_b scale is given as $C_{10} = -4.245$. The corresponding Hamiltonian in the Z' model is given as

$$\mathcal{H}^{Z'}_{eff} = \frac{G_F}{\sqrt{2}} \left(\frac{g' M_Z}{g M_{Z'}}\right)^2 [\bar{d}\gamma^\mu(\eta^L_{db} - \eta^R_{db}\gamma_5)b][\bar{\mu}\gamma_\mu(C^\mu_V - C^\mu_A\gamma_5)\mu] \,, \tag{5.3.14}$$

where C^μ_V and C^μ_A are the vector and axial-vector couplings of the Z' boson to $\mu^-\mu^+$ pair. Including the contribution arising from the Z' exchange to the SM amplitude,

one can write the amplitude for $B_d \to \mu\mu$ process as

$$\begin{aligned}\mathcal{M}(B_d \to \mu^+\mu^-) &= i\frac{G_F}{\sqrt{2}}\frac{\alpha}{\pi} iV_{tb}V_{td}^* f_B m_B m_\mu C_{10}[\bar{\mu}\gamma_5\mu]\left(1 + \frac{g'^2 M_Z^2}{g^2 M_{Z'}^2}\frac{2\pi\eta_{db}^R C_A^\mu}{\alpha V_{tb}V_{td}^* C_{10}}\right) \\ &= \mathcal{M}^{SM}\left(1 + \frac{g'^2 M_Z^2}{g^2 M_{Z'}^2}\frac{2\pi\eta_{db}^R C_A^\mu}{\alpha V_{tb}V_{td}^* C_{10}}\right) . \qquad (5.3.15)\end{aligned}$$

Thus, from Eq. (5.3.15), one can obtain the branching ratio as

$$\mathrm{Br}(B_d \to \mu\mu) = \mathrm{Br}(B_d \to \mu\mu)^{SM}\left|1 + \frac{g'^2 M_Z^2}{g^2 M_{Z'}^2}\frac{2\pi\eta_{db}^R C_A^\mu}{\alpha V_{tb}V_{td}^* C_{10}}\right|^2 . \qquad (5.3.16)$$

Assuming the axial-vector coupling of Z' to muon pair, i.e., C_A^μ has the same form as the corresponding SM Z boson coupling to fermion-antifermion pair with value $C_A^\mu = -1/2$. Now with Eqn. (5.3.16) and considering 1-σ range of experimental and SM predicted branching ratios from (5.3.12) and (5.3.11), the constraint on the parameter η_{db}^R is found to be

$$0.006 \leq |\eta_{db}^R| \leq 0.014, \qquad (5.3.17)$$

for $M_{Z'}$=1 TeV and the particle masses and CKM elements are taken from [106]. Using this allowed range of $|\eta_{db}^R|$, the bounds on the LFV couplings $\eta_{e\tau}^{L,R}$ can be obtained by comparing (5.3.10) with the corresponding branching ratio $\mathrm{Br}(B_d \to \tau e) < 2.8 \times 10^{-5}$ [106] as

$$|\eta_{e\tau}^L| = |\eta_{e\tau}^R| < 19.2 , \quad \text{for } |\eta_{db}^R| = 0.014 , \qquad (5.3.18)$$

where it is assumed that $\eta_{e\tau}^L = \eta_{e\tau}^R$. These couplings can be redefined in terms of another set of new couplings as $\varepsilon_{e\tau} = (g'^2 M_Z^2/g^2 M_{Z'}^2)\eta_{e\tau}$, which can give the relative NP strength in comparison to SM ones as

$$|\varepsilon_{e\tau}^L| = |\varepsilon_{e\tau}^R| < 0.16 , \quad \text{for } |\eta_{db}^R| = 0.014 , \qquad (5.3.19)$$

for $g' \simeq g$ and a TeV scale Z' boson, i.e., $M_{Z'} \simeq 1$ TeV. Since these parameters are related to the corresponding NSI parameters of the neutrino sector by the $SU(2)_L$ symmetry. Analogously, one can obtain the bounds on the NSI couplings $\varepsilon_{e\mu}$ from $B_d \to e\mu$ decay, which are expected to be of the same order as $\varepsilon_{e\tau}$.

5.4 Model independent bound on NSI parameter

Almost all current neutrino oscillation data are consistent with the standard oscillation paradigm. Therefore, the effect of NSI on the oscillation phenomena is expected to be very small. Moreover, some neutrino mass models for instance, triplet seesaw model [116], Zee Babu model [117] predict the value of NSI parameters of the order of $10^{-4} - 10^{-3}$, which depend on the scale of new physics and the neutrino mass ordering. The strong constraints on NSI parameters make them very difficult to be observed in the long baseline experiments. The model independent current upper bounds of NSI parameters at 90 % C.L. are given as [118–123]

$$|\varepsilon_{\alpha\beta}| \; < \; \begin{pmatrix} 4.2 & 0.3 & 0.5 \\ 0.3 & 0.068 & 0.04 \\ 0.5 & 0.04 & 0.15 \end{pmatrix}. \tag{5.4.1}$$

From the above equation, it should be noted that the bound on LFV-NSI parameters as $|\varepsilon_{e\mu}| < 0.3, |\varepsilon_{\mu\tau}| < 0.04$ and $|\varepsilon_{e\tau}| < 0.5$, therefore, in the analysis one can use the representative values for $\varepsilon_{e\mu}, \varepsilon_{\mu\tau}$ and $\varepsilon_{e\tau}$ close to their upper bounds, i.e., as 0.2, 0.03 and 0.3 respectively. It should also be noted that each NSI parameter $\varepsilon_{\alpha\beta}$ has a CP phase $\delta_{\alpha\beta}$, which can vary between $-\pi$ to π.

5.5 Effect of NSI on ν_e appearance probability and event spectra

In general, the measurement of branching ratios (BRs) and the CP violation parameters can be used to probe the New Physics effects or non-standard interactions in the flavor sector. If any inconsistency found between the experimental observed values and the corresponding SM predictions in these observables, it would imply the presence of new physics. However, in the case of neutrinos one can not use branching ratio measurements to study the new physics effects, since the mass difference between neutrinos is really small and also experiments detect neutrinos as flavour states (mixed state of mass eigenstates). The various issues regarding the BR measurement of neutrinos are discussed in [124]. Therefore, in the case of neutrinos, new physics effect

can be studied by using the oscillation probabilities. The super-beam experiments like T2K, NOνA and DUNE use muon neutrino beams as neutrino source. Therefore, this section discusses the consequences of LFV-NSI parameters on neutrino appearance ($\nu_\mu \to \nu_e$) probability.

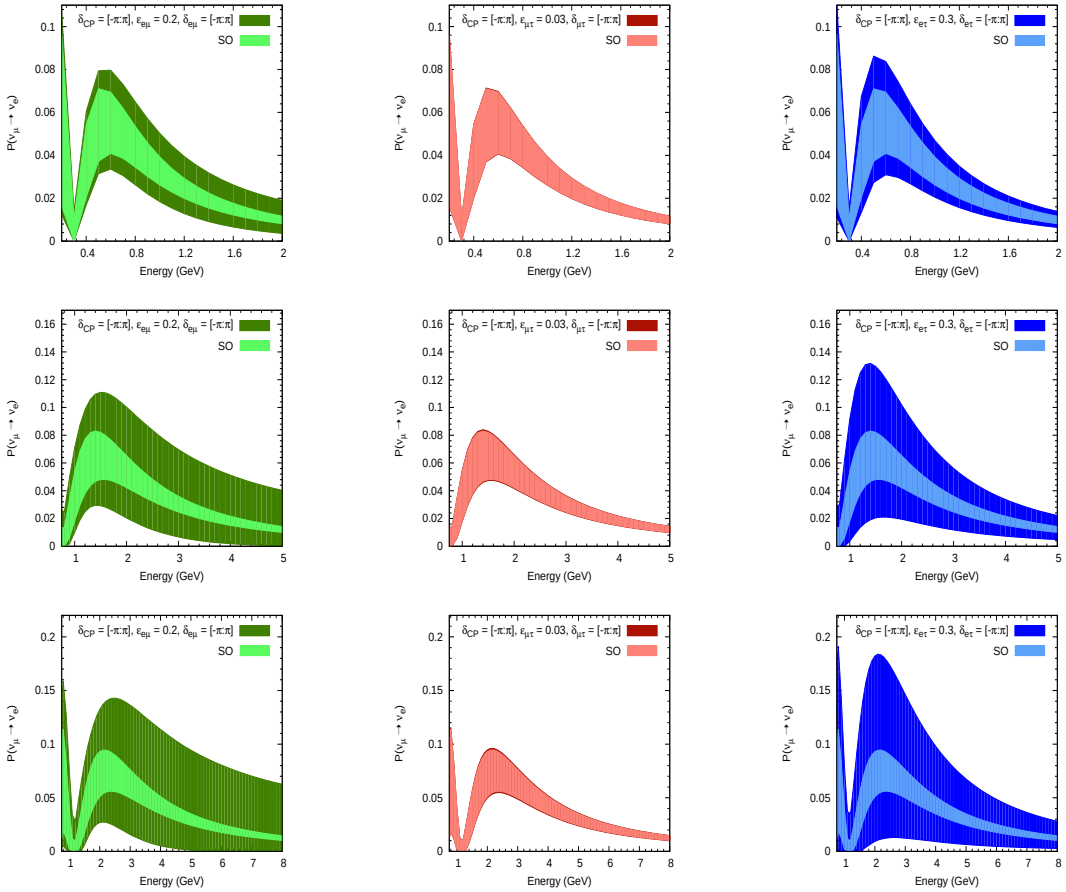

Figure 5.5.1: Neutrino appearance probability for the $\nu_\mu \to \nu_e$ without NSI (light shaded region) and with NSI (dark shaded green, red and blue regions are correspond to $\varepsilon_{e\mu}, \varepsilon_{\mu\tau}$ and $\varepsilon_{e\tau}$ parameters contribution respectively) for T2K (top panel), NOνA (middle panel) and DUNE (bottom panel). The hierarchy is assumed to be NH

To study the implications of LFV-NSI on the propagation of neutrinos, one can use GLoBES package [128, 129] along with snu plugin [130, 131]. This chapter not only focus on the current generation experiments but also study the effect of NSI on the sensitivities of proposed experiment Deep Underground Neutrino Experiment (DUNE). DUNE is a next-generation long-baseline neutrino experiment based at the Fermi National Accelerator Laboratory. It uses Liquid Argon (LAr) detector with fiducial volume 35 kt and the detector is placed at 1300 km away from Fermilab. Moreover, the neutrino beam with energy between 0.5 GeV and 8 GeV is obtained from a proton beam with beam power 700 KW and beam energy 120 GeV (6×10^{20} protons on

Expt. setup	T2K [70–72]	NOνA [37, 53, 64]	DUNE [126, 127]
Detector	Water Cherenkov	Scintillator	Liquid Argon
Beam Power(MW)	0.75	0.77	0.7
Fiducial mass(kt)	22.5	14	35
Baseline length(km)	295	810	1300
Running time (yrs)	5 (3ν+$2\bar{\nu}$)	6 (3ν+$3\bar{\nu}$)	10 (5ν+$5\bar{\nu}$)

Table 5.5.1: The experimental specifications.

target (POT) per year). Furthermore, the GLoBES files and the detector parameter assumptions for DUNE are taken from [125]. In addition, the uncertainty on signal normalization and background normalization that considered in the analysis are 5% and 10% respectively . Moreover, the experimental details of T2K, NOνA and DUNE are given in Table 5.5.1. The values of standard oscillation parameters that are used in the analysis are given in the Table 5.5.2.

Oscillation Parameter	True Value
$\sin^2\theta_{12}$	0.32
$\sin^2 2\theta_{13}$	0.1
$\sin^2\theta_{23}$	0.5, 0.41 (LO), 0.59 (HO)
Δm^2_{atm}	2.4×10^{-3} eV^2 for NH -2.4×10^{-3} eV^2 for IH
Δm^2_{21}	7.6×10^{-5} eV^2
δ_{CP}	0°

Table 5.5.2: The true values of oscillation parameters considered in the simulations are taken from [28].

The Fig. 5.5.1 illustrates the calculated transition probability with and without NSI for T2K (top panel), NOνA (middle panel) and DUNE (bottom panel) by assuming hierarchy as NH for neutrinos. In the figure, the light shaded regions correspond to probability in the standard oscillation (SO) paradigm, whereas the dark shaded green, red, and blue regions represent the additional contribution to the oscillation probability, which are coming from NSI parameters $\varepsilon_{e\mu}, \varepsilon_{\mu\tau}$ and $\varepsilon_{e\tau}$ respectively. From the figure, one can see that the NSI contribution to oscillation probability is noteworthy in presence of $\varepsilon_{e\tau}$ and $\varepsilon_{e\mu}$ parameters, whereas the contribution from $\varepsilon_{\mu\tau}$ is negligible. It can also be seen from the figure that there is significant change in the oscillation probability in the presence of NSIs for both NOνA and DUNE, whereas for T2K, the effect is found to be rather small, i.e., NOνA and DUNE are more sensitive to

NSI effects. It should be noted from the figure that there is a substantial change in the oscillation probability of DUNE experiment in the presence of NSI. Therefore, DUNE experiment can be used to investigate various effect of NSI, which are expected to be observed in the long baseline experiment. Moreover, NSI can even affect the results, which require much precision on their measurements for the determination of the unknowns in neutrino sector, of the currently running experiments like T2K and NOνA.

One of the most convenient way to show the effect of NSI parameter $\varepsilon_{e\tau}$ on oscillation probability, is by obtaining $\Delta P = |P_{NSI} - P_{SI}|$ (where $P_{NSI(SI)}$ denotes the probability with Non-standard (Standard) interactions) for different baseline length and energy using the neutrino oscillation parameters as given in Table 5.5.2. The contour plots for ΔP as a function of neutrino energy and baseline length are given in the Fig. 5.5.2. The different shades in the figure correspond to different ranges of ΔP. It can be seen from the figure that $\Delta P \in$ (0.02,0.03) and (0.04,0.05) for NOνA ($L = 810$ km and $E = 2$ GeV) and DUNE ($L = 1300$ km and $E = 2.5$ GeV) respectively for NH, whereas for IH, $\Delta P \in$ (0.02,0.03) for both NOνA and DUNE. This implies that the non-standard interactions can affect the measurement of oscillation parameters at NOνA and DUNE experiments significantly.

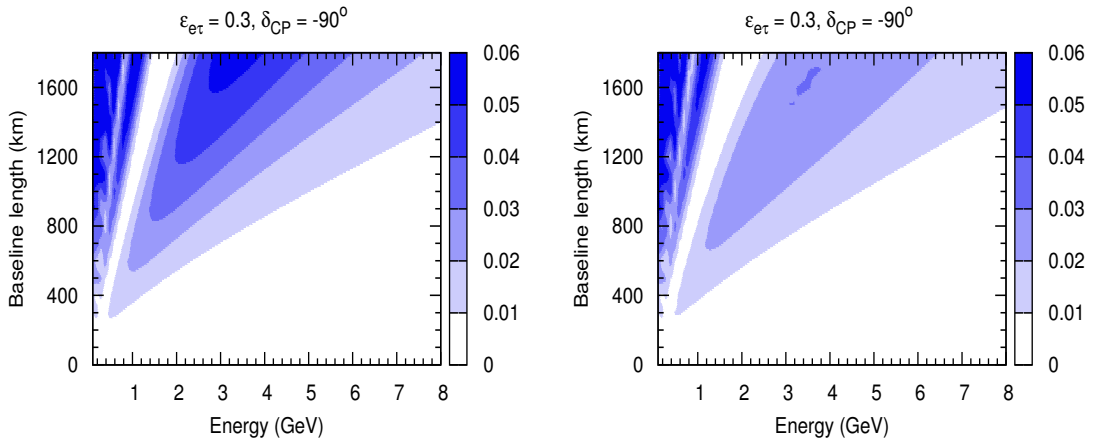

Figure 5.5.2: The $\Delta P = |P_{NSI} - P_{SI}|$ as a function of neutrino energy and baseline length. The left (right) panel corresponds to Normal (Inverted) hierarchy.

The oscillation probabilities as a function of CP- violating phase for NOνA (DUNE) is shown in the left (right) panel of Fig. 5.5.3. The dark solid (dashed) curve in the figure

corresponds to oscillation probability for NH (IH) in the presence of NSI, whereas the light solid (dashed) curve corresponds to oscillation probability for NH (IH) in the standard oscillation. From the figure, it can be seen that there is an enhancement (diminution) in the probability for CP- violating phase in the range $0° \leqslant \delta_{CP} \leqslant 180°$ ($-180° \leqslant \delta_{CP} \leqslant 0°$) for both mass hierarchies, if the NSI phase $\delta_{e\tau}$ is zero. Further, the ν_e appearance event spectra for NOνA and DUNE are shown in Figs. 5.5.4 and 5.5.5 respectively. From these figures, one can see that the event rate in the presence of NSI is larger than that in SO for δ_{CP} =0 or 90°. Whereas for $\delta_{CP} = -90°$, the event rates in presence of NSI is lesser than that in SO for $\delta_{e\tau} = 0$.

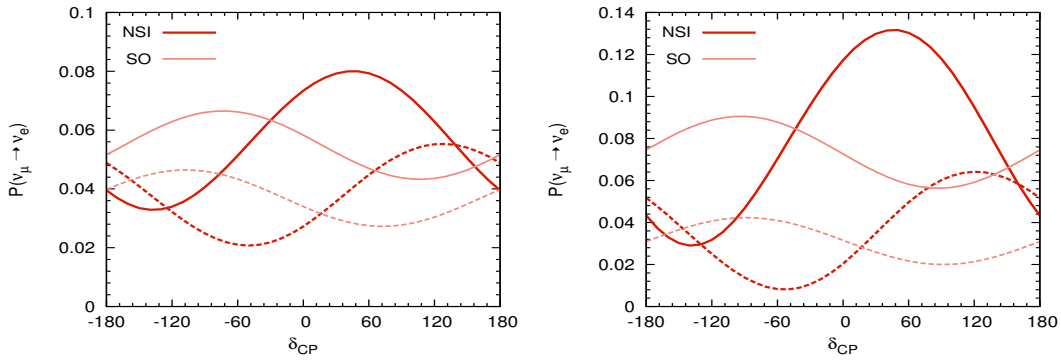

Figure 5.5.3: The left (right) panel shows the appearance oscillation probability for NOνA (DUNE). The dark (light) coloured curves represent the oscillation probability in the presence (absence) of NSI for $\delta_{e\tau} = 0$. The solid (dashed) curves correspond to NH (IH).

5.6 NSI effect on Physics potential of long baseline experiments

As the primary objective of long baseline experiments is the determination of the various unknowns in the phenomenon of neutrino oscillation, it is very crucial to study the effect of LFV-NSI on the determination of these unknowns. This section is devoted to the thorough study of sensitivities of long baseline experiments in presence of NSIs. From the previous section, it can be understood that the NSI parameter $\varepsilon_{e\tau}$ can significantly change the oscillation probability. Therefore, for simplicity, this section focus on the effect of $\varepsilon_{e\tau}$ on the determination of other unknowns in neutrino oscillation sector. Moreover, this chapter also discusses a comparative study of the

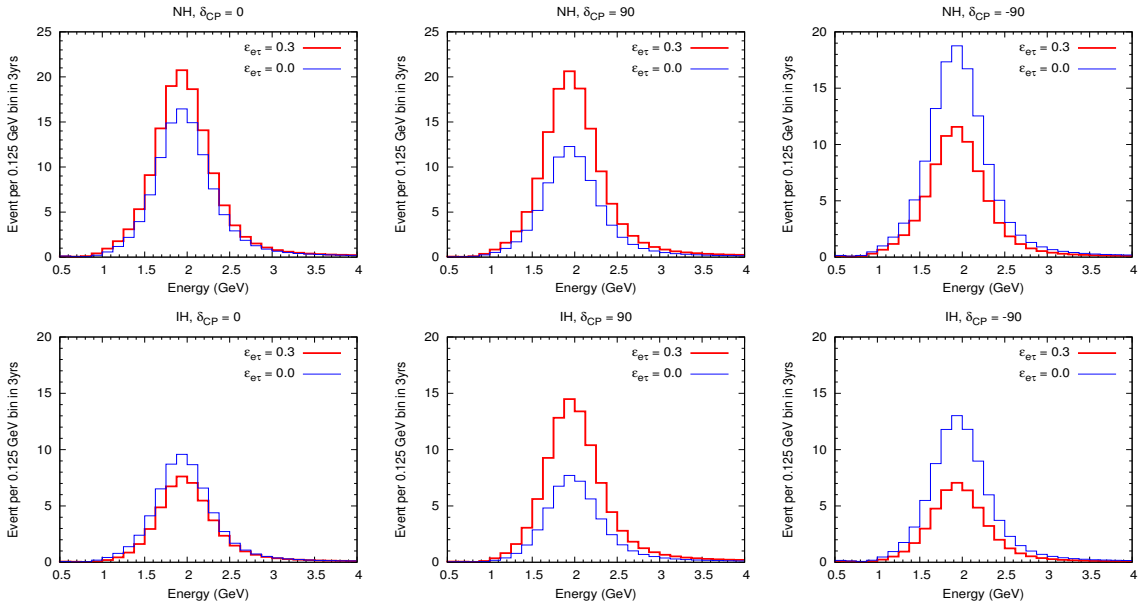

Figure 5.5.4: The event spectra of NOνA for different values of CP violating phase, i.e, $\delta_{CP} = 0°$ (left panel), $\delta_{CP} = 90°$ (middle panel), and $\delta_{CP} = -90°$ (right panel) .

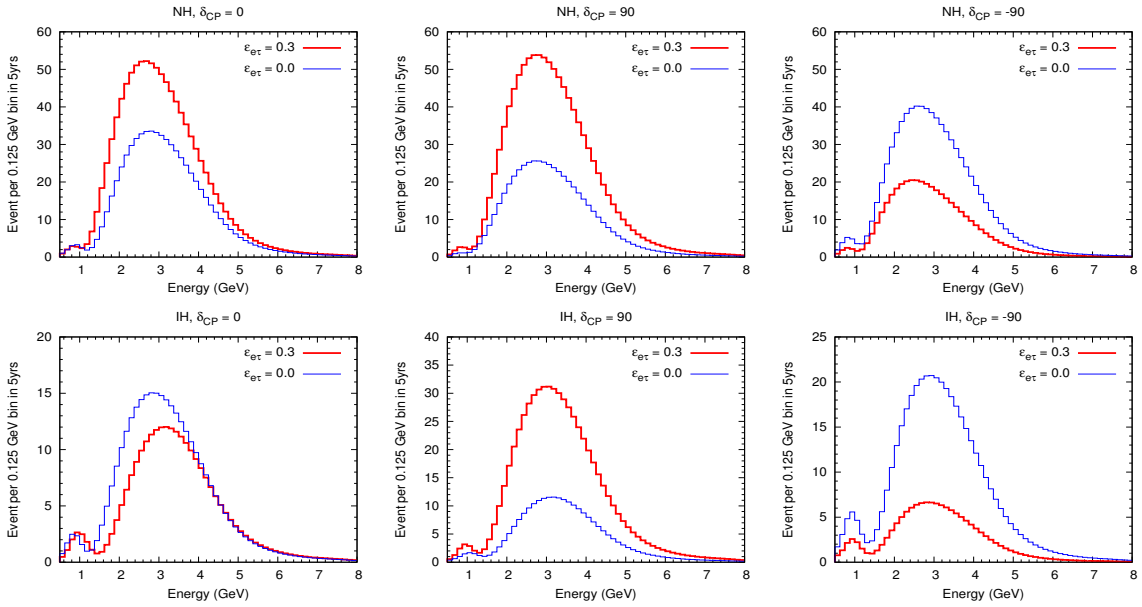

Figure 5.5.5: The event spectra of DUNE for different values of CP violating phase, i.e, $\delta_{CP} = 0°$ (left panel), $\delta_{CP} = 90°$ (middle panel), and $\delta_{CP} = -90°$ (right panel) .

effect of NSIs on physics potential of different experiments. it should be note that all the sensitivities are computed by using GLoBES.

5.6.1 Effect on the determination of neutrino mass ordering

So far, no one know whether the hierarchy of neutrino mass is Normal ($m_1 < m_2 << m_3$) or Inverted ($m_3 << m_1 < m_2$). The MSW effect, the so called matter effect plays a crucial role in the determination of neutrino mass hierarchy, because unlike vacuum oscillation, they give different contributions to oscillation probability for NH and IH, as one can see from the top panel of Fig. 5.6.1. Therefore, a thorough study of effect of NSIs on the determinations of MH is of great importance in oscillation physics.

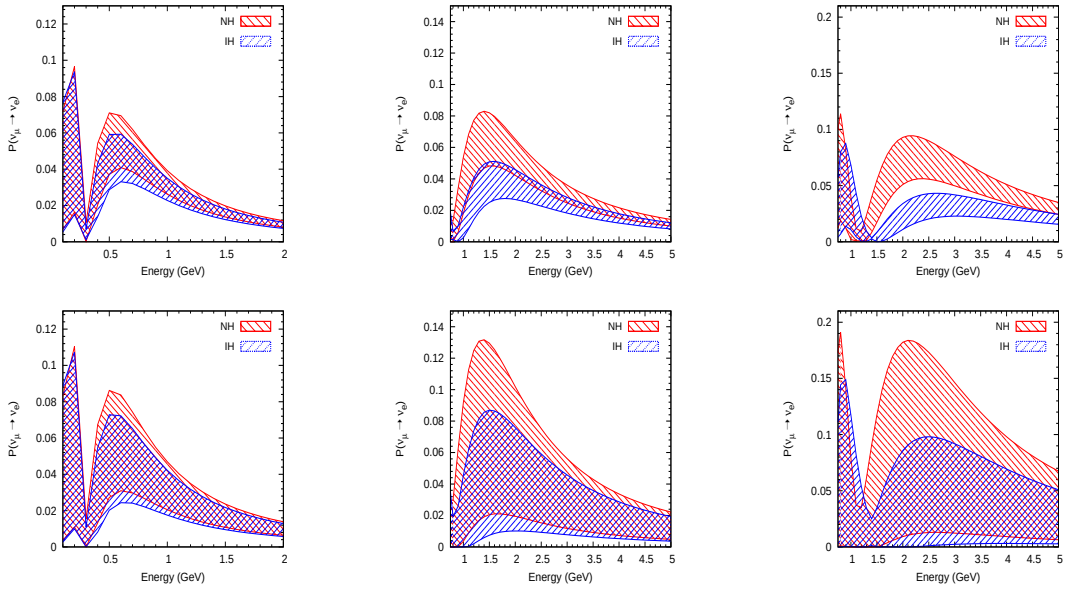

Figure 5.6.1: Neutrino appearance probability for the $\nu_\mu \to \nu_e$ without NSI (top panel) and with NSI (bottom panel) by assuming both NH (red) and IH (blue) for T2K (left panel), NOνA (middle panel) and DUNE (right panel).

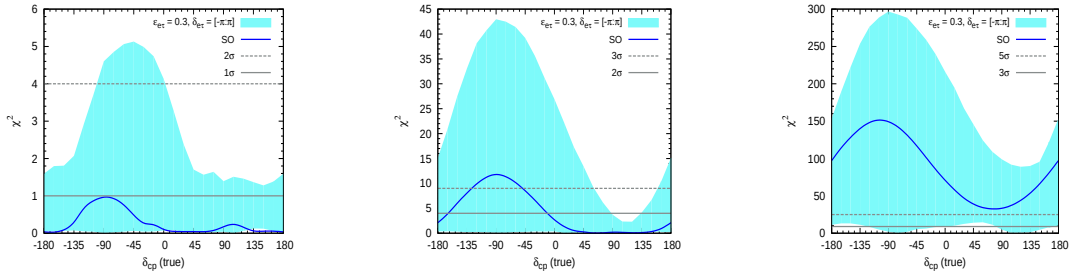

Figure 5.6.2: Mass hierarchy sensitivity as a function of true values of δ_{CP}. The blue solid line in the figure corresponds to MH sensitivity without NSI, whereas blue band in the figure shows the MH sensitivity in presents of NSI ($\varepsilon_{e\tau}$ =0.3) in the allowed range of $\delta_{e\tau}$ for T2K (left panel), NOνA (middle panel) and DUNE (right panel).

However, if one compare the top and bottom panels of Fig. 5.6.1, it can be seen that there is considerable overlap between the hierarchies in the presence of NSIs

and this overlap will worsen the hierarchy determination capability of long-baseline experiments. Further, the MH sensitivity as a function of true values of Dirac CP phase δ_{CP} is shown in Fig. 5.6.2. In the figure, the solid blue line corresponds to the MH sensitivity in SO, which is obtained by comparing true event spectrum as NH and test event spectrum as IH. The blue band in the figure shows the variation in MH sensitivity for different values of $\delta_{e\tau}$ with $\varepsilon_{e\tau} = 0.3$. This sensitivity is obtained by doing marginalization over the SO parameters in their allowed parameter space and adding a prior on $\sin^2 2\theta_{13}$. From the figure, it is clear that though the presence of NSI worsen MH sensitivity, there is a possibility to determine mass hierarchy for T2K (NOνA) above 2σ (3σ) for 30 % (75%) of parameter space of δ_{CP}.

5.6.2 Effect on the determination of octant of θ_{23}

The resolution of the tension between LO and HO of atmospheric mixing angle is one of the challenging goal of long baseline neutrino oscillation experiments. This section discusses the effect of LFV-NSI on the resolution of octant of atmospheric mixing angle.

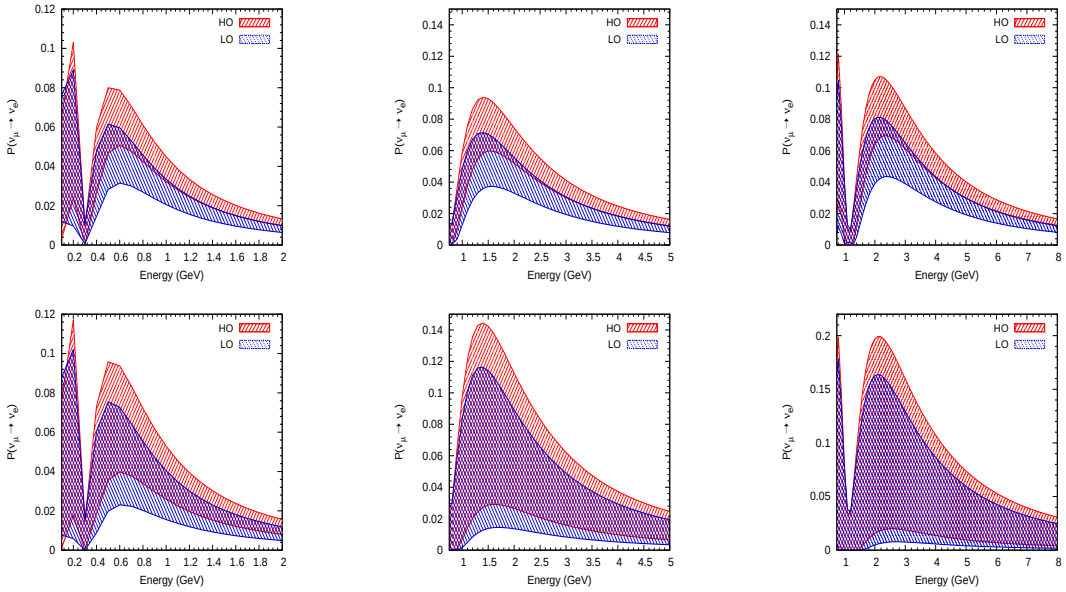

Figure 5.6.3: Neutrino appearance probability for the $\nu_\mu \to \nu_e$ without NSI (top panel) and with NSI (bottom panel) by assuming both HO (red) and LO (blue) for T2K (left panel), NOνA (middle panel) and DUNE (right panel).

The octant degeneracy is merely a consequence of inherent structure of three flavour

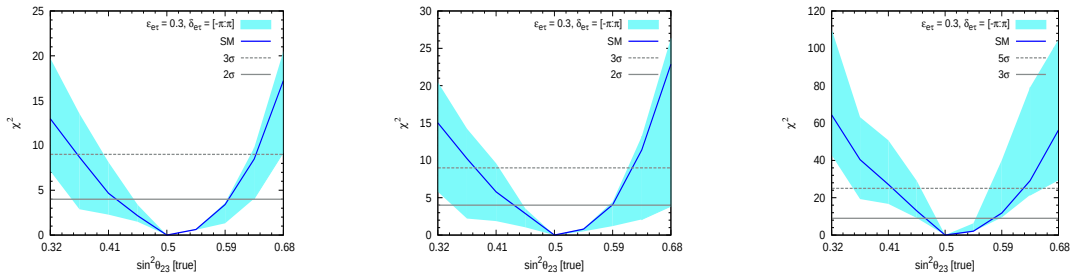

Figure 5.6.4: Octant sensitivity as a function of true values of $\sin^2\theta_{23}$. The blue line in the figure corresponds to octant without NSI, whereas light blue band in the figure shows the octant sensitivity in presents of NSI ($\varepsilon_{e\tau}$ =0.3) in the allowed range of $\delta_{e\tau}$ for T2K (left panel), NOνA (middle panel) and DUNE (right panel). Neutrino MH is assumed to be Normal Hierarchy

neutrino oscillation probability, where a set of oscillation parameters gives disconnected regions in neutrino oscillation parameter space and it makes too difficult to find the true solution. However, the matter effect in long baseline experiments can help to resolve the octant of θ_{23} [132], since the oscillation probability gives different contributions to HO and LO as one can see from the upper panels of Fig. 5.6.3. From the lower panels of the figure, it can be seen that there is considerable overlap between the lower and higher octants in the presence of LFV-NSI, which will worsen the sensitivity of long baseline experiments in the determination of octant of θ_{23}. Moreover, the octant sensitivity as a function of true value of $\sin^2\theta_{23}$ is given in Fig. 5.6.4. The octant sensitivity is obtained by comparing true event spectrum (HO/LO) with test event spectrum (LO/HO). The χ^2 is calculated by doing marginalization over SO parameter space in their allowed values and adding a prior on $\sin^2 2\theta_{13}$. From the figure, it can be seen that there is a possibility of enhancement in the sensitivity of octant of atmospheric mixing angle in the presence of LFV-NSIs, though LFV-NSIs worsen the sensitivity.

5.6.3 Effect on the determination of CP violating phase δ_{CP}

One of the main objectives of long-baseline neutrino oscillation experiments is the determination of the CP violation (CPV) in the leptonic sector. Therefore, it is crucial to study the effect of NSI on the determination of CPV at T2K, NOνA and DUNE experiments. In order to understand the effect of NSI at probability level, the ν_e

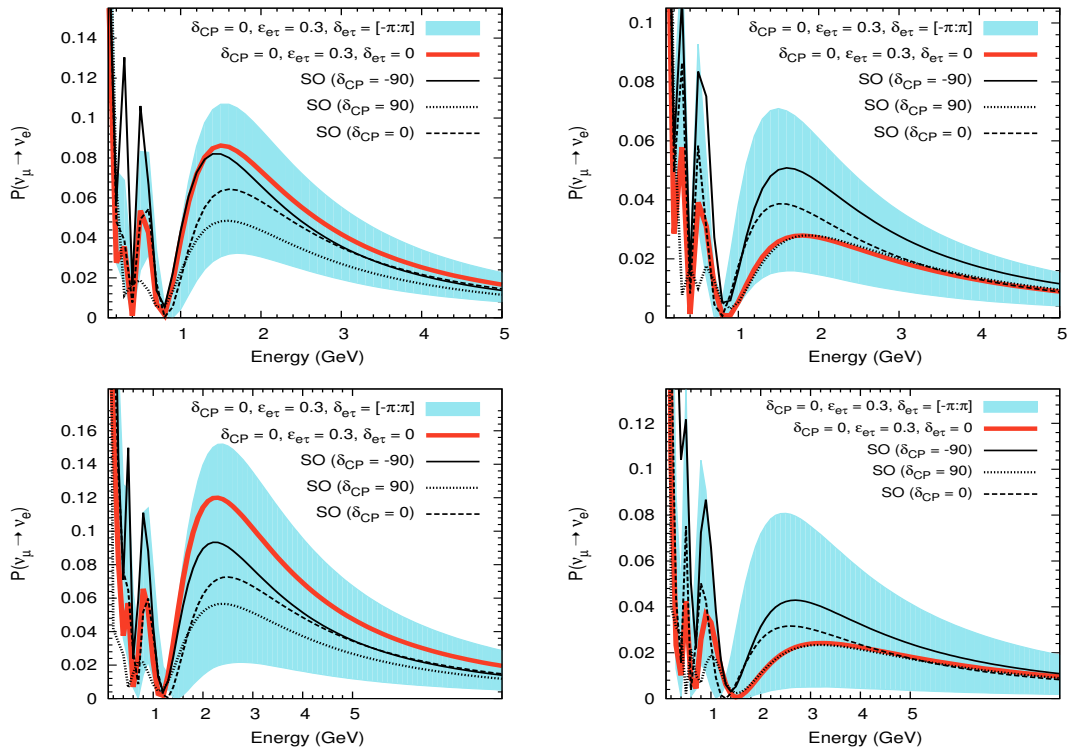

Figure 5.6.5: The $\nu_\mu \to \nu_e$ oscillation probability as a function of neutrino energy for NOνA (DUNE) in the top (bottom) panel.The left (right) panel corresponds to NH (IH).

appearance oscillation probability for NOνA (DUNE) is given in the top (bottom) panels of Fig. 5.6.5. The light coloured band in the figure corresponds to the oscillation probability in the presence of NSI for allowed values of NSI phase parameter $\delta_{e\tau}$ if $\delta_{CP} = 0$. From the figure, one can see that the CP-violating oscillation signals (dark solid and dashed oscillation curves) in SO can mimic the CP-conserving oscillation signal (light solid oscillation curve) in presence of NSI. This leads to misinterpretation of oscillation data if NSIs exists in nature.

Moreover, the direct measurement of CP violation can be obtained by looking at the difference in the transition probability of CP conjugate channels i.e, by analyzing the ν_e appearance and $\bar{\nu}_e$ appearance probabilities.

The observable so called CP asymmetry (A_{CP}) can be used to quantify the effects due to CP violation and it is defined as

$$A_{CP} = \frac{P_{\mu e} - \overline{P}_{\mu e}}{P_{\mu e} + \overline{P}_{\mu e}} \tag{5.6.1}$$

where $P_{\mu e}$ is the ν_e appearance probability and $\overline{P}_{\mu e}$ is $\bar{\nu}_e$ appearance probability.

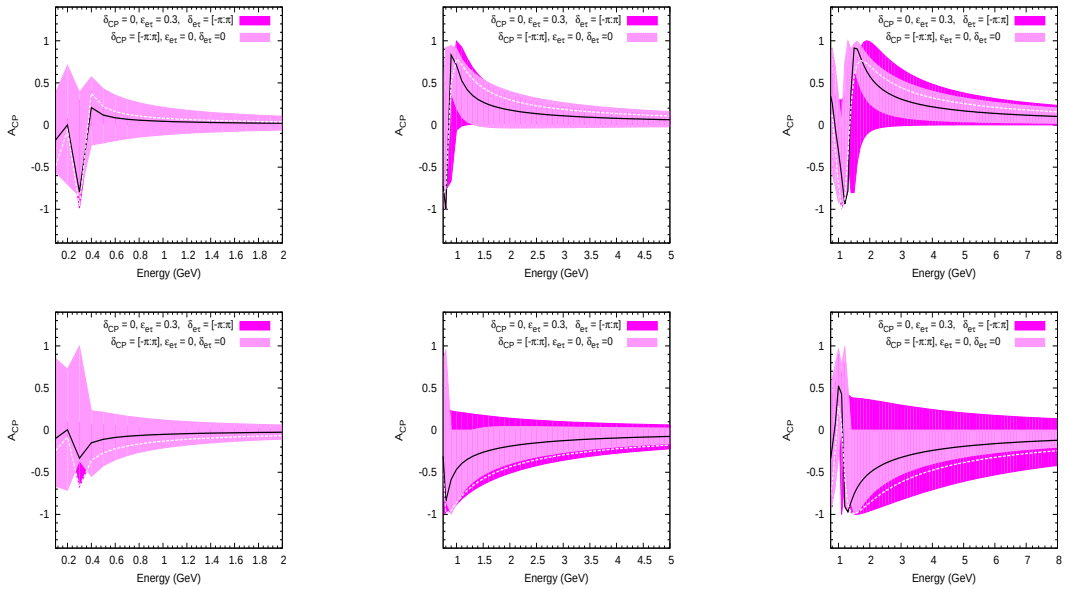

Figure 5.6.6: The CP asymmetry bands for T2K (left panel), NOνA (middle panel) and DUNE (right panel) without NSI (light coloured band) and with NSI (dark coloured band) by assuming both NH (top panel) and IH (bottom panel). The solid black line corresponds to CP asymmetry for $\delta_{CP} = 0$ without NSI, where as the dashed white line corresponds to CP asymmetry for $\delta_{CP} = 0$ with NSI ($\varepsilon_{e\tau} = 0.3$).

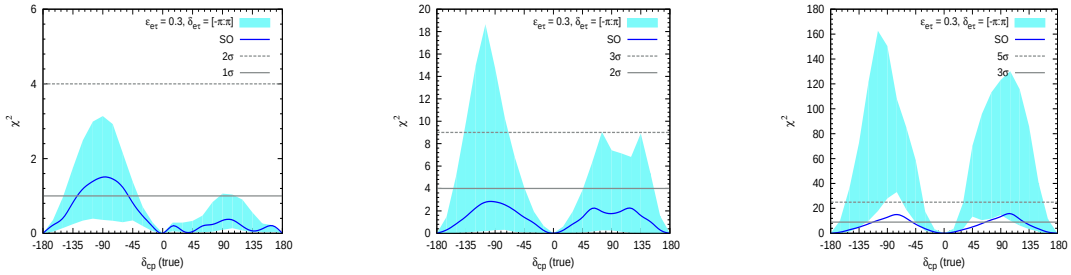

Figure 5.6.7: The CPV potential as a function of true values of δ_{CP} for T2K (left panel), NOνA (middle panel) and DUNE (right panel) without NSI (solid blue line) and with NSI (band).

Fig. 5.6.6 shows the CP asymmetry bands for T2K (left panel), NOνA (middle panel) and DUNE (right panel) without NSI (light coloured band) and with NSI (dark coloured band) by assuming both normal (top panel) and inverted (bottom panel) hierarchies. The solid black line corresponds to CP asymmetry for $\delta_{CP} = 0$ without NSI, whereas the dashed white line corresponds to CP asymmetry for $\delta_{CP} = 0$ with NSI ($\varepsilon_{e\tau} = 0.3$). The dark bands in the figure show the impact of the phase of LFV-NSI parameter on A_{CP}. Therefore, the dark bands correspond to the fake CP signals which are coming from NSI. From the figures, it is clear that there is not much change in the asymmetry with NSI and without NSI in the case of T2K, whereas in the case of NOνA the bands show that there is significant change in the asymmetry with NSI and without NSI. Moreover, the change in the asymmetry is quite large in the case of DUNE. From the figure, it is clear that NSI can give fake CP signals even without considering contributions from the intrinsic phase ($\delta_{e\tau}$) of NSI parameter and therefore, it is very difficult to determine the CP violation in the presence of NSIs.

The CP violation sensitivity as a function of true values of δ_{CP} for T2K (left panel), NOνA (middle panel) and DUNE (right panel) is shown in Fig. 5.6.7. The CP violation sensitivity is obtained by comparing the true event spectrum and test event spectrum with $\delta_{CP}^{test} = 0,\ \pi$. The minimum χ^2 is obtained by doing marginalization over the SO parameter space and adding a prior on $\sin^2\theta_{13}$. From the figure, it is clear that there is a possibility to determine CP violation above 2σ, 3σ and 5σ with 30%, 60 % and 60 % of δ_{CP} parameter space for T2K, NOνA and DUNE respectively.

5.7 Degeneracies among oscillation parameters in presence of LFV-NSI

One of the major issues in neutrino oscillation physics is the parameter degeneracy among the oscillation parameters. In the standard oscillation physics, there are four-fold degeneracies among the oscillation parameters and they are known as octant degeneracy and mass hierarchy (sign of Δm^2_{31}) degeneracy. Therefore, this section discusses a simple way to understand the degeneracies among the oscillation parameters in the presence of LFV-NSI parameter $\varepsilon_{e\tau}$, by using bi-probability plots i.e., CP

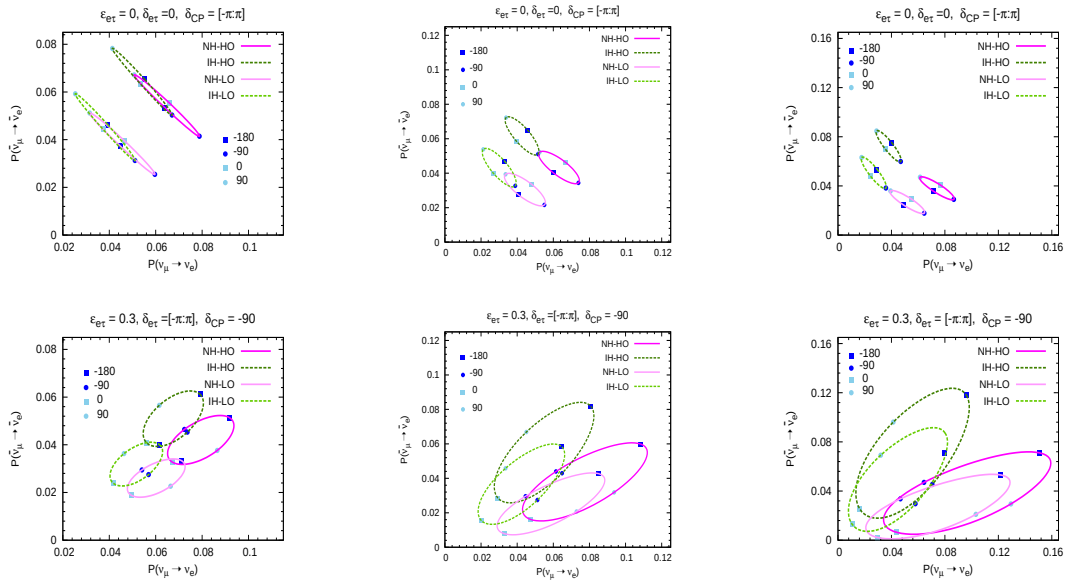

Figure 5.7.1: The CP trajectory for T2K (left), NOνA (middle) and DUNE (right) with (bottom panel) and without (top panel) NSIs.

trajectory in a $P_{(\nu_\mu \to \nu_e)} - P_{(\bar{\nu}_\mu \to \bar{\nu}_e)}$ plane and δ_{CP}-A_{CP} plane.

The Fig. 5.7.1 shows the bi-probability plots for T2K (E = 0.6 GeV, L = 295 km), NOνA (E = 2 GeV, L = 810 km) and DUNE (E = 3 GeV, L = 1300 km) for both NH (solid line) and IH (dashed line) where dark (light) colour plot corresponds to HO (LO). In the figure, the upper panel corresponds to δ_{CP} trajectory without NSIs, whereas the lower panel corresponds to $\delta_{e\tau}$ trajectory with $\varepsilon_{e\tau} = 0.3$ and $\delta_{CP} = -90^\circ$ (it is the presently favoured value of CP phase).

In the standard oscillation paradigm, the NH and IH ellipses are well separated in the case of DUNE experiment, compared with T2K and NOνA experiments. This means that DUNE experiment has highest mass hierarchy determination capability. However, the ellipses in presence of LFV-NSI overlap with each other, which will significantly worsen the hierarchy determination capability of DUNE experiment. It can also be seen from the figure that octant degeneracy can be resolved by using all the three experiments, since the light coloured ellipses are well separated from dark coloured ellipse in the SO. Whereas the octant resolution capability of NOνA and DUNE experiments become worsen in presence of LFV-NSI, because there is significant overlap between the CP trajectories of HO and LO in presence of LFV-NSI. Moreover, there present new types of degeneracies among oscillation parameters in

presents of LFV-NSI.

For a detailed discussion on the resolution of parameter degeneracies among the oscillation parameters, focus on the bi-probability plot of DUNE with NSI i.e., bottom right panel of Fig. 5.7.1. One can see from the figure that

- If $\delta_{e\tau} = -180°$, then the points in the $P_{(\nu_\mu \to \nu_e)} - P_{(\bar{\nu}_\mu \to \bar{\nu}_e)}$ plane are well separated in the case of NH-HO and IH-HO, which is a clear indication of mass hierarchy determination even in presence of LFV-NSI. Whereas, the capability of MH is reduced in the case of IH-LO and NH-LO. It is also noted from the figure that, NH(IH)-HO and NH(IH)-LO are also well separated, which means that octant determination is possible in this case.

- If $\delta_{e\tau} = -90°$, then it is extremely difficult to infer any definitive conclusion about the determination of both mass hierarchy and octant, since all the four degenerate points in $P_{(\nu_\mu \to \nu_e)} - P_{(\bar{\nu}_\mu \to \bar{\nu}_e)}$ plane are very close to each other .

- If $\delta_{e\tau} = 0$, then all the four degenerate points are very close to each other in $P_{(\nu_\mu \to \nu_e)} - P_{(\bar{\nu}_\mu \to \bar{\nu}_e)}$ plane and therefore it is extremely difficult to make any decisive prediction about the determination of both mass hierarchy and octant.

- If $\delta_{e\tau} = 90°$, then the points correspond to NH-HO and IH-HO in $P_{(\nu_\mu \to \nu_e)} - P_{(\bar{\nu}_\mu \to \bar{\nu}_e)}$ plane are very well separated, which is an indication of MH determination. However, the capability of determination of mass hierarchy is reduced in the case of LO. It is also noted that octant determination is poor in this case.

All the above predictions are made under the assumptions that the value of LFV-NSI $\varepsilon_{e\tau}$ is near to its upper bound and the value of CP violating phase is near to its currently preferred value i.e, $\delta_{CP} = -90°$. Moreover, these predictions point toward that the mass hierarchy and octant determinations are possible even in the presence of LFV-NSI, if $\delta_{e\tau} = -180°$ or $90°$.

Another simple way to understand the parameter degeneracies among the oscillation parameters is by simply looking at the CP-asymmetry, which is defined in Eqn. (5.6.1). CP-asymmetry as a function of δ_{CP} for NH-LO, NH-HO, IH-LO and IH-HO for DUNE experiment is given in Fig. 5.7.2. The top left panel of the figure shows the

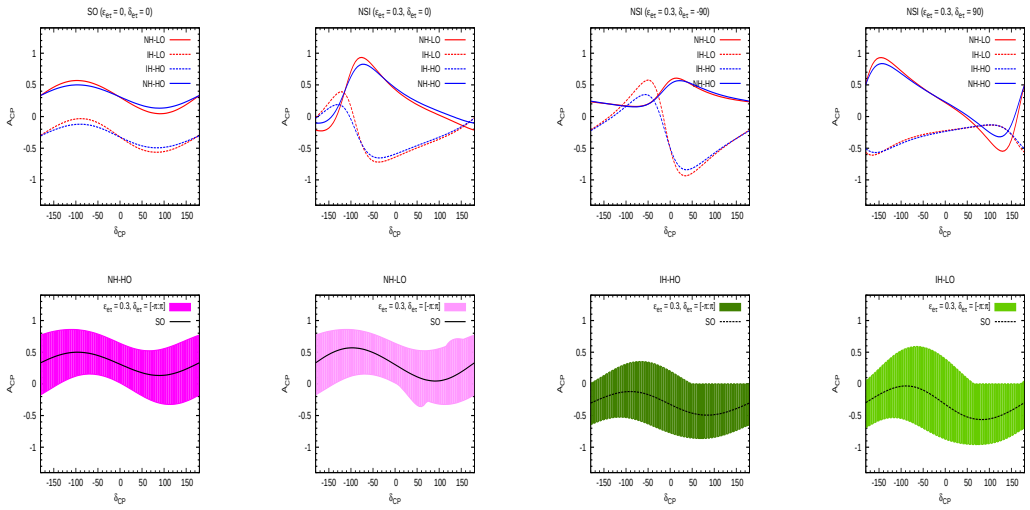

Figure 5.7.2: The parameter degeneracy among the oscillation parameter in δ_{CP}-CP asymmetry plane for DUNE experiment. The top left panel shows the degeneracies in SO, whereas the other three panels show the degeneracy in presence of LFV-NSI with $\delta_{e\tau}$ =0, -90, and 90 respectively. The bottom panel shows the A_{CP} for NH-HO, NH-LO, IH-LO and IH-LO in presence of NSI ($\varepsilon_{e\tau} = 0.3$ and $\delta_{e\tau} = [\pi : \pi]$).

CP asymmetry in standard oscillation and it can be seen from the figure that CP asymmetry is more in LO than in HO for both NH and IH. The rest of three in the top panel show the CP asymmetry in presence of NSI with $\delta_{e\tau} = 0, -90°$, and $90°$ respectively. It is clear from the figure that LFV-NSI introduces other degeneracies among the standard oscillation parameters. Moreover, the bottom panel shows the A_{CP} for NH-HO, NH-LO, IH-LO and IH-LO in presence of NSI ($\varepsilon_{e\tau} = 0.3$ and $\delta_{e\tau} = [\pi : \pi]$). Therefore, degeneracy resolution in presence of NSI extremely complicated. It also noted that degeneracy resolution capability is mainly depend on the value of $\delta_{e\tau}$, for instance if $\delta_{e\tau} = 90°$, then CP-asymmetry for IH-LO and IH-HO are almost same and one cannot distinguish between them.

5.7.1 Correlation between δ_{CP} and θ_{23}

This subsection discusses the effect of LFV-NSI on the allowed parameter space of $\sin^2\theta_{23}$ and δ_{CP}. Further, the Fig. 5.7.3 shows the 2σ C.L. regions for $\sin^2\theta_{23}$ vs. δ_{CP} with true $\sin^2\theta_{23} = 0.41$ (0.59) for LO (HO) and true $\delta_{CP} = -90°$, for T2K (top panel) and DUNE (bottom panel) experiments. From the figure, one can see that there is significant change in the allowed parameter space in presence of LFV-NSI for DUNE.

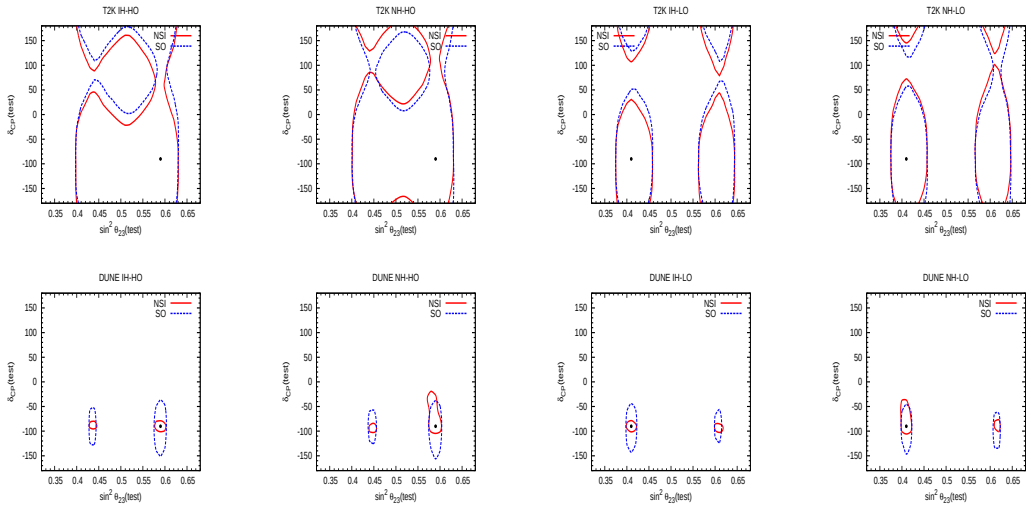

Figure 5.7.3: The 2σ C.L. regions for $\sin^2\theta_{23}$ vs. δ_{CP} with true $\sin^2\theta_{23} = 0.41$ (0.59) for LO (HO) and true $\delta_{CP} = -90°$. The top panel corresponds to T2K and bottom panel corresponds to DUNE experiments.

5.8 Summary and Conclusions

This chapter is devoted to study role the non-standard interactions of neutrino that are coming from various extensions of SM on physics potential of long baseline experiments. Moreover, this chapter is mainly focused on the lepton flavor violating propagation NSIs. Though the conservation of lepton flavour is one of the unique feature of the SM, recently there are a series of experimental results in B physics pointing towards possible violations of LFU, both in the charged and neutral current mediated semileptonic decays. Such lepton flavour universality violation could in principle also induce lepton flavour violating interactions. Further, the lepton flavour violating couplings in the Z' model is constrained by using the upper limits of the corresponding branching ratios of the lepton flavour violating decays of B meson, i.e, $B_d \to \tau^{\pm} e^{\mp}$ decay. In this way obtained the bound on NSI parameters as $|\varepsilon_{e\tau}| < 0.7$ from the decay rate. And studied the possible implications of these new physics interactions in the long-baseline neutrino oscillation experiments by assuming these NSI parameters in the charged lepton sectors to be related to the corresponding NSI parameters in the neutrino sector by $SU(2)_L$ symmetry. From the analysis, it is found that the discovery reach for the unknowns in oscillation physics by these experiments can be altered significantly in the presence of LFV-NSIs. Moreover, it is found that the degeneracy discrimination capability of all the experiment will worsen in the presence

of LFV-NSI, since it leads to new degeneracies among the oscillation parameters other than the existing degeneracies in standard oscillation physics. It is also found that the possibility of misinterpretation of oscillation data in the presence of new physics scenarios (NSIs), give rise to wrong determination of octant of atmospheric mixing angle, neutrino mass hierarchy and the CP violation. Moreover, the δ_{CP} coverage of NOνA for CPV sensitivity above 1σ is reduced in presence NSIs. However, the CPV sensitivity is enhanced in the presence of NSI and it is above 5σ for more than 50% allowed values of δ_{CP} in the case of both NH and IH for DUNE.

CHAPTER 6

Summary and Conclusions

The ultimate aim of the theories and experiments which are mainly focussing on neutrinos is to construct a theoretical model which can explain both observed neutrino masses and lepton mixing pattern. Such a theoretical formulation requires the best knowledge of neutrino oscillation parameters especially neutrino mass hierarchy, octant of θ_{23}, and CP violating phase δ_{CP}. The long baseline neutrino oscillation experiments are indented to determine all these unknowns in neutrino sector, which are mainly looking for $\nu_\mu(\bar{\nu}_\mu)$ to $\nu_e(\bar{\nu}_e)$ oscillation channel since this channel is sensitive to all the unknowns. This thesis sheds light on the present knowledge of neutrino oscillation parameters by examining the sensitivity of current and future long baseline experiments.

The first chapter of this thesis started with a brief historical review of neutrino and it is followed by the discussions on the nature of neutrino in the Standard Model and beyond the Standard Model by which one can understand what makes neutrino so special among all other fundamental particles in SM. Further, this chapter is ended with an overview of the whole thesis work. Chapter 2 of this thesis discussed theoretical framework of neutrino oscillation, which emphasized the role of matter effect. Moreover, this chapter also discussed the evidence of neutrino oscillation, the various neutrino oscillation experiments and the current status of neutrino oscillation parameters.

Chapter 3 of this thesis presented a study towards extracting best possible results from the currently running long baseline experiment, NuMI Off-Axis ν_e Appearance (NOνA). The determination of unknown parameters by an oscillation experiment like NOνA, which is mainly rely on the oscillation probability, is extremely difficult due to the parameter degeneracies, since various combination of these parameters give the same probability. In this context, this chapter investigated whether it is possible to extract the best results from NOνA with a shorter time-span than its scheduled run period by analysing its capability to discriminate the degeneracy among various neutrino oscillation parameters within four years of run time, with two years each in neutrino and anti-neutrino modes. This chapter also discussed the synergy between NOνA and T2K experiment with a total of five years run with 3.5 years in neutrino mode and 1.5 years in anti-neutrino mode. It is found that the parameter degeneracy discrimination capability of NOνA (2+2) is quite good when compared with NOνA (3+1). Looking all the results from the analysis, it is strongly urged that after two years of neutrino running, NOνA should run for two years in anti-neutrino mode to provide better information about the determination of neutrino mass ordering and the octant of atmospheric mixing angle.

Chapter 4 of this thesis discussed a comprehensive study of the discovery potential of currently running accelerator based neutrino experiments NOνA and T2K and the forthcoming T2HK experiment. This chapter investigated the prospects of the determination of current unknowns with these experiments. The following results can be inferred from the analysis:

- Octant resolution: It is found that T2K experiment with (3ν +$2\bar{\nu}$) years of runs can resolve the octant degeneracy with nearly 2σ C.L. if the true value of θ_{23} to be around $\sin^2\theta_{23} = 0.41$ (LO) or $\sin^2\theta_{23} = 0.59$ (HO). The sensitivity increases to nearly 3σ with (3ν +$3\bar{\nu}$) years running of NOνA. However, if one combines the data from these two experiments the sensitivity increases significantly than the sensitivities of individual experiments. It is also found that octant degeneracy can be resolved with NOνA experiment alone with more than 3σ significance, if

one assumes that NOνA continues data taking for 10 years.

- Mass hierarchy determination: It is also found that one can rule out nearly one-third of the δ_{CP} space at 3σ C.L. for mass hierarchy determination, if one uses the synergy between NOνA and T2K experiments. Further, the sensitivity increases significantly for ten years of running of NOνA and NOνA with (5ν+$5\bar{\nu}$) combination is found to be more suitable than the combination of (7ν+$3\bar{\nu}$).

- Determination of CP-Violation: It is found that T2K by itself has marginal CP violation sensitivity at 1σ CL. For NOνA with (3+3) years of running there will be CP violation sensitivity above 1.5σ level for about one-third of the CP violating phase δ_{CP} space. The sensitivity increases slightly for 10 years of run time, with (5ν + $5\bar{\nu}$) combination having sensitivity than that of (7ν + $3\bar{\nu}$) combination. The data from T2HK experiment will improve the CPV sensitivity significantly. It is also found that the CP violating phase δ_{CP} can be determined to be better than 35°, 21° and 9° for all values of δ_{CP} for T2K, NOνA and T2HK experiments.

Chapter 5 of this thesis dealt with the impact of non-standard neutrino interactions (NSIs), which can be considered as sub-leading effects in neutrino oscillation, on the physics potential of long baseline experiments. This chapter mainly discussed the implications of Lepton Flavor Violating propagation NSIs on the physics potential of various neutrino oscillation experiments in both model independent and model-dependent ways. In model independent method, the constraints on the NSI parameters are taken from [118, 119]. Whereas in model dependent analysis, there considered a model with an additional Z' boson,which is quite successful in explaining the observed LFU anomalies in the B meson sector. And analysed its effect in the lepton flavour violating (LFV) $B_d \to \tau^{\pm} e^{\mp}$ decay modes. Moreover, the constraints on the new physics parameters is obtained from the present upper bound of the $B_d \to \tau^{\pm} e^{\mp}$ branching ratio. These parameters are related to the corresponding NSI parameters in the neutrino sector by $SU(2)_L$ symmetry and investigated the possibility of observing the effects of these interactions in currently running and upcoming long-baseline experiments, i.e., NOνA and DUNE respectively. It is found that the NSI parameters in the $e\tau$ sector remarkably affect the ν_e appearance oscillation probability. Moreover, it is also found that the possibility of misinterpretation of oscillation data in the

presence of new physics scenarios (NSIs), give rise to wrong determination of octant of atmospheric mixing angle, neutrino mass hierarchy and the CP violation. The δ_{CP} coverage of NOνA for CPV sensitivity above 1σ is reduced in presence NSIs. However, the CPV sensitivity is enhanced in the presence of NSI and it is above 5σ for more than 50% allowed values of δ_{CP} in the case of both NH and IH for DUNE. It also found that the degeneracy discrimination capability of all the experiment will worsen in the presence of LFV-NSI, since it leads to new degeneracies among the oscillation parameters other than the existing degeneracies in standard oscillation physics.

The current generation accelerator-based long baseline experiments have played crucial role in the measurements of neutrino oscillations parameters. To avoid the misinterpretation of oscillation data in presence of New Physics (NSI) as discussed in this thesis, one should need high statistics (large event rates). The experiments with very intense and well understood neutrino beam and very large detectors ensure large statistics and leads to the complete understandings of the neutrino oscillation parameters. In this way, over the next few years, long baseline experiments promise a rich program of research with the sensitivity to make the fundamental discoveries.

APPENDIX A

Relation between the measured and standard atmospheric oscillation parameters

In general, the atmospheric oscillation parameters are measured by using two flavor framework. However, the three flavor framework has become the standard picture of neutrino oscillation. Therefore, this subsection discuss the relation between the measured atmospheric oscillation parameters $(\Delta m^2_{\mu\mu}, \theta_{\mu\mu})$ and that in the standard three flavor framework $(\Delta m^2_{31}, \theta_{23})$. In order to find this, consider the ν_μ disappearance probability in two flavor framework,

$$P^{\mu\mu}_{2f} = 1 - \sin^2 2\theta_{\mu\mu} \sin^2 \hat{\Delta}_{\mu\mu}, \tag{A.0.1}$$

where $\hat{\Delta}_{\mu\mu} = \frac{\Delta m^2_{\mu\mu} L}{E}$. The disappearance oscillation probability in three flavor framework is given by,

$$P^{\mu\mu}_{3f} = 1 - 4|U_{\mu3}|^2|U_{\mu1}|^2 \sin^2 \hat{\Delta}_{31} - 4|U_{\mu3}|^2|U_{\mu2}|^2 \sin^2 \hat{\Delta}_{32} - 4|U_{\mu2}|^2|U_{\mu1}|^2 \sin^2 \hat{\Delta}_{21}, \tag{A.0.2}$$

where $\hat{\Delta}_{31} = \frac{\Delta m^2_{31}}{E}$. Neglecting the last term in the above equation yields,

$$\begin{aligned} P^{\mu\mu}_{3f} &= 1 - 4|U_{\mu 3}|^2|U_{\mu 1}|^2 \sin^2 \hat{\Delta}_{31} - 4|U_{\mu 3}|^2|U_{\mu 2}|^2 \sin^2 \hat{\Delta}_{32} \\ \frac{1 - P^{\mu\mu}_{3f}}{4} &= |U_{\mu 3}|^2 \left(|U_{\mu 1}|^2 \sin^2 \hat{\Delta}_{31} + |U_{\mu 2}|^2 \sin^2 \hat{\Delta}_{32}\right), \\ &= |U_{\mu 3}|^2 \left(|U_{\mu 1}|^2 + |U_{\mu 2}|^2\right) \left(a_1 \sin^2 \hat{\Delta}_{31} + a_2 \sin^2 \hat{\Delta}_{32}\right), \qquad \text{(A.0.3)} \end{aligned}$$

where $a_1 = \frac{|U_{\mu 1}|^2}{|U_{\mu 1}|^2 + |U_{\mu 2}|^2}$ and $a_2 = \frac{|U_{\mu 2}|^2}{|U_{\mu 1}|^2 + |U_{\mu 2}|^2}$ with $a_1 + a_2 = 1$.

$$\frac{1 - P^{\mu\mu}_{3f}}{4} = \frac{|U_{\mu 3}|^2}{2} \left(|U_{\mu 1}|^2 + |U_{\mu 2}|^2\right) \left[a_1 \left(1 - \cos 2\hat{\Delta}_{31}\right) + a_2 \left(1 - \cos 2\hat{\Delta}_{32}\right)\right],$$

Substituting for $\Delta_{32} = \Delta_{31} - \Delta_{21}$ yields,

$$\begin{aligned} \frac{1 - P^{\mu\mu}_{3f}}{4} &= \frac{|U_{\mu 3}|^2}{2} \left(|U_{\mu 1}|^2 + |U_{\mu 2}|^2\right) \\ &\quad \left[a_1 \left(1 - \cos 2\hat{\Delta}_{31}\right) + a_2 \left(1 - (\cos 2\hat{\Delta}_{31} \cos 2\hat{\Delta}_{21} + \sin 2\hat{\Delta}_{31} \sin 2\hat{\Delta}_{21})\right)\right], \end{aligned}$$

Since $\hat{\Delta}_{21}$ is really small, which indicates that $\cos 2\hat{\Delta}_{21} \approx 1$ and $\sin 2\hat{\Delta}_{21} \approx 2\hat{\Delta}_{21}$,

$$\begin{aligned} \frac{1 - P^{\mu\mu}_{3f}}{4} &= \frac{|U_{\mu 3}|^2}{2} \left(|U_{\mu 1}|^2 + |U_{\mu 2}|^2\right) \\ &\quad \left[a_1 \left(1 - \cos 2\hat{\Delta}_{31}\right) + a_2 \left(1 - (\cos 2\hat{\Delta}_{31} + 2\hat{\Delta}_{21} \sin 2\hat{\Delta}_{31})\right)\right], \\ &= \frac{|U_{\mu 3}|^2}{2} \left(|U_{\mu 1}|^2 + |U_{\mu 2}|^2\right) \\ &\quad \left[a_1 - a_1 \cos 2\hat{\Delta}_{31} + a_2 - a_2 \cos 2\hat{\Delta}_{31} - 2\hat{\Delta}_{21} a_2 \sin 2\hat{\Delta}_{31}\right], \\ &= \frac{|U_{\mu 3}|^2}{2} \left(|U_{\mu 1}|^2 + |U_{\mu 2}|^2\right) \left[1 - \cos 2\hat{\Delta}_{31} - 2\hat{\Delta}_{21} a_2 \sin 2\hat{\Delta}_{31}\right], \end{aligned}$$

Now define $\cos\alpha = \frac{1}{\sqrt{1 + 4a_2^2 \hat{\Delta}_2 1^2}}$ and $\sin\alpha = \frac{2a_2\hat{\Delta}_{21}}{\sqrt{1 + 4a_2^2 \hat{\Delta}^2_{21}}}$, then

$$\begin{aligned} \frac{1 - P^{\mu\mu}_{3f}}{4} &= \frac{|U_{\mu 3}|^2}{2} \left(|U_{\mu 1}|^2 + |U_{\mu 2}|^2\right) \left[1 - (\cos\alpha \cos 2\hat{\Delta}_{31} - \sin\alpha \sin 2\hat{\Delta}_{31}) \sqrt{1 + 4a_2^2 \hat{\Delta}^2_{21}}\right], \\ &= \frac{|U_{\mu 3}|^2}{2} \left(|U_{\mu 1}|^2 + |U_{\mu 2}|^2\right) \left[1 - \cos(2\hat{\Delta}_{31} - \alpha) \sqrt{1 + 4a_2^2 \hat{\Delta}^2_{21}}\right], \end{aligned}$$

Ignoring the higher order terms of $\hat{\Delta}_{21}$ yields,

$$\frac{1 - P^{\mu\mu}_{3f}}{4} = \frac{|U_{\mu 3}|^2}{2} \left(|U_{\mu 1}|^2 + |U_{\mu 2}|^2\right) \left[1 - \cos(2\hat{\Delta}_{31} - \alpha)\right].$$

It should be note that $\alpha = tan^{-1}(2a_2\hat{\Delta}_{21}) \approx 2a_2\hat{\Delta}_{21}$. Therefore,

$$\begin{aligned}\frac{1-P^{\mu\mu}_{3f}}{4} &= \frac{|U_{\mu 3}|^2}{2}\left(|U_{\mu 1}|^2+|U_{\mu 2}|^2\right)\left[1-\cos 2(\hat{\Delta}_{31}-a_2\hat{\Delta}_{21})\right], \\ &= |U_{\mu 3}|^2\left(|U_{\mu 1}|^2+|U_{\mu 2}|^2\right)\sin^2(\hat{\Delta}_{31}-a_2\hat{\Delta}_{21}).\end{aligned}$$

$$P^{\mu\mu}_{3f} = 1-4|U_{\mu 3}|^2\left(|U_{\mu 1}|^2+|U_{\mu 2}|^2\right)\sin^2(\hat{\Delta}_{31}-a_2\hat{\Delta}_{21}). \quad \text{(A.0.4)}$$

Compare above equation with Eqn A.0.1 gives,

$$\begin{aligned}\hat{\Delta}_{\mu\mu} &= \hat{\Delta}_{31}-a_2\hat{\Delta}_{21} \\ \sin^2 2\theta_{\mu\mu} &= 4|U_{\mu 3}|^2\left(|U_{\mu 1}|^2+|U_{\mu 2}|^2\right)\end{aligned}$$

$$\begin{aligned}\Delta m^2_{\mu\mu} &= \Delta m^2_{31}-a_2\Delta m^2_{21} \\ &= \Delta m^2_{31}-\frac{|U_{\mu 2}|^2}{|U_{\mu 1}|^2+|U_{\mu 2}|^2}\Delta m^2_{21} \\ &= \Delta m^2_{31}-\frac{|U_{\mu 2}|^2}{1-|U_{\mu 3}|^2}\Delta m^2_{21} \qquad\qquad ||U_{\mu 1}|^2+|U_{\mu 2}|^2+|U_{\mu 3}|^2=1 \\ \sin^2 2\theta_{\mu\mu} &= 4|U_{\mu 3}|^2\left(1-|U_{\mu 3}|^2\right).\end{aligned}$$

The PMNS matrix for three flavor mixing

$$U_{PMNS} = \begin{pmatrix} c_{12}c_{13} & s_{12}c_{13} & s_{13}e^{-i\delta_{CP}} \\ -s_{12}c_{23}-c_{12}s_{23}s_{13}e^{i\delta_{CP}} & c_{12}c_{23}-s_{12}s_{23}s_{13}e^{i\delta_{CP}} & s_{23}c_{13} \\ s_{12}s_{23}-c_{12}c_{23}s_{13}e^{i\delta_{CP}} & -c_{12}s_{23}-s_{12}s_{23}s_{13}e^{i\delta_{CP}} & c_{23}c_{13} \end{pmatrix}$$

Using $U_{\mu 2} = c_{12}c_{23}-s_{12}s_{23}s_{13}e^{i\delta_{CP}}$, $U_{\mu 3} = s_{23}c_{13}$ and neglecting higher powers of s_{13} gives

$$\begin{aligned}\frac{|U_{\mu 2}|^2}{1-|U_{\mu 3}|^2} &= \frac{c^2_{12}c^2_{23}+s^2_{12}s^2_{23}s^2_{13}-2c_{12}c_{23}s_{12}s_{23}s_{13}\cos\delta_{CP}}{1-s^2_{23}c^2_{13}}, \\ &\approx c^2_{12}-2c_{12}s_{12}\frac{s_{23}}{c_{23}}s_{13}\cos\delta_{CP}, \\ &= \cos^2\theta_{12}-\sin 2\theta_{12}\tan\theta_{23}\sin\theta_{13}\cos\delta_{CP}, \quad \textit{and} \qquad \text{(A.0.5)} \\ \sin^2 2\theta_{\mu\mu} &= 4s^2_{23}c^2_{13}\left(1-s^2_{23}c^2_{13}\right), \qquad \text{(A.0.6)} \\ &\approx 4s^2_{23}c^2_{13}\end{aligned}$$

Finally, the relation between the atmospheric parameters in a 2 flavor framwork and three flavor framework is given by,

$$\begin{aligned} \Delta m^2_{\mu\mu} &= \Delta m^2_{31} - \left(\cos^2\theta_{12} - \sin 2\theta_{12}\tan\theta_{23}\sin\theta_{13}\cos\delta_{CP}\right)\Delta m^2_{21}, \quad \textit{and} \\ \sin\theta_{\mu\mu} &= \sin\theta_{23}\cos\theta_{13}. \end{aligned}$$

Therefore, it can be written as,

$$\Delta m^2_{31} = \Delta m^2_{\mu\mu} + \left(\cos^2\theta_{12} - \sin 2\theta_{12}\tan\theta_{23}\sin\theta_{13}\cos\delta_{CP}\right)\Delta m^2_{21}, \textit{and} \quad \text{(A.0.7)}$$

$$\sin\theta_{23} = \frac{\sin\theta_{\mu\mu}}{\cos\theta_{13}}. \quad \text{(A.0.8)}$$

More details can be seen in [66–68].

Bibliography

[1] Frederick Reines and Clyde L. Cowan, Jr., *"Detection of the Free Neutrino"*, Phys. Rev. **92**, 830 (1953).

[2] C. L. Cowan, Jr., F. Reines, F.B. Harrison, H. W. Kruse, A. D. McGuire, *"Detection of the Free Neutrino: A Confirmation"*, Science **124**, 3212 (1956).

[3] F. Reines and C. L. Cowan, Jr., *"Free Antineutrino Absorption Cross Section. I. Measurement of the Free Antineutrino Absorption Cross Section by Protons"*, Phys. Rev. **113**, 273 (1959).

[4] F. Reines, C. L. Cowan, Jr., F. B. Harrison, A. D. McGuire, H. W. Kruse, *"Detection of the Free Antineutrino"*, Phys. Rev. **117**, 159 (1960).

[5] S.L. Glashow, *"Partial-symmetries of weak interactions"*, Nucl. Phys. **22**, 579 (1961).

[6] S. Weinberg, *"A Model of Leptons"*, Phys. Rev. Lett. **19**, 1264 (1967).

[7] S. L. Glashow, J. Iliopoulos and L. Maiani, *"Weak Interactions with Lepton-Hadron Symmetry"*, Phys. Rev. D **2**, 1285 (1970).

[8] F. Halzen, A. D. Martin, *"Quarks and Leptons: An Introductory Course in Modern Particle Physics"*.

[9] S. Weinberg, *"Baryon- and Lepton-Nonconserving processes"*, Phys. Rev. Lett. **43**, 1566 (1979).

[10] J. W. F. Valle, *" Neutrino physics overview"*, J. Phys. Conf. Ser. **53**, 473(2006), [arXiv: 0608101 (hep-ph)].

[11] F. Bonnet, D. Hernandez, T. Ota, W. Winter, *"Neutrino masses from higher than $d = 5$ effective operators"*, JHEP **0910**, 076 (2009), [arXiv: 0907.3143 (hep-ph)].

[12] A. Abada, C.Biggio, F. Bonnet, M.B. Gavela, T. Hambye, *"Low energy effects of neutrino masses"*, JHEP **0712**, 061 (2007), [arXiv: 0707.4058 (hep-ph)].

[13] Zhi-zhong Xing, *"Theoretical Overview of Neutrino Properties"*, Int.J.Mod.Phys. A **23**, 4255 (2008), [arXiv: 0810.1421 (hep-ph)].

[14] Zhi-zhong Xing, *"Naturalness and Testability of TeV Seesaw Mechanisms"*, Prog. Theor. Phys. Suppl. **180**, 112 (2009), [arXiv:0905.3903 (hep-ph)].

[15] A. Broncano, M.B. Gavela, E. Jenkins, *"Neutrino Physics in the Seesaw Model"*, [arXiv: 0307058 (hep-ph)].

[16] P. Minkowski, *"$\mu \to e\gamma$ at a rate of one out of 109 muon decays?"*, Phys. Lett. B **67**, 421 (1977).

[17] T. Yanagida, *"Horizontal Symmetry and Masses of Neutrinos"*, Prog. Theor. Phys. **64**, 1103 (1980).

[18] Rabindra N. Mohapatra and Goran Senjanovic, *"Neutrino Mass and Spontaneous Parity Nonconservation"*, Phys. Rev. Lett. **44**, 912 (1980).

[19] Rabindra N. Mohapatra, *"Massive neutrinos"*.

[20] Manfred Lindner, Tommy Ohlsson, Gerhart Seidl, *"See-saw Mechanisms for Dirac and Majorana Neutrino Masses"*, Phys.Rev. D **65**, 053014 (2002), [arXiv: 0109264 (hep-ph)].

[21] A. Zee, *"A theory of lepton number violation and neutrino Majorana masses"*, Phys. Lett. B **93** , 389 (1980), [Erratum: Phys. Lett. B 95 , 461 (1980)].

[22] A. Zee, *"Quantum numbers of Majorana neutrino masses"*, Nucl. Phys. B **264**, 99 (1986); K. S. Babu, *"Model of 'Calculable' Majorana Neutrino Masses"*, Phys.Lett. B **203**, 132 (1988).

[23] E. Ma, *"Verifiable radiative seesaw mechanism of neutrino mass and dark matter"*, Phys. Rev. D **73**, 077301 (2006), [arXiv: 0601225 (hep-ph)].

[24] M. Lindner, T. Ohlsson, G. Seidl, "See-saw Mechanisms for Dirac and Majorana Neutrino M
Phys. Rev. D **65**, 053014 (2002), [arXiv: 0109264 (hep-ph)].

[25] C. Giunti and C. W. Kim, *"Fundamentals of neutrino physics and astrophysics"*.

[26] B. Pontecorvo, *"Inverse Beta Processes and Nonconservation of Lepton Charge"*, Soviet Phys. JETP **7**, 172 (1958).

[27] J. A. Formaggio and G. P. Zeller, *"From eV to EeV: Neutrino cross sections across energy scales"*, Rev. Mod. Phys. **84**, 1307 (2012), [arXiv:1305.7513 (hep-ex)].

[28] D. Forero, M. Tortola, and J. Valle, *"Neutrino oscillations refitted"*, Phys. Rev. D **90**, 093006 (2014), [arXiv: 1405.7540 (hep-ph)].

[29] P. Adamson et al., [MINOS Collaboration], *"Measurement of Neutrino and Antineutrino Oscillations Using Beam and Atmospheric Data in MINOS"*, Phys. Rev. Lett. **110**, 251801 (2013), [arXiv:1304.6335 (hep-ex)].

[30] H. Minakata, H. Sugiyama, O. Yasuda, K. Inoue, and F. Suekane, *"Reactor measurement of θ_{13} and its complementarity to long-baseline experiments"*, Phys. Rev. D **68**, 033017 (2003), [arXiv: 0211111 (hep-ph)].

[31] K. Abe et al. (T2K Collaboration), *"Indication of Electron Neutrino Appearance from an Accelerator-Produced Off-Axis Muon Neutrino Beam"*, Phys. Rev. Lett.**107**, 041801 (2011), [arXiv: 1106.2822 (hep-ex)].

[32] P. Adamson et al. (MINOS Collaboration), *"Improved Search for Muon-Neutrino to Electron-Neutrino Oscillations in MINOS"*, Phys. Rev. Lett. **107**, 181802 (2011), [arXiv: 1108.0015 (hep-ex)].

[33] Y. Abe *et al.* (DOUBLE-CHOOZ Collaboration), *"Indication of Reactor $\bar{\nu}_e$ Disappearance in the Double Chooz Experiment"*, Phys. Rev. Lett. **108**, 131801 (2012), [arXiv: 1112.6353 (hep-ex)].

[34] F. P. An *et al.* (DAYA-BAY Collaboration), *"Observation of Electron-Antineutrino Disappearance at Daya Bay"*, Phys. Rev. Lett. **108**, 171803 (2012), [arXiv: 1203.1669 (hep-ex)]..

[35] J. K. Ahn *et al.* (RENO Collaboration), *"Observation of Reactor Electron Antineutrinos Disappearance in the RENO Experiment"*, Phys. Rev. Lett. **108**, 191802 (2012), [arXiv; 1204.0626 (hep-ex)].

[36] K. Abe *et al.* (T2K Collaboration), *"Observation of Electron Neutrino Appearance in a Muon Neutrino Beam"*, Phys. Rev. Lett. **112**, 061802 (2014), [arXiv:1311.4750 (hep-ex)].

[37] P. Adamson et al. (NOvA), *"First measurement of electron neutrino appearance in NOvA"*, Phys. Rev. Lett. **116**, 151806 (2016), [arXiv: 1601.05022 (hep-ex)].

[38] Y. Fukuda *et al.* [Super-Kamiokande Collaboration], *"Evidence for oscillation of atmospheric neutrinos"*, Phys. Rev. Lett. **81** 1562 (1998), [arXiv: 9807003 (hep-ex)].

[39] Q. R. Ahmad *et al.* [SNO Collaboration], *"Direct Evidence for Neutrino Flavor Transformation from Neutral-Current Interactions in the Sudbury Neutrino Observatory"*, Phys. Rev. Lett. **89**, 011301 (2002), [arXiv: 0204008 (nucl-ex)].

[40] K. Eguchi *et al.* [KamLAND Collaboration], *"First Results from KamLAND: Evidence for Reactor Antineutrino Disappearance"*, Phys. Rev. Lett. **90**, 021802 (2003), [arXiv: 0212021 (hep-ex)].

[41] V. Barger, D. Marfatia, K. Whisnant, *"Breaking eightfold degeneracies in neutrino CP violation, mixing, and mass hierarchy"*, Phys. Rev. **D 65**, 073023 (2002), [arXiv: 0112119 (hep-ph)].

[42] H. Minakata, H. Nunokawa, S. Parke, *"Parameter Degeneracies in Neutrino Oscillation Measurement of Leptonic CP and T Violation"*, Phys. Rev. **D 66**, 093012 (2002), [arXiv: 0208163 (hep-ph)].

[43] M. Ishitsuka, T. Kajita, H. Minakata, H. Nunokawa, *"Resolving Neutrino Mass Hierarchy and CP Degeneracy by Two Identical Detectors with Different Baselines"*, Phys. Rev. **D 72**, 033003 (2005), [arXiv: 0504026 (hep-ph)].

[44] S. Prakash, U. Rahaman and S. Uma Sankar, *"The need for an early anti-neutrino run of NOνA"*, JHEP **07**, 070 (2014), [arXiv: 1306.4125 (hep-ph)].

[45] Y. Fukuda *et al.* (Super-Kamiokande Collaboration), *"Evidence for oscillation of atmospheric neutrinos"*, Phys. Rev. Lett. **81**, 1562-1567 (1998), [arXiv: 9807003 (hep-ex)].

[46] M. Apollonio *et al.* (CHOOZ Collaboration), *"Search for neutrino oscillations on a long baseline at the CHOOZ nuclear power station"*, Eur. Phys. J. C **27**, 331-374 (2003), [arXiv: 0301017 (hep-ex)].

[47] M. Ahn *et al.* (K2K Collaboration), *"Measurement of Neutrino Oscillation by the K2K Experiment"*, Phys. Rev. D **74**, 072003 (2006), [arXiv: 0606032 (hep-ex)].

[48] I. Ambats *et al.* (MINOS Collaboration), *"The MINOS Detectors Technical Design Report"*, (1998).

[49] F. Arneodo *et al.* (ICARUS), *"The ICARUS experiment, a second-generation proton decay experiment and neutrino observatory at the Gran Sasso Laboratory"*, (2001), [arXiv: 0103008 (hep-ex)].

[50] R. Acquafredda *et al.*, *"The OPERA experiment in the CERN to Gran Sasso neutrino beam"*, JINST **4**, P04018 (2009).

[51] K. Abe et al. (T2K Collaboration), *"The T2K Experiment"*, Nucl. Instrum. Meth. A **659**, 106-135 (2011), [arXiv: 1106.1238 (physics.ins-det)].

[52] D. Ayres et al, *"Letter of Intent to build an Off-axis Detector to study numu to nue oscillations with the NuMI Neutrino Beam"*, (2002), [arXiv: 0210005 (hep-ex)].

[53] D. Ayres et al. (NOvA Collaboration), *"NOvA: Proposal to build a 30 kiloton off-axis detector to study $\nu_\mu \to \nu_e$ oscillations in the NuMI beamline "*, Fermilab-Proposal-0929 (2004), [arXiv: 0503053 (hep-ex)].

[54] Olga Mena Requejo, Sergio Palomares-Ruiz, Silvia Pascoli, *" Super-NOvA: a long-baseline neutrino experiment with two off-axis detectors"*, Phys. Rev. D **72**, 053002 (2005), [arXiv: 0504015 (hep-ph)].

[55] E. K. Akhmedov, R. Johansson, M. Lindner, T. Ohlsson, and T. Schwetz, *"Series expansions for three-flavor neutrino oscillation probabilities in matter"*, JHEP **0404**, 078 (2004), [arXiv: 0402175 (hep-ph)].

[56] A. Cervera *et al.*, *"Golden measurements at a neutrino factory"*, Nucl. Phys. B **579**, 17 (2000), [arXiv: 0002108 (hep-ph)].

[57] M. Freund, *"Analytic Approximations for Three Neutrino Oscillation Parameters and Probabilities in Matter"*, Phys. Rev. D **64**, 053003 (2001), [arXiv: 0103300 (hep-ph)].

[58] P. Huber, M. Lindner and W. Winter, *"From parameter space constraints to the precision determination of the leptonic Dirac CP phase"*, JHEP **0505**, 020 (2005), [arXiv: 0412199 (hep-ph)].

[59] P. Huber, M. Lindner, T. Schwetz and W. Winter, *"First hint for CP violation in neutrino oscillations from upcoming superbeam and reactor experiments"*, JHEP **0911**, 044 (2009), [arXiv: 0907.1896 (hep-ph)].

[60] M. C. Gonzalez-Garcia and M. Maltoni, *"Atmospheric Neutrino Oscillations and New Physics"*, Phys. Rev. D **70**, 033010 (2004), [arXiv: 0404085 (hep-ph)].

[61] G. L. Fogli, E. Lisi, A. Marrone, D. Montanino, and A. Palazz, *"Getting the most from the statistical analysis of solar neutrino oscillations"*, Phys. Rev.D **66**, 053010 (2002), [arXiv: 0206162 (hep-ph)].

[62] G. L. Fogli, E. Lisi, A. Marrone, and D. Montanino, *"Status of atmospheric neutrino(mu)<–>neutrino(tau) oscillations and decoherence after the first K2K spectral data"*, Phys. Rev. D **67**, 093006 (2003), [arXiv: 0303064 (hep-ph)].

[63] E. Paschos and J. Yu, *"Neutrino interactions in oscillation experiments"*, Phys. Rev. D**65**, 033002 (2002), [arXiv: 0107261 (hep-ph)].

[64] S. K. Agarwalla, S. Prakash, S. K. Raut, and S. Uma Sankar, *"Potential of optimized NOvA for large theta(13) & combined performance with a LArTPC & T2K"*, JHEP **1212**, 075 (2012), [arXiv: 1208.3644 (hep-ex)].

[65] K. Abe *et al.*, [T2K Collaboration], *" Neutrino Oscillation Physics Potential of the T2K Experiment"*, Prog. Theor. Expt. Phys.**4**, 043C01 (2015), [arXiv: 1409.7469 (hep-ex)].

[66] A. de Gouvea, J. Jenkins, and B. Kayser, *"Neutrino mass hierarchy, vacuum oscillations, and vanishing $|U_{e3}|$"*, Phys. Rev. D **71**, 113009 (2005), [arXiv: 0503079 (hep-ph)].

[67] Hiroshi Nunokawa, Stephen Parke, and Renata Zukanovich Funchal, "Another possible way to determine the Neutrino Mass Hierarchy", Phys. Rev. D **72**, 013009 (2005), [arXiv: 0503283 (hep-ph)].

[68] S. K. Raut, *"Effect of non-zero θ_{13} on the measurement of θ_{23}"*, Mod. Phys. Lett. A **28**, 1350093 (2013), [arXiv: 1209.5658 (hep-ph)].

[69] K. Abel et al., *"A Long Baseline Neutrino Oscillation Experiment Using J-PARC Neutrino Beam and Hyper-Kamiokande"*, [arXiv: 1412.4673 (physics.ins-det)].

[70] P. Huber, M. Lindner and W. Winter, *"Superbeams versus neutrino factories"*, Nucl. Phys. **B645**,3 (2002), [arXiv: 0204352 (hep-ph)].

[71] Y. Itow *et al.*, [T2K Collaboration], *"The JHF-Kamioka neutrino project"*, [arXiv: 0106019 (hep-ex)].

[72] M. Ishitsuka *et al.*, *"Resolving neutrino mass hierarchy and CP degeneracy by two identical detectors with different baselines"*, Phys. Rev. D **72**, 033003 (2005), [arXiv: 0504026 (hep-ph)]; K. Abe *et al.*, [T2K Collaboration], *"Neutrino Oscillation Physics Potential of the T2K Experiment"*, Prog. Theor. Expt. Phys.**4**, 043C01 (2015) [arXiv:1409.7469 (hep-ex)].

[73] A. Chatterjee, P. Ghoshal, S. Goswami, S. K. Raut, JHEP**06** 010 (2013), *"Octant sensitivity for large theta$_{13}$ in atmospheric and long baseline neutrino experiments"*, JHEP **06**, 010 (2013), [arXiv: 1302.1370 (hep-ph)].

[74] S. K. Agarwalla, S. Prakash, S. Uma Sankar, *"Resolving the octant of theta23 with T2K and NOvA"*, JHEP **1307**, 131 (2013), [arXiv: 1301.2574 (hep-ph)].

[75] S. K. Agarwalla, *"Physics Potential of Long-Baseline Experiments"*, [arXiv: 1401.4705 (hep-ph)].

[76] L. Wolfenstein, *"Neutrino oscillations in matter"*, Phys. Rev. D **17**, 2369 (1978).

[77] L. Wolfenstein, *"Neutrino oscillations and stellar collapse"*, Phys. Rev. D **20**, 2634 (1979).

[78] S. Davison, C. Pena-Garay, N. Rius and A. Santamaria, *"Present and Future Bounds on Non-Standard Neutrino Interactions"*, JHEP **03**, 011 (2003), [arXiv: 0302093 (hep-ph)].

[79] M. C. Gonzalez-Garcia and M. Maltoni, *" Determination of matter potential from global analysis of neutrino oscillation data"*, JHEP **1309**, 152 (2013), [arXiv: 1307.3092 (hep-ph)].

[80] M. C. Gonzalez-Garcia, M. Maltoni and J. Salvado, *" Testing matter effects in propagation of atmospheric and long-baseline neutrinos"*, JHEP **1105**, 075 (2011), [arXiv: 1103.4365 (hep-ph)].

[81] G. Mitsuka et al. [Super-Kamiokande Collaboration], *"Study of Non-Standard Neutrino Interactions with Atmospheric Neutrino Data in Super-Kamiokande I and II"*, Phys. Rev. D **84**, 113008 (2011), [arXiv: 1109.1889 (hep-ex)].

[82] O. G. Miranda, M. A. Tortola and J. W. F. Valle, *"Are solar neutrino oscillations robust?"*, JHEP **0610**, 008 (2006), [arXiv: 0406280 (hep-ph)].

[83] A. Bolanos, O. G. Miranda, A. Palazzo, M. A. Tortola and J. W. F. Valle, *" Probing non-standard neutrino-electron interactions with solar and reactor neutrinos"*, Phys. Rev. D **79** 113012 (2009), [arXiv: 0812.4417 (hep-ph)].

[84] A. Palazzo and J. W. F. Valle, *"Confusing non-zero theta_13 with non-standard interactions in the solar neutrino sector"*, Phys. Rev. D **80**, 091301 (2009), [arXiv: 0909.1535 (hep-ph)].

[85] F. J. Escrihuela, O. G. Miranda, M. A. Tortola and J. W. F. Valle, *"Constraining nonstandard neutrino-quark interactions with solar, reactor and accelerator data"*, Phys. Rev. D **80**, 105009 (2009), [arXiv: 0907.2630 (hep-ph)].

[86] A. Friedland, C. Lunardini and C. Pena-Garay, *"Solar neutrinos as probes of neutrino-matter interactions"*, Phys. Lett. B **594**, 347 (2004), [arXiv: 0402266 (hep-ph)].

[87] H. Oki and O. Yasuda, *" Sensitivity of T2KK to the non-standard interaction in propagation"*, Phys. Rev. D **82**, 073009 (2010), [arXiv: 1003.5554 (hep-ph)].

[88] A. Bandyopadhyay *et al.*, *"Physics at a future Neutrino Factory and super-beam facility"*, ISS Physics Working Group, Rept. Prog. Phys. **72**, 106201 (2009),[arXiv: 0710.4947 (hep-ph)].

[89] D. Meloni, T. Ohlsson, W. Winter and H. Zhang, *"Non-standard interactions versus non-unitary lepton flavor mixing at a neutrino factory"*, JHEP **1004**, 041v (2010), [arXiv: 0912.2735 (hep-ph)].

[90] A. M. Gago, H. Minakata, H. Nunokawa, S. Uchinami and R. Zukanovich Funchal, *"Resolving CP Violation by Standard and Nonstandard Interactions and Parameter Degeneracy in Neutrino Oscillations"*, JHEP **1001**, 049 (2010), [arXiv: 0904.3360 (hep-ph)].

[91] J. Kopp, T. Ota and W. Winter, *"Neutrino factory optimization for non-standard interactions"*, Phys. Rev. D **78**, 053007 (2008), [arXiv: 0804.2261 (hep-ph)].

[92] N. C. Ribeiro, H. Minakata, H. Nunokawa, S. Uchinami and R. Zukanovich Funchal, *" Probing Non-Standard Neutrino Interactions with Neutrino Factories"*, JHEP **0712**, 002 (2007), [arXiv: 0709.1980 (hep-ph)].

[93] M. Campanelli and A. Romanino, *"Effects of new physics in neutrino oscillations in matter"*, Phys. Rev. D **66**, 113001 (2002), [arXiv: 0207350 (hep-ph)].

[94] P. Huber, T. Schwetz and J. W. F. Valle, *" How sensitive is a neutrino factory to the angle θ_{13}?"*, Phys. Rev. Lett. **88**, 101804 (2004), [arXiv: 0111224 (hep-ph)].

[95] T. Ota, J. Sato and N. Yamashita, *"Oscillation enhanced search for new interaction with neutrinos"*, Phys. Rev. D **65**, 093015 (2002), [arXiv: 0112329 (hep-ph)].

[96] A. M. Gago, M. M. Guzzo, H. Nunokawa, W. J. C. Teves and R. Zukanovich Funchal, *"Probing Flavor Changing Neutrino Interactions Using Neutrino Beams from a Muon Storage Ring"*, Phys. Rev. D **64**, 073003 (2001), [arXiv: 0105196 (hep-ph)].

[97] N. C. Ribeiro, H. Nunokawa, T. Kajita, S. Nakayama, P. Ko and H. Minakata, *"Probing Nonstandard Neutrino Physics by Two Identical Detectors with Different Baselines"*, Phys. Rev. D **77** 073007 (2008), [arXiv: 0712.4314 (hep-ph)].

[98] A. Esteban-Pretel, R. Tomas and J. W. F. Valle, *"Probing non-standard neutrino interactions with supernova neutrinos"*, Phys. Rev. D **76**, 053001 (2007), [arXiv: 0704.0032 (hep-ph)].

[99] H. Duan, G. M. Fuller, J. Carlson and Y. Z. Qian, *"Coherent Development of Neutrino Flavor in the Supernova Environment"*, Phys. Rev. Lett. **97**, 241101 (2006), [arXiv: 0608050 (astro- ph)].

[100] G. L. Fogli, E. Lisi, A. Mirizzi and D. Montanino, *"Reexamining nonstandard interaction effects on supernova neutrino flavor oscillations"*, Phys. Rev. D **66** 013009 (2002), [arXiv: 0202269 (hep-ph)].

[101] A. de Gouvea, K. J. Kelly, *"Non-standard Neutrino Interactions at DUNE"*, Nucl. Phys. B 908, 318 (2016) [arXiv: 1511.05562 (hep-ph)].

[102] P. Coloma, *"Non-Standard Interactions in propagation at the Deep Underground Neutrino Experiment"*, JHEP **1603**, 016 (2016), [arXiv: 1511.06357 (hep-ph)].

[103] D. V. Forero, P. Huber, *"Hints for leptonic CP violation or New Physics?"*, Phys. Rev. Lett. **117**, 031801 (2016), [arXiv: 1601.03736 (hep-ph)].

[104] K. Huitu, T. J. Karkkainen, J. Maalampi, and S. Vihonen, *"Constraining the non-standard interaction parameters in long baseline neutrino experiments"*, Phys. Rev. D **93** 053016 (2016), [arXiv: 1601.07730 (hep-ph)].

[105] J. Liao,D. Marfatia, and K. Whisnant, *"Degeneracies in long-baseline neutrino experiments from nonstandard interactions"*, Phys. Rev. D **93**, 093016 (2016), [arXiv: 1601.00927 (hep-ph)].

[106] K. A. Olive *et al.*, (Particle Data Group), *"REVIEW OF PARTICLE PHYSICS"*, Chin. Phys. C **38**, 090001 (2014).

[107] B. Kronenbitter *et al.*, [Belle Collaboration], *"Measurement of the branching fraction of $B^+ \to \tau^+ + \nu_\tau$ decays with the semileptonic tagging method"*, [arXiv: 1503.05613 (hep-ex)].

[108] M. Bona *al.* [UTFit Collaboration], `http://www.utfit.org/UTfit/ResultsSummer2014PostMoriondSM`.

[109] S. Fajfer, J.F. Kamenik, I. Nisandzic and Z. Zupan, *"Implications of lepton flavor universality violations in B decays"*, Phys. Rev. Lett. **109**, 161802 (2012), [arXiv: 1206.1872 (hep-ph)].

[110] A. Crivellin *et al.*, *"Lepton-flavor violating B decays in generic Zâ\Šš models"*, Phys. Rev. D **92**, 054013 (2015), [arXiv: 1504.07928 (hep-ph)].

[111] D. Becirevic, O. Sumensari, R. Z. Funchal, *"Lepton Flavor Violation in Exclusive $b \to s$ Decays"*, Euro. Phys. J. C **76**, 134 (2016), [arXiv: 1602.00881 (hep-ph)].

[112] R. Aaij *et al.*, [LHCb Collaboration], *"Measurement of the $B^0 \to \mu^+\mu^-$ branching fraction and search for $B^0 \to \mu^+\mu^-$ decays at the LHCb experiment"*, Phys. Rev. Lett. **111**, 101805 (2013) [arXiv: 1307.5024 (hep-ex)].

[113] S. Chatrchyan *et al.*, [CMS Collaboration], *"Measurement of the $B^0(s) \to \mu^+\mu^-$ branching fraction and search for $B^0 \to \mu^+\mu^-$ with the CMS Experiment"*, Phys. Rev. Lett. **111**, 101805 (2013) [arXiv: 1307.5025 (hep-ex)].

[114] V. Khachatryan *et al.*, [CMS Collaboration], and I. Bediaga *et al.* [LHCb Collaboration], *"Observation of the rare $B^0(s) \to \mu^+\mu^-$ decay from the combined analysis of CMS and LHCb data"*, Nature, **522**, 68 (2015), [arXiv: 1411.4413 (hep-ex)].

[115] C. Bobeth, M. Gorbahn, T. Hermann, M. Misiak, E. Stamou, M. Steinhauser, *"$B_{s,d} \to l^+l^-$ in the Standard Model with Reduced Theoretical Uncertainty"*, Phys. Rev. Lett. **112**, 101801 (2014) [arXiv: 1311.0903 (hep-ph)].

[116] M. Malinsky, T. Ohlsson, H. Zhang, *"Study of the decay $K^+ \to \pi^+\bar{\nu}\nu$ in the momentum region 140<P_π<199* MeV/c*"*, Phys. Rev. D **79** 011301 (2009), [arXiv: 1307.5025 (hep-ex)].

[117] T. Ohlsson, T. Schwets,H. Zhang, *"Non-standard neutrino interactions in the Zee-Babu model"*, Phys. Lett. B **681**, 269 (2009), [arXiv: 0909.0455 (hep-ph)].

[118] C. Biggio, M. Blennow, E. Fernandez-Martinez, *"General bounds on non-standard neutrino interactions"*, JHEP **08** 090 (2009)[arXiv: 0907.0097 (hep-ph)].

[119] G. Mitsuka *et al.*, *"Analytic Approximations for Three Neutrino Oscillation Parameters and Probabilities in Matter"*, Phys. Rev. D **84**, 113008 (2011), [arXiv: 0103300 (hep-ph)].

[120] T. Ohlsson, *"Status of non-standard neutrino interactions"*, Rept. Prog. Phys. **76**, 044201 (2013),[arXiv: 1209.2710 (hep-ph)].

[121] P. Adamson *et al.*, [MINOS Collaboration], *"A search for flavor-changing non-standard neutrino interactions by MINOS"*, Phys. Rev. D **88** (7),072011 (2013), [arXiv: 1303.5314 (hep-ex)].

[122] J. Kopp, P. A. Machado and S. J. Parke, *"Interpretation of MINOS data in terms of nonstandard neutrino interactions"*, Phys.Rev. D **82** 113002 (2010), [arXiv: 1009.0014 (hep-ph)].

[123] S. Choubey, A. Ghosh, T. Ohlsson, D. Tiwari, *"Neutrino physics with non-standard interactions at INO"*, JHEP **12**, 126 (2015), [arXiv: 1507.02211 (hep-ph)].

[124] Y. Grossman, *"Non-Standard Neutrino Interactions and Neutrino Oscillation Experiments"*, Phys. Lett. B **359**, 141 (1995), [arXiv: 9507344 (hep-ph)].

[125] T. Akiri *et al.* [LBNE Collaboration], *"The 2010 Interim Report on the Long-Baseline Neutrino Experiment Collaboration Physics Working Groups"*, [arXiv: 1110.6249 (hep-ex)]; `http://lbne2-docdb.fnal.gov/cgi-bin/ShowDocument?docid=5823`.

[126] R. Acciarri *et al.*, [DUNE Collaboration], *"Long-Baseline Neutrino Facility (LBNF) and Deep Underground Neutrino Experiment (DUNE) Conceptual Design Report Volume 2: The Physics program for DUNE at LBNF"*, [arXiv: 1512.06148 (physics.ins-det)].

[127] R. Acciarri *et al.*, [DUNE Collaboration], *"Long-Baseline Neutrino Facility (LBNF) and Deep Underground Neutrino Experiment (DUNE) Conceptual Design Report Volume 1: The LBNF and DUNE Projects"*, [arXiv: 1601.05471 (physics.ins-det)].

[128] P. Huber, M. Lindner and W. Winter, *"From parameter space constraints to the precision determination of the leptonic Dirac CP phase"*, JHEP **0505**, 020 (2005) [arXiv: 0412199 (hep-ph)].

[129] P. Huber, M. Lindner, T. Schwetz and W. Winter, *"First hint for CP violation in neutrino oscillations from upcoming superbeam and reactor experiments"*, JHEP **0911** (2009) 044, [arXiv: 0907.1896 (hep-ph)].

[130] J. Kopp, *"Efficient numerical diagonalization of hermitian* 3×3 *matrices"*, Int. J. Mod. Phys. C **19**, 523 (2008). Erratum ibid C **19** (2008), [arXiv: 0610206 (physics.comp-ph)].

[131] J. Kopp, M. Lindner, T. Otta and J. Sato, *" Non-standard neutrino interactions in reactor and superbeam experiments"*, Phys. Rev. D **77**, 013007 (2008), [arXiv: 0708.0152 (hep-ph)].

[132] H. Minakata, M. Sonoyama, and H. Sugiyama, *"Determination of* θ_{23} *in Long-Baseline Neutrino Oscillation Experiments with Three-Flavor Mixing Effects"*, Phys. Rev. D **70**, 113012 (2004), [arXiv: 0406073 (hep-ph)].

List of Publications

Thesis Publications

[1] **C. Soumya** and R. Mohanta, *"Towards Extracting the best possible results from NOνA experiment"*, Eur. Phys J. C **76**, 302 (2016), [arXiv:1605.00523(hep-ph)].

[2] **C. Soumya**, K. N. Deepthi and R. Mohanta, *"A comprehensive study of the discovery potential of NOνA, T2K and T2HK experiments"*, Adv. High Energy Phys. **2016**, 9139402 (2016), [arXiv:1408.6071 (hep-ph)].

[3] **C. Soumya** and R. Mohanta, *"Implications of lepton flavour violation on long baseline neutrino oscillation experiments"*, Phys. Rev. D **94**, 053008 (2016), [arXiv:1603.02184 (hep-ph)].

[4] **Soumya C.** and R. Mohanta, *"Impact of lepton flavour universality violation on CP violation sensitivity of long baseline neutrino oscillation experiments"*, [arXiv:1701.00327 (hep-ph)], (To appear in Eur. Phys J. C).

Other Publications

[1] K. N. Deepthi, **C. Soumya**, and R. Mohanta, *"Revisiting the sensitivity studies for leptonic CP-violation and mass hierarchy with T2K, NOνA and LBNE experiments"*, New J. Phys. **17** 023035 (2015), [arXiv:1409.2343(hep-ph)].

[2] Sruthilaya M., **Soumya C.**, K. N. Deepthi and R. Mohanta, *"Predicting Leptonic CP phase by considering deviations in charged lepton and neutrino sector"*, New J. Phys. **17** 083028 (2015), [arXiv:1408.4392(hep-ph)].

Conference Proceedings

- Sruthilaya M., **Soumya C.**, K. N. Deepthi and R. Mohanta, "*Predicting Leptonic CP phase by considering deviations in charged lepton and neutrino sectors*", XXI DAE-BRNS High Energy Physics Symposium, Springer proceedings in Physics **174** (page 401-406).

- **Soumya C.** and R. Mohanta, "*Impact of active-sterile neutrino mixing on physics potential of long baseline experiment*", Presented at XXII DAE-BRNS High Energy Physics Symposium.

PHENOMENOLOGICAL ASPECTS OF NEUTRINO OSCILLATIONS

ORIGINALITY REPORT

%23	%6	%21	%2
SIMILARITY INDEX	INTERNET SOURCES	PUBLICATIONS	STUDENT PAPERS

PRIMARY SOURCES

1	Soumya, C., and R. Mohanta. "Towards extracting the best possible results from NO $$\nu $$ v A", The European Physical Journal C, 2016. Publication	%8
2	arxiv.org Internet Source	<%1
3	Deepthi, K N, Soumya C, and R Mohanta. "Revisiting the sensitivity studies for leptonic CP-violation and mass hierarchy with T2K, NOvA and LBNE experiments", New Journal of Physics, 2015. Publication	<%1
4	A Bandyopadhyay. "Physics at a future Neutrino Factory and super-beam facility", Reports on Progress in Physics, 10/01/2009 Publication	<%1
5	www.i-scholar.in Internet Source	<%1
6	Rukmani Mohanta. "Effect of FCNC mediated Z boson on lepton flavor violating decays",	<%1

	The European Physical Journal C, 04/2011 Publication	
7	Submitted to University of Hyderabad, Hyderabad Student Paper	<%1
8	Sruthilaya, M, C Soumya, K N Deepthi, and R Mohanta. "Predicting leptonic CP phase by considering deviations in charged lepton and neutrino sectors", New Journal of Physics, 2015. Publication	<%1
9	Klapdor-Kleingrothaus, . "Original Articles", Sixty Years of Double Beta Decay From Nuclear Physics to Beyond Standard Model Particle Physics, 2001. Publication	<%1
10	Advanced Topics in Science and Technology in China, 2011. Publication	<%1
11	Abe, K., H. Aihara, C. Andreopoulos, I. Anghel, A. Ariga, T. Ariga, R. Asfandiyarov, M. Askins, J. J. Back, P. Ballett, M. Barbi, G. J. Barker, G. Barr, F. Bay, P. Beltrame, V. Berardi, M. Bergevin, S. Berkman, T. Berry, S. Bhadra, F. d. M. Blaszczyk, A. Blondel, S. Bolognesi, S. B. Boyd, A. Bravar, C. Bronner, F. S. Cafagna, G. Carminati, S. L. Cartwright, M. G. Catanesi, K. Choi, J. H. Choi, G. Collazuol, G. Cowan, L. Cremonesi, G.	<%1

This is to certify that the thesis entitled "Phenomenological Aspects of Neutrino Oscillation" has been screened by the Turnitin software at the library of University of Hyderabad. The software shows 23% similarity index out of which, 8% came from the candidate's research article related to this thesis. The major part of remaining 15% might have come from the three other articles (published in Advances in High Energy Physics, Physical Review D, and European Physical Journal C), which has not been detected by the software. Therefore, this thesis is free from plagiarism.

Prof. Rukmani Mohanta
(Thesis Supervisor)